CHALMERS
UNIVERSITY OF TECHNOLOGY

Analysis of GNSS signal measurement accuracy

Investigating error models for phase residuals with respect to antenna phase center corrections

Master thesis in Wireless, Photonics and Space Engineering

ALIF RACHMAN HARFIAN

DEPARTMENT OF SPACE, EARTH AND ENVIRONMENT
CHALMERS UNIVERSITY OF TECHNOLOGY
Gothenburg, Sweden 2024
www.chalmers.se

Master thesis 2024

Analysis of GNSS signal measurement accuracy

Investigating error models for phase residuals with respect to antenna phase center corrections

ALIF RACHMAN HARFIAN

CHALMERS
UNIVERSITY OF TECHNOLOGY

Department of Space, Earth and Environment
Division of Onsala Space Observatory
Research Unit of Space Geodesy and Geodynamics
Chalmers University of Technology
Gothenburg, Sweden 2024

Analysis of GNSS signal measurement accuracy
Investigating error models for phase residuals with respect to antenna phase center corrections
ALIF RACHMAN HARFIAN

Supervisor: Sten Bergstrand, RISE Research Institutes of Sweden AB
Examiner: Rüdiger Haas, Department of Space, Earth and Environment

Master Thesis 2024
Department of Space, Earth and Environment
Division of Onsala Space Observatory
Research Unit of Spacegeodesy and Geodynamics
Chalmers University of Technology
SE-412 96 Gothenburg
Telephone +46 31 772 1000

Cover: GNSS station D501 and 20 m telescope at Onsala Space Observatory.

Gothenburg, Sweden 2024

Analysis of GNSS signal measurement accuracy
Investigating error models for phase residuals with respect to antenna phase center corrections

ALIF RACHMAN HARFIAN
Department of Space, Earth and Environment
Chalmers University of Technology

Abstract

Receiver-related errors significantly influence the accuracy of GNSS signal measurements. One of these errors pertains to the antenna phase center correction. Several antenna calibration techniques, such as robot calibration, can mitigate the impact of such errors. However, there is a possibility that calibration corrections may not completely eliminate the errors in the antenna phase center. To address this issue, calibrated antenna phase center corrections were investigated by measuring GNSS signal observations at four different stations, each tilted to various angles in specific directions, involving up to six baseline length formations. This experiment was distinct from previous studies, which only involved one baseline length between two different stations with antennas physically tilted towards each other. Observation data from the four different stations were retrieved and processed using GipsyX with the Precise Point Positioning (PPP) method, and Bernese with the single difference technique (DGNSS). Additionally, a laser tracker was utilized to measure the station positions and baseline lengths, providing more precise measurements. The phase residual error models were derived from L1, L2 and L3 frequency observations. The error models indicate that all three frequency observations are influenced by errors corresponding to antenna phase center corrections, with an error of -0.8867 mm for L1, -1.5728 mm for L2, and -0.3901 mm for L3.

Keywords: GNSS, GPS, Carrier Phase, Antenna Phase Center, Single Difference, PPP, GipsyX, Bernese.

Acknowledgements

I would like to express my gratitude to all my supervisors and examiner Sten Bergstrand, Rüdiger Haas, and Jan Johansson for the invaluable support and guidance during the project work, as well as the constructive feedback that improved the thesis project. I would also like to thank Uttama Dutta for her technical helps processing the observation data within the Bernese software.

I would like to furthermore extend my sincere to the RISE Research Institutes of Sweden AB for giving the great opportunity to undertake the thesis, particularly the people in the Division Unit of Safety and Transport including Jörgen Spetz, Sten Bergstrand, Magnus Herbertsson, etc., and also for providing their assistance and sharing their knowledge to make this thesis project possible.

Lastly, I would like to thank the people at the Onsala Space Observatory and people in the Department of Space, Earth and Environment (4ö) for making me feel welcome and creating a friendly working environment.

Alif Rachman Harfian, Gothenburg, March 2024

List of Acronyms

Below is the list of acronyms that have been used throughout this thesis listed in alphabetical order:

ADC	Attitude Determination & Control
ADC	Analog-to-Digital Converter
AIUB	Astronomical Institute of the University of Bern
ARNS	Aeronautical Radio Navigation Service
ARP	Antenna Reference Point
AUT	Antenna Under Test
C/A	Course Acquisition
CRF	Celestial Reference System
CRS	Celestial Reference System
DGNSS	Differential GNSS
DORIS	Doppler Orbitography and Radiopositioning Integrated by Satellite
DSP	Digital Signal Processor
ECEF	Earth-Center, Earth-Fixed
ERPs	Earth's Rotation Parameters
ESA	European Space Agency
GAs	Ground Antennas
GDOP	Geometric Dilution of Precision
GLONASS	Global'naya Navigatsionnaya Sputnikovaya Sistema
GNSS	Global Navigation Satellite System
GPS	Global Positioning System
IERS	International Earth Rotation and Reference System
IF	Intermediate Frequency
IGN	Institut Géographique National
IGS	International GNSS Service
IRNSS	Indian Regional Navigation Satellite System
ITRF	International Terrestrial Reference Frame
KASI	Korea Astronomy and Space Science Institute
LNA	Low Noise Amplifier
LOS	Line-of-Sight
MCS	Master Control Station
MEO	Medium Earth Orbit
MSs	Monitor Stations

NASA JPL	National Aeronautics and Space Administration Jet Propulsion Laboratory
NGS	U.S. National Geodetic Survey
OCS	Operational Control System
OSO	Onsala Space Observatory
PCO	Phase-Center Offset
PCV	Phase-Center Variation
PPP	Precise Point Positioning
PRN	Pseudorandom Noise
PZ-90	Parametry Zemli 1990
QSS	QZS System Service
RF	Radio Frequency
RHCP	Right-Hand Circular Polarization
RL	Return Loss
RTG	Real Time Gipsy
SA	Selective Availability
SBAS	Satellite-Based Augmentation Systems
SD	Single-Difference
SLR	Satellite Laser Ranging
SNR	Signal-to-Noise Ratio
SOPS	Space Operations Squadron
SV	Satellite Vehicle
TEC	Total Electron Content
TOA	Time-of-Arrival
TRF	Terrestrial Reference Frame
TRS	Terrestrial Reference System
TT&C	Tracking, Telemetry and Command
USAF	United States Air Force
USNO	United States Naval Observatory
UTC	Coordinated Universal Time
WGS	World Geodetic System
ZTD	Zenith Tropospheric Delay

Contents

List of Figures

List of Tables

1

Introduction

Global Navigation Satellite System (GNSS) is a technology consisting of multiple satellite constellations that provide positioning, navigation, and timekeeping services globally or in specific regions. Currently, there are only six different authorities responsible for managing and controlling navigation satellites worldwide. These authorities are either individual countries or unions of multiple countries. The GPS (Global Positioning System) constellation is owned and operated by the USA, Galileo by the European Union, GLONASS by the Russian Federation, COMPASS/Beidou by the People's Republic of China, NavIC/IRNSS by the Government of India, and QZSS is owned by the Government of Japan and operated by QZS System Service Inc. (QSS).

The first operational GNSS was the United States' GPS, initially intended for military applications. Developed by the US Department of Defense in 1973, it was first launched in 1978. Nowadays, GNSS technology serves many purposes, not only military as initially intended, but also scientific research, civilian use, shipping monitoring, construction, aviation, and defense, among others. One of the most common GNSS applications today is map navigation in smartphones for consumer use.

Furthermore, more specific fields of application, such as space geodesy and geodynamics, extensively utilize GNSS technology. These fields of study focus on the Earth's shape, structure, and its dynamic activities over time, aiming to gain comprehensive knowledge about the Earth's behavior as a planet. In addition to these studies, GNSS technology can also be used for predicting and analyzing natural disasters like earthquakes caused by either tectonic plate movements or volcanic eruptions. This type of analysis involves measuring the movement of ground-based instruments that receive GNSS satellite signals from space.

There are numerous GNSS stations spread out around the world, covering all seven continents. This global network can be accessed through the International GNSS Service (IGS), which provides high-precision data from the GNSS station network, making it easily accessible for a variety of applications. Moreover, many nations have established their regional networks of GNSS stations to serve various purposes. In Sweden, for instance, the local GNSS stations are managed by Lantmäteriet through the SWEPOS network, consisting of more than 500 stations distributed across the country. Through this local SWEPOS network, a local coordinate reference system can be established and determined, known in this case as SWEREF99.

Errors in GNSS measurements stem from various sources, necessitating the resolution of these discrepancies for more precise results. The error sources arise from multiple factors, including hardware-related issues such as receivers and antennas, both on the ground station or satellite, atmospheric properties, satellite trajectory and location, and the surrounding environment of the station. These errors influence the signals from satellites, consequently affecting the measurement precision. One specific error arises from the antenna element, which crucially requires calibration using specific techniques to determine the phase-center offsets (PCO) as well as phase-center variations (PCV).

The main focus of this project is to analyze the quality assurance of GNSS measurements from the perspective of ground segment receivers, with a particular experimental setup, and assess the remaining errors that are hypothetically expected to arise from the antenna phase-center calibration corrections. The data processing involves correcting signal errors, determining the final coordinate positions of the stations, and validating such data using externally estimated data from another type of measurement. By comparing the results of two different types of measurements, it can identify the error correction related to the phase-center calibration.

The project aims to achieve the local error of the station-dependent phase center offset by employing multiple combinations of differentials between antennas setup, each antenna independently, and an external high-precision geometric measurement as the benchmark. The ultimate goal is to ensure optimal outcomes with minimal errors. The experiment setup includes five point coordinates around the Onsala Space Observatory area. One of the stations, ONSA (also known as ONS0), has been part of the IGS global network for decades, while the rest of the stations (O302, O303, O304, and O501) form a local network. Data was collected from these five stations and processed using two different techniques and software: the Precise Point Positioning (PPP) method using GipsyX and Single-Difference (SD) using Bernese.

The fundamental part of this project is to apply a new method developed by [1] in the field experiment setup and measurement. By intentionally tilting the antennas using this method, it creates a geometric constraint that influences the data processing and results regarding the antenna phase-center calibration data. These antennas have been previously calibrated by IGS-approved service providers. The investigation aims to characterize a mobile reference antenna system and verify its performance at a different independent site.

2

Theory

A GNSS satellite is designed to determine and provide precise time and positioning. This technology utilizes signals from satellites following established orbits to approximate position, speed, and time. Equipped with suitable receivers, users can obtain precise and continuous three-dimensional position and velocity details globally, while also receiving time aligned with the Coordinated Universal Time (UTC) standard [2]. Before the emergence of global navigation satellite systems (GNSS), accurate navigation was limited to professional navigators or individuals with the means to purchase costly navigation systems. However, GNSS technology has made precise navigation accessible to a broader range of users due to its affordability [3].

Global constellations of satellite navigation mostly orbit in MEO (Medium Earth Orbit) at an altitude of approximately 20,000-30,000 km above the Earth's surface. The fundamental principle of satellite navigation is to ascertain position by measuring the distance from known coordinate points, either moving or stationary. This determination process is known as trilateration [4]. Trilateration requires a minimum of four satellites to calculate four unknown variables: the three-dimensional position coordinates and the receiver clock error. The two fundamental measurements of GNSS signals take place within the user segment. This involves comparing the received code signal with a locally produced version to determine the time delay between the satellite and the receiver. This measurement process is known as Pseudorange [5].

2.1 Global Navigation Satellite Systems (GNSS)

GNSS generally consists of three segments to operate and provide continuous positioning data, i.e., the space segment, control segment, and user segment [5].

2.1.1 Space Segment

The space segment consists of multiple constellations of satellites that constantly transmit signals to users, both on the ground (Earth) and in space (other types of satellites). These satellite constellations contain navigation payloads, highly accurate atomic clocks, antennas, and additional systems such as thermal, attitude determination & control (ADC), Tracking, Telemetry, and Command (TT&C), and power subsystems. In general, the satellite constellation is designed to ensure access to a minimum of four satellites simultaneously and globally at any given time [5].

The primary role of the space segment involves sending radio-navigation signals and storing and transmitting navigation messages from the Control Segment. It relies on extremely precise atomic clocks installed within the satellites [6]. There are currently multiple established GNSS constellations around the world, as well as regionally operated systems. The most recognized operational GNSS is GPS, developed by the United States Department of Defense and operated by the formal United States Air Force (USAF) GPS Directorate [2].

The space segment, particularly satellites, transmit pseudorandom noise (PRN)-coded signals used for ranging measurements, also known as pseudorange. This characterizes the GPS satellite as a passive system for users, where the signals are solely transmitted, and the user passively receives them [2]. The satellites are designed and positioned across various orbital planes to optimize the geometric dilution of precision (GDOP), which measures satellite geometry [5].

Another counterpart of the U.S. GPS is the Russian GLONASS (Global Navigation Satellite System). Similar to GPS, GLONASS serves both military and civil purposes for positioning and timing in a multi-frequency system. Moreover, the People's Republic of China and the European Union (EU) have developed and launched their respective GNSS constellations, Beidou and Galileo. These constellations operate globally on similar principles with slight variations [2].

Conversely, countries such as India and Japan have established their own regional systems: the Indian Regional Navigation Satellite System (IRNSS) and the Quasi-Zenith Satellite System (QZSS), respectively. These regional constellations are designed to enhance the performance of the current global GNSS constellations [2].

2.1.2 Control Segment

In general, the primary responsibility of the Control Segment is to monitor, operate, and maintain the Space Segment [4]. This involves calculating the location of satellites, managing their orientation, and controlling their orbital trajectory. Furthermore, the Control Segment is also responsible for transmitting navigation messages and ensuring highly accurate clock synchronization to the satellites [5].

In the United States' GPS control segment, the Operational Control System (OCS) consists mainly of three different subgroups, i.e., the Master Control Station (MCS), L-band monitor stations (MSs), and S-band ground antennas (GAs) [2]. These subdivisions, except for the MCS, are spread around the globe to enable greater monitoring and operation of the global satellite constellations [7]. The MCS ensures the continuous operation of GPS services 24/7 and serves as the central hub for controlling GPS operations. It is located in Colorado, USA, and operated under the U.S. Air Force Space Command, Second Space Operations Squadron (2 SOPS) [2].

2.1.3 User Segment

The User Segment generally involves GNSS receivers that analyze signals received from satellites to determine the user's position. Common receiver functions include identifying the visibility of satellites, calculating user-to-satellite distances, and employing triangulation to determine positions [5]. It should also be noted that the clock of a ground receiver is not as accurate as the clock on the satellites [8].

2.2 Satellite Orbits and Clocks

Orbital information and errors are crucially important in the field of timing and positioning using satellite navigation. Orbital errors are closely linked to positional inaccuracy. Orbital information parameters can be transmitted from the satellites through broadcast messages or retrieved from various agencies. Several agencies are responsible for determining post-observation analysis of satellite orbit information, typically several days after observation [9]. These agencies, namely NASA JPL (USA), ESA (EU), IGN (France), KASI (South Korea), etc., estimate precise orbital information parameters that can be used as error solutions for post-processing analysis by users. The solution includes satellite orbit, satellite and station clocks, and Earth's rotation parameters (ERPs), which are submitted to worldwide data hubs on a sub-daily, daily, or weekly basis.

In general, the movements of satellites in orbit are described by Kepler's laws of motion, which are further supported by Newton's laws of gravitation [10]. Particularly, satellite navigation can be confined to elliptical orbit motions, and the six main orbit parameters. These orbit parameters are the inclination (i), semi-major axis of orbital ellipse (a), argument of perigee (ω), right ascension of ascending node (Ω), eccentricity (e), and epoch of perigee passage (T_0) [9]. A brief summary detail of a few GNSS constellation parameters from multiple different systems is described in Table 2.1 [11, 12, 13].

Table 2.1: GNSS constellations orbital parameters

Constellation	Number of Satellites	Altitude (km)	Number of Orbital Planes	Inclination (°)
GPS	24	20,180	6	55
GLONASS	24	19,100	3	64.8
Galileo	30	23,222	3	56

Furthermore, the clock plays a crucial role in the accuracy of timing and positioning in GNSS applications. Although it operates on a similar concept, clock accuracy requires detailed specifications depending on various applications, especially those used in reference timescale centers (i.e., UTC). These applications utilize extremely stable clocks that are kept under specific controlled environments. For example, in the US Naval Observatory (USNO), clocks include multiple commercial cesium beam frequency standards, hydrogen masers, and custom-made rubidium fountain standards. These clocks are physically isolated and operate within highly regulated environment conditions [14].

2.3 GNSS Signals and Frequencies

GNSS signals are principally generated by the atomic clocks in satellite, normally using cesium standards [4]. The clocks generate one or multiple radio frequency carriers, representing nearly ideal sinusoidal voltages in the satellite transmitter. Nowadays, the majority of GNSS signals utilize carrier frequencies within the L-band spectrum (1-2 GHz). The L-band frequency spectrum offers various benefits for GNSS signals compared to other frequency ranges. Lower frequencies tend to encounter greater delays due to the Earth's atmosphere, leading to inconsistencies in atmospheric properties that weaken satellite signals. Conversely, higher frequencies require increased satellite power and are susceptible to notable attenuation caused by precipitation, such as rain [2].

The L-band spectrum in GNSS is differentiated in two parts, the upper L-band (1559-1620 MHz) and the lower L-band (1164-1300 MHz). All these frequency ranges are allocated and regulated by the ITU (International Telecommunication Union). This specific GNSS spectrum is also known as RNSS (radio navigation satellite service) band. In addition, ARNS (Aeronautical Radio Navigation Service) band is allocated with the spectrum to ensure the protection of GNSS signals from any threats and interferences [15]. A summary of allocated frequencies used by multiple GNSS signals is shown in Figure 2.1.

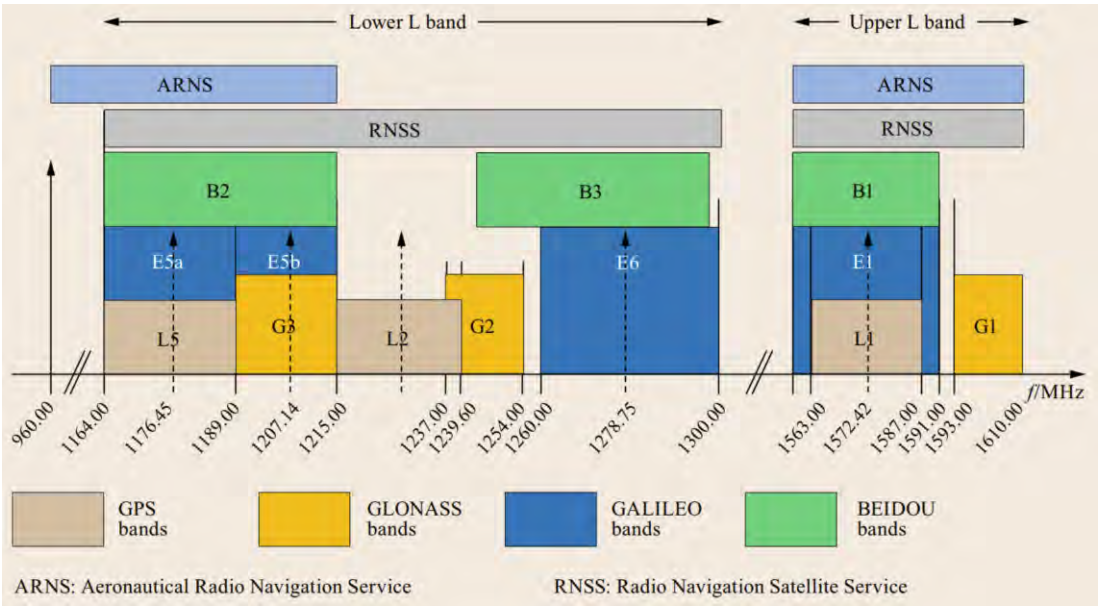

Figure 2.1: GNSS frequency band allocated by the ITU [15].

2.3.1 Carrier Signals

The satellite navigation signal is primarily generated by the onboard oscillators on satellites. These oscillators create a fundamental frequency that is used for all components of the satellite signal. In GPS signals, for instance, the signals are driven by a 10.23 MHz clock oscillator. The carrier signals are derived from integer

multiplication of the clock frequency [9]. Currently, the GPS provides three different L-band frequency services, L1, L2, and L5 [16]. Table 2.2 summarizes the existing GPS carrier signals.

Table 2.2: GPS carrier signals [16]

Component	Frequency (MHz
Frequency clock (f_o)	10.23
L1	$154f_o = 1575.42$
L2	$120f_o = 1227.60$
L5	$115f_o = 1176.45$

All three carrier GPS signals (L1, L2, and L5) are composed of two carrier components that are in-phase quadrature with each other, and all transmitted with the minimum received power of -158.5 dBW, -160.0 dBW, and -157.9 dBW, respectively [16]. These carriers are modulated by codes to provide satellite clock data to the receiver and convey other information such as orbital parameters. The codes consist of sequences with states of +1 or -1, corresponding to the binary values of 0 or 1. This type of process is also known as binary phase modulation [9].

2.3.2 Ranging Codes

The codes fundamentally consist of the C/A (Coarse Acquisition) code and P (Precise) code. The C/A code is present on the L1 channel, while the P code is present on both L1 and L2 channels [4]. Satellite clock readings employ two codes distinguished by a pseudorandom noise (PRN) sequence. The C/A code operates at frequency of $f_o/10$ and repeats every millisecond. Moreover, the P code has a frequency of the satellite clock f_o, repeating roughly once every 266.4 days [9]. In addition, another type called W-code is used to encrypt the P(Y) code. Initially, both the C/A and the P(Y) code, along with the L1 and L2 carrier frequencies, were supposed to be encrypted, along with time-varying frequency adjustments (known as dither) and encrypted offsets in ephemeris and almanac data, a feature also known as Selective Availability (SA) [2]. Nonetheless, Selective Availability (SA) was deactivated on all GPS satellites since 2000, and the United States, as the owner and operator of GPS, has no plans to reinstate SA [17].

The bits in the pseudorandom noise (PRN) sequences are generally referred to as chips, emphasizing that these codes do not contain data. The C/A code is produced by a combination of two 10-bit tapped feedback shift registers. The output of both registers is combined through binary operations to generate the code sequences, which are accessible to civilian users. With a frequency of 1.023 MHz and a repetition rate of 1 millisecond, the code has a length of 1023 chips. Consequently, the time gap between two chips is slightly less than 1 microsecond, roughly equivalent to a 300 m chip length [9].

Similarly, the P code is also created by two registers. The initial bit sequence recurs every 1.5 seconds and possesses a length of 1.5345×10^7 bits, corresponding to

the clock frequency f_o. The second sequence extends by an additional 37 bits. Combining both sequences yields a code with roughly 2.3547×10^{14} bits, corresponding to a duration of approximately 266.4 days as mentioned previously [9].

2.3.3 Navigation Message

The navigation message encompasses all the essential information required for users to conduct positioning. This includes ephemeris parameters for determining satellite coordinates, time parameters, and crucially clock corrections for calculating satellite clock offsets and time conversions. Furthermore, it includes service parameters indicating satellite health status, ionospheric model parameters as required for single-frequency receivers, and the almanac data that provides information about the details of the entire constellation orbit and clocks [15].

This information is transmitted at a rate of 50 bps, comprising 25 frames per second, each consisting of 1500 bits. As a result, it requires 12.5 minutes for complete transmission [4]. A single frame contains five subframes, which are sent within a 6-second interval and comprise 10 words, each consisting of 30 bits. Consequently, the transmission time required for one word is 0.6 seconds. It is worth noting that a receiver needs a minimum of 30 seconds to establish a connection with a satellite [9].

2.4 Data Acquisition

Utilizing the correlation method, the fundamental concept of GNSS involves deriving observable satellites by comparing the transmitted signal with the self-generated replica within the receiver. This determination utilizes two clocks, on the satellite and one on the ground receiver. Hence, the distance calculations are highly influenced by clock errors in both the satellite and the receiver, which are also referred to as pseudoranges [18]. GNSS signal measurement is defined in two categories, the pseudorange and the carrier phase. The carrier phase measurement, also referred to as the carrier beat phase, serves as the foundation in high-precision GNSS survey applications these days, as it is considered to be more accurate than pseudorange measurement [8].

2.4.1 Code Pseudorange

The fundamental measurement conducted by a GNSS receiver involves determining the time taken for the GNSS signal to travel from a satellite to the receiver. This process is achieved by monitoring the PRN code modulation of the signal. The pseudorange measurement is considered to have accuracy within the decimeter-level range. As the signal travels at the speed of light (c), the time duration can be transformed into a distance or range by multiplying it directly with c [19]. A simplified pseudorange observation from satellite S to receiver k can be defined in Equation 2.1

$$P_k^S = (T_k - T^S)c \tag{2.1}$$

where T_k represents the known value of the receiver clock when satellite signal is receiver, T^S denotes the time signal of the satellite clock is transmitted, and c is the speed of light in vacuum (3×10^8 m/s).

$$T_k = t_k + \tau_k \tag{2.2}$$

$$T^S = t^S + \tau^S \tag{2.3}$$

The modeled time signal for both satellite and receiver correspond to the true receive time t and clock bias τ, as shown in Equation 2.2 and 2.3. The substitutions yield the pseudorange model observation as a function of the true time when the signal is received in receiver, as defined in the following Equation 2.4.

$$P_k^S = \rho_k^S(t_k, t^S) + c\tau_k - c\tau^S \tag{2.4}$$

where $\rho_k^S(t_k, t^S)$ is the so-called true range from the ground receiver to the satellite.

However, other error parameters should be taken into account during the pseudorange measurement, which can result in significant delays. These delays are generally related to Earth's atmospheric properties, such as dispersive effects in the ionosphere and non-dispersive effects in the troposphere [18]. It results to more complex model of pseudorange measurement. An extended pseudorange measurement model is described in Equation 2.5.

$$P_k^S = \rho_k^S(t_k, t^S) + c\tau_k - c\tau^S + I_k^S + Z_k^S \tag{2.5}$$

where the ionospheric and tropospheric delay between the receiver and the satellite are denoted as I_k^S and Z_k^S, respectively.

The measured pseudorange data signal is combined with initial estimations to determine the residuals using Taylor approximation [18]. Hence, the pseudoranges are transformed into position values. Furthermore, the true range ρ_k^S can be determined using Pythagoras Theorem from the three-dimensional position between the satellite and the receiver in the same reference coordinate [4], which can be defined in the following Equation 2.6.

$$\rho_k^S = \sqrt{(x^S(t^S) - x_k(t_k))^2 + (y^S(t^S) - y_k(t_k))^2 + (z^S(t^S) - z_k(t_k))^2} \tag{2.6}$$

The information of satellite positions (x^S, y^S, z^S) can be readily retrieved and calculated from the navigation messages, as well as the satellite clock bias τ^S. Hence, the remaining four unknown variables, receiver position (x_k, y_k, z_k) and the receiver clock bias τ_k, are determined by tracking a minimum of four distinct satellites at the same time [4, 19].

2.4.2 Phase Pseudorange

The phase pseudorange, also known as carrier phase measurement, is fundamentally operated similarly to code measurement. The principle for the carrier phase measurement involves combining the received carrier from a GNSS satellite with a

duplicate carrier generated within the receiver. The phase discrepancy between the incoming signal and the internal reference of the receiver refers to the fractional component of the carrier phase measurement in GNSS signal. This type of measurement is also referred to as the carrier beat phase observable. In GNSS signal, a beat refers to the pulsation arising from the two waves combined with distinct frequencies. This phenomenon occurs whenever there is a combination of oscillators with different frequencies [8]. A phase as a function of time ($\varphi(t)$) can be characterized as the angle by which its line has rotated [4].

The carrier beat signal can be formulated as the following Equation 2.7.

$$\varphi_B(T) = \varphi^S(T) - \varphi_k(T) \tag{2.7}$$

where $\varphi_B(T)$ is the carrier beat phase, $\varphi^S(T)$ is the transmitted signal phase from satellite, and $\varphi_k(T)$ is the reference phase in the receiver.

Although the carrier phase measurement is considered to produce higher accuracy than the code pseudorange, the carrier phase process is more susceptible to errors. In carrier phase observations, the receiver is unable to ascertain the travel time, making it challenging to calculate the number of entire cycles from the satellite to the ground. This phenomenon of the unknown amount of cycles is known as phase ambiguity N (or integer ambiguity) [8].

Moreover, variations in carrier phase over time indicate alterations in the pseudorange but with significantly greater precision (≈ 2 orders). In instances of interrupted satellite tracking, the accumulated cycle unit is then reset, resulting in cycle slips in carrier phase measurement [19]. Thus, a new model of carrier phase signal is introduced, taking the phase ambiguity parameter of the satellite into account, as shown in Equation 2.8.

$$\Phi(T) = \varphi^S(T) - \varphi_k(T) - N^S \tag{2.8}$$

where $\Phi(T)$ is the carrier phase signal as a function of time (t) and N^S is the satellite phase ambiguity.

The observation can also be modeled to describe the clock time as a function of phase and reference frequency f_o, which in this case is the frequency of clock oscillator. It introduced in Equation 2.9.

$$T(t) = \frac{\varphi(t) - \varphi_0}{f_o} \tag{2.9}$$

Hence, the carrier observable in the receiver yields to Equation 2.10

$$\Phi_k^S(T_k) = f_o(T_k - T^S) + \varphi_{o_k} - \varphi_o^S - N^S \tag{2.10}$$

It should be noted that the time T^S may exhibit slight variations among satellites because the transmission time from each satellite must have differed for all signals to reach the receiver simultaneously [4].

Furthermore, carrier phase measurements can be formulated in unit of range or distance. This simplifies the phase measurement model by multiplying it with the wavelength. Thus, the carrier phase model in distance is described in Equation 2.11 and 2.12.

$$L_k^S(T_k) = \lambda_o f_o(T_k - T^S) + \lambda_o(\varphi_{o_k} - \varphi_o^S - N^S) \tag{2.11}$$

$$L_k^S(T_k) = c(T_k - T^S) + \lambda_o(\varphi_{o_k} - \varphi_o^S - N^S) \tag{2.12}$$

It is worth noting that the last three terms are treated constant, and combined together as a new term known as carrier phase bias B_k^S.

$$B_k^S = \lambda_o(\varphi_{o_k} - \varphi_o^S - N^S) \tag{2.13}$$

Previously, it was mentioned that GNSS signal observation can experience significant delays caused by the atmosphere. Therefore, the atmospheric properties during signal transmission, such as ionospheric and tropospheric delay, should also be taken into account in the carrier phase measurement model. The final model of carrier phase measurement is defined in Equation 2.14.

$$L_k^S(T_k) = \rho_k^S(t_k, t^S) + c\tau_k - c\tau^S + Z_k^S - I_k^S + B_k^S \tag{2.14}$$

Comparing Equation 2.5 and 2.14, the code pseudorange and carrier phase model are fundamentally similar. However, a few slight differences between the two type measurements are noted, especially the minus sign for the ionosphere parameter ($-I_k^S$), suggesting that the phase velocity experiences an actual increase in the carrier phase measurement model [4].

2.5 GNSS Receiver

A GNSS receiver is principally built with three main subsystems, i.e., the radio frequency (RF) front-end, the digital signal processor (DSP), and the navigation processor. The RF front-end is responsible for controlling and receiving incoming signals from satellites, lowering the signal frequency to an intermediate frequency (IF) using a down-converter, and sampling the signals using an analog-to-digital converter (ADC). All types of data measurements are then processed in the DSP block. These data include code pseudorange, carrier phase, Doppler frequency, and navigation data. Moreover, the navigation processor utilizes the navigation data to extract time, ephemeris information, and almanac data, ultimately determining velocity, time, and position [18]. Figure 2.2 shows the building of main GNSS receiver block.

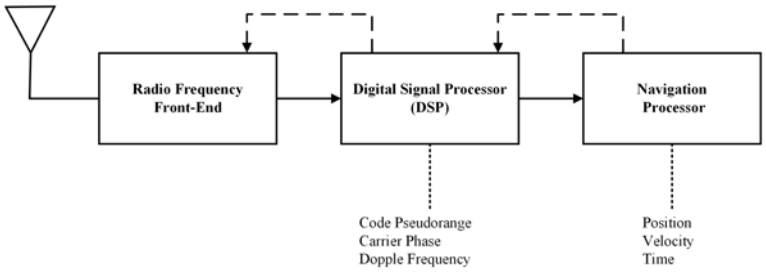

Figure 2.2: GNSS receiver block diagram.

2.5.1 Radio Frequency (RF) Front-end

The receiver antenna is the first component that receives electromagnetic waves in signal transmission from the satellite. It then transforms these waves into electric signals, which are sent to the RF front-end [20]. In GNSS applications, antennas are commonly designed to have an omnidirectional gain pattern, providing a uniform pattern in every direction for incoming signals from satellites. For static receiver observations, the gain is primarily minimized in the upper hemisphere. This is achieved by using certain types of antennas with a ground plane or choke ring design to reject signals originating from below the horizon, including those reflected from the ground [18]. Furthermore, it should also be noted that the antenna design is highly dependent to the type of applications, i.e., civil, military, space, geodesy, aviation, etc. [20].

There are several key parameters of antenna design, namely center frequency, bandwidth, radiation pattern and gain, polarization, and return loss (RL). GNSS antennas can be technically defined in two different characteristics: active and passive antennas. In active antenna design, the low noise amplifier (LNA) plays a significant role as it is integrated into the antenna, providing advantages to compensate signal loss by adjusting approximate gain at the output of the LNA. However, in passive antenna design, the LNA is embedded in the RF parts of the receiver [20].

Generally, GNSS antennas are designed to have right-hand circular polarization (RHCP), implying that the electric field of a GNSS signal consists of two perpendicular waves of identical amplitude and separated by a 90° phase shift. However, during the transmission process, this polarization might alter to left-hand circular polarization due to reflections from the surrounding environment. Furthermore, one of the significant errors in the antenna aspect is multipath, which poses a substantial risk to the precision of GNSS measurements. Multipath occurs when the receiver receives multiple identical signals from various directions. This phenomenon takes place when the line-of-sight (LOS) signal is reflected or diffracted from the surrounding objects of the antenna [21]. Moreover, this specific error source can be compensated by designing the antenna with specific shapes, e.g., choke-ring ground plane. The utilization of a ground plane with a choke ring helps diminish side- and back-lobe levels as well as enhance the antenna gain, consequently minimizing reflections [22]. An example of choke-ring antenna design is shown in Figure 2.3.

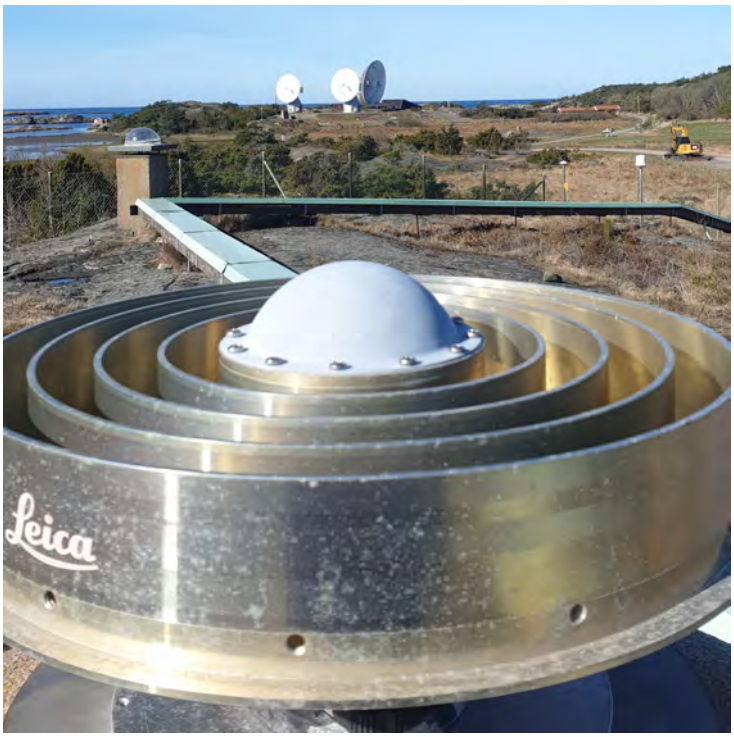

Figure 2.3: Choke-ring antenna design.

Another crucial error source is the phase center of the GNSS antenna. The antenna phase center is identified as the point where the transmitted signal from the satellite arrives in the antenna plane. Thus, it refers to as the reference point for all types of GNSS signal measurements. The geometric representation is defined as the Antenna Reference Point (ARP) [23]. This reference can be characterized as a function of elevation and azimuth, where the measurements depend on the direction of the incoming signals. In practice, the phase contour of the signal is not entirely spherical. This implies that the signal has a distorted form with frequency-dependent variations [22].

Moreover, it should be noted that the phase center of the antenna is not quite identical to its ARP. Therefore, the so-called phase center offset (PCO) is defined to correct the offset between the ARP and the mean phase center. Furthermore, considering that the incoming signal depends on the frequency, elevation, and azimuth, another term is introduced: the phase center variation (PCV). Unlike the PCO, which is considered a constant offset, PCV represents the change of phase center correction with respect to the received signal from the satellite as a function of elevation, azimuth, and frequency [21].

These phase center-related errors can be corrected by calibrating the antenna, either for the receiver (ground) or the transmitter (satellite) antenna. A precise calibration of both PCO and PCV plays an essential role in high-precision measurements, such as geodetic applications. This ensures positions derived from GNSS measurements can be accurately correlated with the actual locations of the antenna physically [22]. Antenna calibration is utilized to determine the phase center as well as its pattern at

particular frequencies. Multiple standard methods for calibrating GNSS antennas include anechoic chamber and absolute field calibration [21].

- **Anechoic chamber calibration:** The determination of the antenna phase center involves observing the phase changes of the received signal in the AUT (Antenna Under Test) while being rotated and tilted around two independent axes to vary its elevation and azimuth angles. The signal is transmitted and generated by the signal simulator, making it considerably convenient to measure PCO and PCV of the antenna since there is no need for actual satellite signals. The simulator can be easily adjusted to generate signals depending on the particular frequencies of the GNSS constellations [22]. However, it is worth noting that the anechoic chamber calibration only provides the mean values of PCO and PCV of the antenna, limiting the information on phase center errors that are dependent on signal directions (elevation and azimuth) in more detail [21].
- **Field calibration:** There are fundamentally two types of field calibrations, namely relative antenna calibration and absolute robot-based antenna calibration. The relative antenna calibration technique involves two antennas closely separated by a short baseline that is precisely calculated using relative measurements. The received satellite signals are then subsequently utilized to estimate the phase center position based on the elevation and azimuth angles of the satellites. This method maintains accuracy when the difference in satellite elevation, as observed by both antennas, is minimal [22]. However, such antenna reference is not required for the absolute robot-based calibration. In this particular calibration, the robot provides swift alterations of the boresight direction and rotation angle. This allows the collection of carrier phase observations, ensuring seamless hemispherical coverage of the antenna during the observation test. Thus, both PCO and PCV can be estimated from these observations [21]. Furthermore, this absolute calibration eliminates errors originating from multipath in both far-field and near-field [22].

2.5.2 Digital Signal Processor (DSP)

There are several signal processes that are conducted in the DSP section. In general, all type of data about the signal measurement as well as satellite information are split into several channels, this process known as channel multiplexing. The amount of channels in the DSP correlates to the maximum observable satellite multiplied by the quantity of the amount of frequencies and ranging codes. However, before the data is being channeled, the first task that is conducted by the DSP is to track the observable satellites upon the receiver initial activation. This done by examining the input signal to all ranging codes of observable satellites. After the observable satellites are tracked and determined, the DSP generates the replicas of all the signals. Subsequently, finding the highest autocorrelation between the two signals (replica and satellite). This process known as signal acquisition [18, 22].

2.5.3 Navigation Processor

This subsystem part of the RF front-end carries out three primary functions. First, the navigation processor decodes the navigation message and calculates the satellite positions using the outcomes of the data demodulation process. Additionally, it utilizes the code, phase, and Doppler measurements for timing, positioning, and velocity determinations. The third responsibility involves assisting such information to the tracking loops and filters [22].

2.6 Error Sources

It is crucial to determine and estimate various types of errors from any sources in high-precision applications of GNSS measurements. Both code pseudorange and carrier phase measurements are highly influenced by these errors. In general, error sources can be defined into several types, including atmospheric properties, satellite, ground receiver, and multipath [24]. Therefore, these error sources should be taken into account of during the measurement process in order to achieve highest precised results of timing and positioning.

2.6.1 Atmospheric Properties

The transmitted signal from the satellite to the ground receiver fundamentally experiences different properties of the atmosphere, which significantly affect the signal's travel and quality. Specifically, the signal is influenced by two atmospheric characteristics, it slows down and deviates during transmission [8].

2.6.1.1 Ionospheric Effect

The ionosphere is located approximately between 70 km and 1000 km above the Earth's surface, and it exhibits dispersive characteristics. This means that its effects depend on the frequency of the signal [8]. In the ionosphere region, specific gas molecules are ionized by ultraviolet rays from the Sun, resulting in the region being electron-free. These free electrons have an impact on the propagation of electromagnetic waves from satellite signals [2].

As mentioned in the previous section and considering the dispersive characteristic of this atmospheric region, signal data such as code pseudorange and navigation information are affected, resulting in delays. Additionally, the carrier phase experiences a phenomenon known as ionospheric divergence. The presence of free electrons causes degradation of the signal information [2]. The error is directly correlated with the so-called total electron content (TEC) within a tube of cross-sectional area of 1 m^2 along the propagation path. The propagation delay along the path for a satellite at zenith position normally fluctuates approximately from 1 m during the night to 5–15 m in the late afternoon. Lower elevation angle corresponds to a longer path in the ionosphere, leading to few meters higher delays at night and up to 50 m during the day. Moreover, error caused by lower satellite elevation angles can be reduced by

increasing certain amount of elevation mask angle. Mask angles between 5°-10° can compensate the reduction in the measurements and the probability of encountering substantial ionospheric errors [24].

It is noted that ionospheric delay is frequency-dependent, and therefore it can be effectively mitigated by conducting measurements using a dual-frequency receiver. By taking the difference between the code pseudorange measurements obtained at two frequencies, it is possible to estimate the delays on both frequencies. The so-called ionospheric-free frequency, such as L3 in GPS satellites, is constructed from two different frequency bands (L1 and L2) [2]. Equation 2.15 describes the formulated ionospheric-free frequency for code pseudorange measurement.

$$\rho_{L_3} = \frac{f_{L_1}^2}{f_{L_1}^2 - f_{L_2}^2}\rho_{L_1} - \frac{f_{L_2}^2}{f_{L_1}^2 - f_{L_2}^2}\rho_{L_2} \tag{2.15}$$

where the ρ_{L_3} is the ionspheric-free code pseudorange, f_{L_1} is the L1 (1575.42 MHz) frequency, f_{L_2} is the L2 frequency (1227.60 MHz), ρ_{L_1} is the measured code of L1, and ρ_{L_2} is the measured code of L2.

The formulated inospheric-free frequency in Equation 2.15 pricipally can also be applied for carrier phase measurement. Nevertheless, in non-differential processing, it is noted that the remaining carrier phase error may surpass the wavelength of both L1 and L2 carrier, leading to ambiguity [24].

2.6.1.2 Tropospheric Effect

In GNSS measurements, the troposphere is often referred to as the neutral atmosphere. This term signifies its characteristic as a non-dispersive medium for radio waves up to frequencies of 15 GHz. Therefore, signal propagation in the troposphere is independent of frequency [9]. Moreover, the tropospheric medium affects both the phase and group velocities of the GNSS carrier and signal information data, resulting in delays in free-space propagation. It is estimated that these delays can range from 2.4 meters when the satellite is directly overhead (zenith direction) and the user is at sea level, to up to 25 meters for a low satellite elevation angle, such as 5° [2].

Unlike the ionospheric delay, the delay caused by the troposphere cannot be estimated by employing dual-frequency measurements, as it is not frequency-dependent. Several techniques, such as modeling or differential methods, need to be used in order to compensate for this error delay. The characteristics of the tropospheric region can primarily be defined by two components: the dry-gas (hydrostatic) component and the water vapor (non-hydrostatic) component [24].

It is noted that the majority of the delay is contributed by the dry component, approximately up to 90 % of the tropospheric delay. Although the water vapor only contributes 10 % of the delay, the estimation is more tricky to model since the water vapor distribution in the atmosphere is uncertain [24]. Both delay components can

be characterized in terms of altitude in the troposphere. The dry layer is experienced in the altitude approximately of 40 km, while the wet component is about 10 km [2].

Furthermore, tropospheric delay error can be estimated by utilizing meteorological information such as pressure and temperature in the surrounding area of the ground receiver. Initial error estimations can be modeled with respect to the zenith direction of the satellite, referred to as zenith tropospheric delay (ZTD). However, a mapping function model is necessary to estimate the expected increase in tropospheric delay due to the longer path of the satellite when it is not at zenith elevation [2].

2.6.2 Satellite-related Errors

There are certain error parameters that can be identified from the satellite system. One major error from the satellite can be caused by the clock data. The timing and positioning determination from each satellite is utilized by its individual atomic clock without any error corrections adjusted, and this is referred to as the SV (satellite vehicle) process. Error correction needs to be estimated since it corresponds directly to clock synchronization in all satellites. The clocks may experience a certain level of relative drift, which is observed by ground stations and subsequently used to generate clock correction information included in the navigation message. Typical errors caused by satellite clocks are below 1 millisecond and they undergo gradual variations [24].

Another error source can also be cause by satellite antenna. It causes error bias, leading to phase and group delay of the that is slightly shifted with off-boresight angles. This phenomenon may lead to code pseudorange biases approximately ± 0.5 m, and ± 2 cm for carrier phase measurement biases. In addition, these estimated errors as antex (antenna exchange format) data information can easily be obtained from the International GNSS Service (IGS) portal for data processing since it is free for users [2].

Furthermore, all GNSS satellite positions in the precise orbit are continuously known and monitored by the master control station. Although the satellites are fundamentally positioned in nearly the same orbital path over time, minor positional shifts occur in the orbit due to gravitational forces. The primary sources of these shifts include the Earth's non-spherical gravitational field, gravitational attractions exerted by the Sun and the Moon, as well as pressure from solar radiation [8].

These orbital errors must be considered, as they affect the accuracy of the ephemeris data for each satellite, leading to inaccuracies in estimated satellite positions. The satellite ephemeris data is calculated by the GNSS master control station on the ground through continuous monitoring of signals from individual satellites. Since the positions of the satellites are accurately known, a reverse positioning determination process can be conducted to calculate the orbital parameters of the satellites. This process is supported by precise clocks at the monitoring stations. Subsequently,

the master control station calculates the estimated orbital parameters and transmits this information to users through the navigation message [24].

2.6.3 Receiver-related Errors

Fundamentally similar to satellite clock errors, inaccuracies in the receiver clock can lead to imprecise measurements. However, it is impractical to use highly accurate atomic clocks in receivers due to their complexity and cost [8]. Typical receiver clocks utilize quartz crystal oscillators with absolute accuracy around 1–10 ppm (parts per million) across standard temperature variations. In addition, more advanced oscillators commonly provide higher precise stability of 0.01–0.05 ppm over a few seconds [24]. Receiver clock error can be compensated by doing synchronization between the clock of both receiver and satellite. By simultaneously receiving signals from at least four satellites, the clock errors in the receiver can be identified, and the three-dimensional coordinates can be determined at the same time [8].

Another tricky error related to the receiver stems from the antenna itself. As mentioned previously, the phase center of the receiver antenna significantly influences the accuracy of GNSS signals, particularly in precise measurements such as land surveying in geodesy applications. This type of error correction can be characterized as constant offsets, which are estimated by calibrating the antenna using several calibration techniques [21]. It is also worth noting that the estimated phase centers are dependent on the type of antenna as well as its manufacturer, implying that for a certain estimated calibration phase center errors of an antenna may not be applicable to another [9].

Moreover, multipath contributes to significant errors in GNSS signal measurements. This phenomenon occurs when the satellite signal reaches the receiver through multiple paths, including one direct path and one or more indirect paths. As a result, the received signal exhibits relative phase offsets, and these phase variances correspond directly to the different lengths of the signal paths [9]. Figure 2.4 illustrates the multipath phenomenon in GNSS signal measurement. Multipath error is heavily influenced by surrounding objects near the receiver, causing the signal to reflect. It's important to note that differential GNSS methods cannot mitigate multipath errors, as these errors are influenced by the local reflection geometry around the receiver antenna. Receivers lacking the ability to compensate for multipath errors, such as those using C/A-code ranging, may experience errors of up to 10 meters [24].

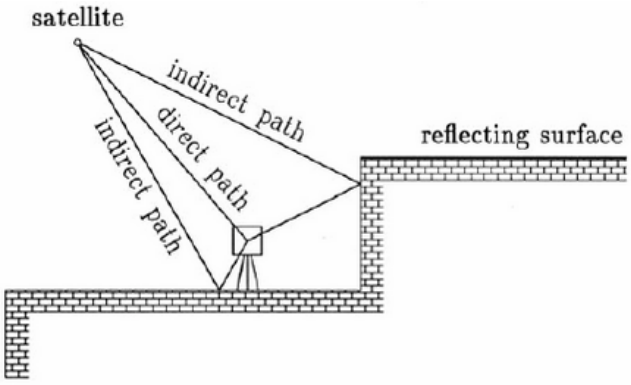

Figure 2.4: Multipath effect [9]

Multipath propagation error can be categorized into two types, static and dynamic. In stationary receivers, changes in signal propagation occur gradually relative to the movements of satellites in orbit, resulting in relatively constant multipath error parameters during certain observation times. Conversely, in dynamic receivers such as mobile phones, there can be larger and more rapid variations in multipath errors over short periods of time [24]. Multipath effects can be assessed by utilizing dual-frequency combinations of L1 and L2 in code pseudorange and carrier phase measurements. This approach relies on the effects of the troposphere, clock errors, and relativistic effects affecting both code pseudorange and carrier phase measurements to a similar extent [9]. Several methods can be applied to mitigate the multipath effect. The most effective technique is to select the antenna location carefully to minimize signal reflections from surfaces or surrounding objects. Another method, as mentioned previously, is to use a ground plane antenna design. Additionally, high directive antenna arrays can be employed to mitigate specific errors by providing high gain towards the direct signal path and attenuation in paths of indirect signals. Furthermore, more practical approaches, known as time-domain processing, are commonly integrated into receivers, especially those used for high-precision measurements. However, since the majority of practical techniques are developed by receiver manufacturers, they are often hesitant to disclose these techniques in detail [24].

Furthermore, the phase ambiguity parameter is also a complex error to compensate for. This error specifically affects the carrier phase measurement technique. The presence of multipath constrains the measurement performance in precision applications, particularly as it affects carrier phase ambiguity resolution [24]. Carrier phase ambiguity is a time-independent parameter as it only correlates to continuous satellite tracking by the receiver. As long as tracking remains uninterrupted, the phase ambiguity resolution remains unaffected. This ambiguity is defined as an integer value of the wavelength, meaning it depends on the frequency of the GNSS signals. Calculating these integer values is challenging due to various factors that can affect this error parameter and make it ambiguous. Additionally, a processing technique known as double-differences can be used to mitigate phase ambiguity, although there is no guarantee of complete error mitigation. Through the double-differences process, the clock error parameter is removed from the measurement

data, potentially isolating the ambiguities of the signal [9]. The amount of error due to the phase ambiguity generates from the integer value of wavelength, in GPS L1 for instance, varies at least from 19 cm.

2.6.4 Carrier Phase Wind-up

In principle, a GNSS signal can be illustrated as an electromagnetic wave with the rotation of the electrical field propagating from the satellite in space to the ground receiver. Ideally, the angle of the observed carrier phase at the receiver antenna corresponds to the geometric angle projected by the reference direction of the antenna and the arriving electric field. However, altering the orientation of the antenna influences the reference direction, consequently affecting the phase measurement. Additionally, changes in the orientation of the antenna affect the direction of the electric field. This phenomenon is referred to as carrier phase wind-up or phase wrap-up. It should be noted that the term applies to antennas on both sides, the satellite antenna, and the ground receiver antenna [25]. A complete cycle rotation phase of received and transmitted signal from satellite or receiver antenna along its boresight results a carrier phase measurement shift by one cycle across all frequency bands of the satellite. In GPS system, for instance, this leads to an approximate range error of 19 cm and 25 cm for the frequency of L1 and L5, respectively [26].

Considering the carrier phase wind-up effect characterizes to be orientation-dependent, the error can be estimated and modeled with respect to vector position parameters of both satellite antenna and receiver antenna. Figure 2.5 illustrates the phenomenon of carrier phase wind-up.

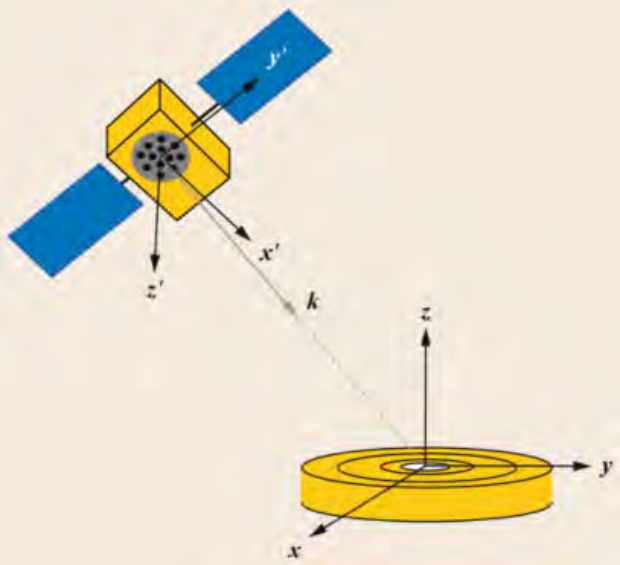

Figure 2.5: Carrier phase wind-up [26]

Initially, an effective dipole vector of both satellite and receiver antenna need to characterized. Equation 2.16 and Equation 2.17 formulate the effective dipole vector of the antennas.

$$D = x - k(k \cdot x) + k \times y \tag{2.16}$$

$$D^{'} = x^{'} - k(k \cdot x^{'}) - k \times y^{'} \tag{2.17}$$

where k is assumed as a unit vector directed from satellite transmitter to the ground receiver. D and $D^{'}$ denotes the effective dipole vector of the receiver and antenna, respectively. Here, x and y correspond to the unit vector of receiving antenna, while $x^{'}$ and $y^{'}$ are the unit vector for transmitting antenna. Thus, the phase wind-up (ω) parameter can be modeled in the following Equation 2.18.

$$\omega = sign(\gamma) \arccos\left(\frac{D^{'} \cdot D}{||D'|| \cdot ||D||}\right) \tag{2.18}$$

where γ can be defined as

$$\gamma = k \cdot (D^{'} \times D) \tag{2.19}$$

Furthermore, phase wind-up errors originating from the transmitting antennas are varied for each satellite, implying such model estimation needs to be conducted in the dependency of every observed satellites [26].

2.7 Coordinate Reference System

To ensure the precision of GNSS positioning measurements, a well-defined reference system for both the coordinate position of the satellite and the receiver needs to be established. Coordinate reference systems are utilized for positioning measurements since the satellite and receiver are on different segments (space and ground). In GNSS applications, the reference system can be defined in two different references, i.e., the Celestial Reference System (CRS) and the Terrestrial Reference System (TRS) [27].

The Celestial Reference System (CRS) primarily utilizes the center of mass of the Earth as the reference origin. The practical application of this reference concept is referred to as the Celestial Reference Frame (CRF), which is established and commonly used to define the coordinates of extra-galactic radio sources. On the other hand, the Terrestrial Reference System (TRS) rotates together with the Earth's daily rotation, and this concept is also known as Earth-Centered, Earth-Fixed (ECEF). It comprises a model of the Earth's characteristics as a physical object, where coordinate points are described and exhibit minor influences due to the geophysical factors of the Earth, such as earth tides or tectonic plate movements. The implementation of this framework is referred to as the Terrestrial Reference Frame (TRF), established by utilizing particular Earth coordinates as reference points [27].

GNSS applications primarily utilize the TRS concept to describe the position of

satellites and receivers. However, the TRS concept can be defined in several different reference system characteristics, generally depending on the satellite navigation systems. For instance, GPS utilizes its own TRS known as WGS84, while GLONASS uses PZ-90. Therefore, it is crucial to take these discrepancies in reference system characteristics into account and correct them to ensure precise measurements, especially when multiple satellite navigation systems are involved [28].

2.7.1 Helmert Transformation

As mentioned earlier, discrepancies exist between different concepts of TRS/TRF, leading to inaccuracies in measurements, especially in high-precision applications such as geodetic surveying. Due to the different reference systems used by various GNSS systems, an International Terrestrial Reference Frame (ITRF) has been established to provide a universal reference for all these systems.

However, to accurately process the transformations between these reference frame systems, a robust algorithm is required. The Helmert transformation method can be utilized for this purpose. The Helmert transformation involves two 3D coordinate systems characterized by differences in their origins, axes, and scale. This method allows for the accurate transformation and estimation of stable coordinate information between two different references [29]. These can be represented by seven parameters, i.e., three translations of the coordinate (t_x, t_y, t_z) along the axes, three rotation angles (r_x, r_y, r_z) between the axes, and scale factor $(1 + k)$. Helmert parameters of coordinate reference transformation can be seen in Figure 2.6.

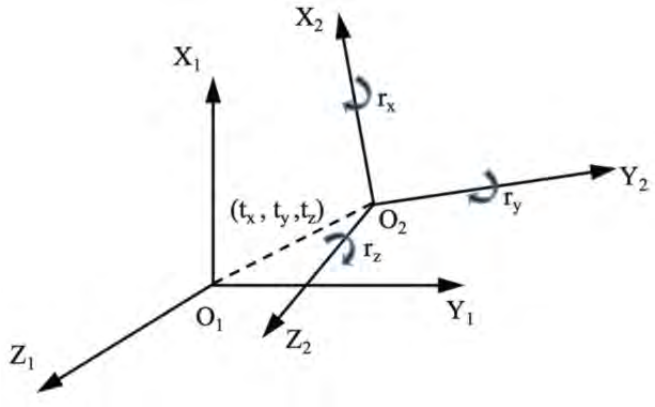

Figure 2.6: Helmert transformation parameters [29]

The seven Helmert parameters are modeled by utilizing two common known coordinates in both different reference systems. Equation 2.20 defines the Helmert transformation model.

$$\begin{bmatrix} X_2^i \\ Y_2^i \\ Z_2^i \end{bmatrix} = (1+k) \begin{bmatrix} 1 & r_z & -r_y \\ -r_z & 1 & r_x \\ r_y & -r_x & 1 \end{bmatrix} \begin{bmatrix} X_1^i \\ Y_1^i \\ Z_1^i \end{bmatrix} + \begin{bmatrix} t_x \\ t_y \\ t_z \end{bmatrix} \tag{2.20}$$

where (X_1, Y_1, Z_1) and (X_2, Y_2, Z_2) are the common known coordinates position in

the reference system-1 and reference system-2, respectively, and i represents a common point. It should be noted that in order to compute the seven Helmert parameters, it requires at least three common known positions in both reference systems. Equation 2.20 can then be reformed as follow,

$$\begin{bmatrix} X_2^i - X_1^i \\ Y_2^i - Y_1^i \\ Z_2^i - Z_1^i \end{bmatrix} = \begin{bmatrix} 1 & 0 & 0 & 0 & -Z_1^i & Y_1^i & X_1^i \\ 0 & 1 & 0 & Z_1^i & 0 & -X_1^i & Y_1^i \\ 0 & 0 & 1 & -Y_1^i & X_1^i & 0 & Z_1^i \end{bmatrix} \begin{bmatrix} t_x \\ t_y \\ t_z \\ r_x \\ r_y \\ r_z \\ k \end{bmatrix} \tag{2.21}$$

It is seen that the Equation 2.21 can be treated in terms of Least-Square estimation formula. The general model of Least-Square estimation is defined in Equation 2.22.

$$\bar{L} = \bar{A}X \tag{2.22}$$

where $\bar{L}$ usually is a vector matrix observation, $\bar{A}$ is a matrix design, and X is the estimated values. In this case, the matrix observation, matrix design, and estimated values are formed in Equation 2.23, 2.24, 2.25, respectively.

$$\bar{L} = \begin{bmatrix} X_2^i - X_1^i \\ Y_2^i - Y_1^i \\ Z_2^i - Z_1^i \end{bmatrix} \tag{2.23}$$

$$\bar{A} = \begin{bmatrix} 1 & 0 & 0 & 0 & -Z_1^i & Y_1^i & X_1^i \\ 0 & 1 & 0 & Z_1^i & 0 & -X_1^i & Y_1^i \\ 0 & 0 & 1 & -Y_1^i & X_1^i & 0 & Z_1^i \end{bmatrix} \tag{2.24}$$

$$X = \begin{bmatrix} t_x \\ t_y \\ t_z \\ r_x \\ r_y \\ r_z \\ k \end{bmatrix} \tag{2.25}$$

Thus, the seven Helmert parameters of X in Equation 2.21 can be derived by employing Least-Square estimation, as formulated in Equation 2.26.

$$X = (\bar{A}^T\bar{A})^{-1}(\bar{A}^T\bar{L}) \tag{2.26}$$

The estimated values of seven Helmert parameters corresponding to X then can be applied in Equation 2.20 to calculate the position coordinates transformation of reference system-1 into reference system-2 [29].

2.8 Data Processing

In the previous sections, it was noted that GNSS signals are highly influenced by various types of errors during measurement. While methods like dual-frequency measurement can mitigate some of these errors by generating ionospheric-free signals, certain applications require even greater precision, reliability, and continuous observation. To achieve this, specific techniques can be employed to process GNSS data signals, aiming for greater accuracy. These techniques include Differential GNSS (DGNSS) and Precise Point Positioning (PPP) [2]. The following subsections elaborate the two fundamental concept of DGNSS and PPP processing methods.

2.8.1 Differential GNSS (DGNSS)

The fundamental principle of Differential GNSS (DGNSS) involves the use of one or more reference receivers at predetermined locations. These receivers broadcast error estimations of GNSS satellite measurements to user receivers, allowing them to subtract these errors from their own signal measurements. Essentially, the DGNSS method aims to mitigate nearly all spatially correlated errors caused by various parameters, including inaccuracies in satellite clock and ephemeris data, as well as ionospheric and tropospheric delays [3].

It is important to note that the correlation of GNSS signal errors tends to be higher over shorter distances. As a result, applying the Differential GNSS (DGNSS) processing technique often yields greater improvements when the reference stations are placed close to the end user. DGNSS processing generates error estimations that can be utilized for the raw data measurements of the end user or for every visible satellite and its navigation messages. Furthermore, the DGNSS technique is fundamentally categorized into two applications, absolute differential and relative differential. In the absolute differential application, the position of reference station(s) must be accurately known or predetermined in the same coordinate system as the user receiver, such as the Earth-Centered, Earth-Fixed (ECEF) reference. Therefore, the reference station(s) ideally remain stationary to provide error estimations for end users. On the other hand, relative differential involves determining the position of the user relative to the desired coordinate system of the reference station(s), where in this case, the absolute position of reference station(s) may not be precisely predetermined [2].

Furthermore, DGNSS can be utilized for both code pseudorange and carrier phase measurements to achieve greater accuracies. Typical code pseudorange calculations result in errors of approximately 3–5 meters, while applying the DGNSS method for these determinations can lower the errors to approximately 0.5–1.0 meters. However, it is worth noting that carrier phase measurements produce much higher accuracy results than code pseudorange. Therefore, for applications requiring high precision levels such as surveying, code pseudorange DGNSS is considered insufficient [3]. Code-based DGNSS can deliver accuracy up to the decimeter level, while differential carrier phase processing can achieve performance at the millimeter-level accuracy [2].

The DGNSS technique can be principally characterized into three different approaches, i.e., single difference, double difference, and triple difference. The fundamental concept of single difference involves simultaneous carrier phase measurements from the same visible satellite by two distinct receivers. Observing a single satellite from two receivers enables the complete elimination of the satellite clock error by computing the difference at any epoch observation. Single difference is ideally used when the baseline between two receivers is relatively small [8]. The single difference concept is illustrated in the following Figure 2.7.

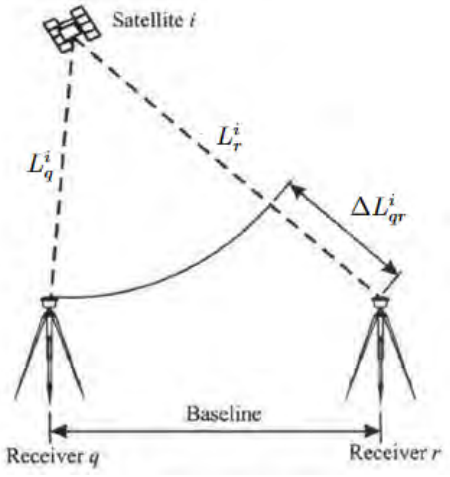

Figure 2.7: Single difference method

A single satellite observation from two difference receivers can be defined as follow,

$$L_q^i(t) = \rho_q^i(t) + c\tau_q - c\tau^i + Z_q^i - I_q^i + B_q^i \tag{2.27}$$

$$L_r^i(t) = \rho_r^i(t) + c\tau_r - c\tau^i + Z_r^i - I_r^i + B_r^i \tag{2.28}$$

Utilizing the single difference method to Equation 2.27 and Equation 2.28 by differentiating two difference receivers for a single satellite signal, the satellite orbital and clock errors (τ^i) can be eliminated. This process is defined in Equation 2.29 and 2.30.

$$\Delta L_{qr}^i = L_q^i - L_r^i \tag{2.29}$$

$$\Delta L_{qr}^i = \Delta_{qr}^i + c\Delta\tau_{qr} + \Delta Z_{qr}^i - \Delta I_{qr}^i + \Delta B_{qr}^i \tag{2.30}$$

Errors influenced by atmospheric properties, tropospheric error (ΔZ_{qr}^i) and ionospheric error (ΔI_{qr}^i), can be compensated by placing the two receivers close to each other [8]. This implies that the receivers may highly experience similar atmospheric properties, which can be almost completely cancelled out during the differential process.

Furthermore, the double difference method can principally be defined as two single differences for two satellite observations at the same epoch. Figure 2.8 illustrates the

concept of double difference. By utilizing such method, it enables the elimination of both receiver clock errors (τ_q and τ_r) since the differences are computed at the same epoch for both satellite observations [8].

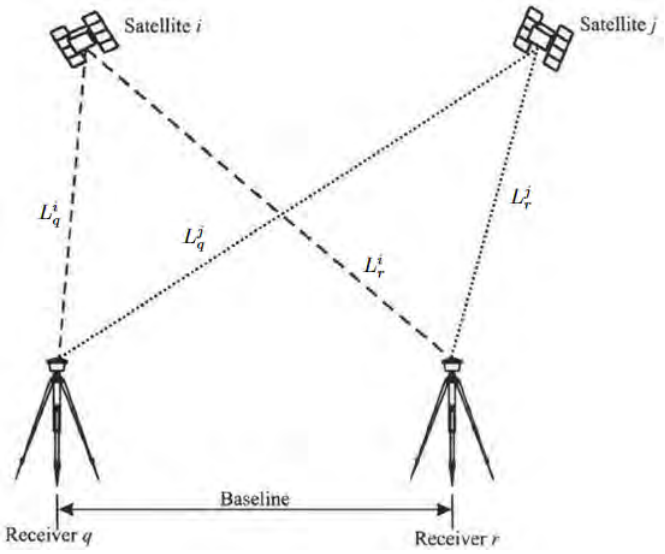

Figure 2.8: Double difference method

The double difference can be formulated in the following Equation 2.31 and 2.32.

$$\Delta\nabla L_{qr}^{ij} = \Delta L_{qr}^{i} - \Delta L_{qr}^{j} \tag{2.31}$$

$$\Delta\nabla L_{qr}^{ij} = \Delta\nabla\rho_{qr}^{ij} + \Delta\nabla Z_{qr}^{ij} - \Delta\nabla I_{qr}^{ij} + \Delta\nabla B_{qr}^{ij} \tag{2.32}$$

It can be seen in Equation 2.32 that the clock errors for both receivers (τ_r and τ_q) are eliminated as a receiver takes simultaneous measurements of two satellites, making the receiver clock error to be constant for both satellites which leads to differential result of zero. Previously, it is noted by placing the two receivers in a close proximity can be used to encounter atmospheric errors (I and Z). However, both single difference and double difference methods are not able to solve the carrier phase ambiguities (B_{qr}^{ij}). Moreover, it should also be noted that double difference method may generate more receiver noise by a factor of two for every difference operation, making it as a drawback and need to be compensated carefully [8].

In addition, triple difference method can be utilized to compensate the carrier phase ambiguities. Almost in similar principle as other difference methods, this can be accomplished by doing differential operation of two double differences at two consecutive epochs of observation. The triple difference method is illustrated in Figure 2.9.

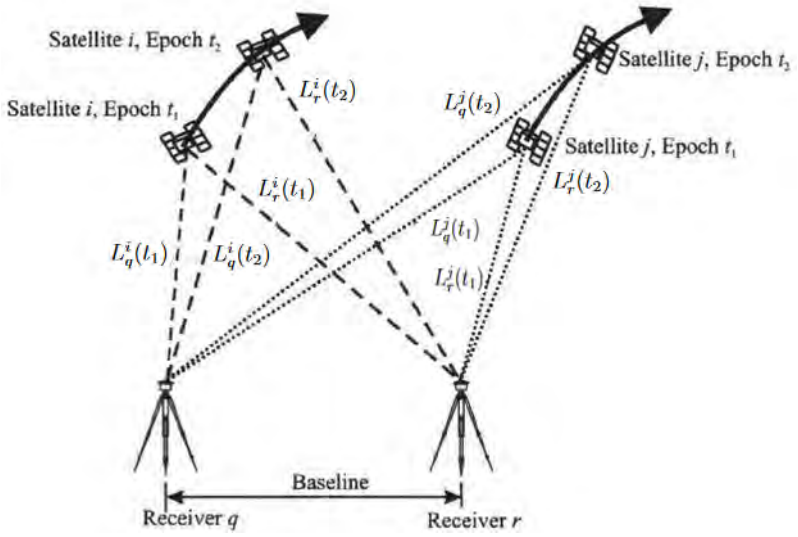

Figure 2.9: Triple difference method

The triple difference method mathematically can be formulated in the following Equation 2.33. This model utilizes two consecutive epochs (t_1 and t_2) for both two similar satellites to analyze the integer phase ambiguity (N), which then be used to cancel out the carrier phase ambiguities in both receivers. This method can be utilized considering that the integer phase ambiguity (N) fundamentally remains constant on the two consecutive epoch observations.

$$\Delta\nabla\varphi_{qr}^{ij}(t_1,t_2) = \Delta\nabla\varphi_{qr}^{ij}(t_1) - \Delta\nabla\varphi_{qr}^{ij}(t_2) \tag{2.33}$$

However, in practical, it is noted that triple difference lacks sufficient accuracy to solve the carrier phase ambiguities. Moreover, it is more ideal to estimate the integer phase ambiguity using particular techniques separately, then apply either single or double difference method for data processing [8]. One of the examples of GNSS processing software, Bernese, utilizes DGNSS principle is briefly discussed in the following section [30].

2.8.1.1 Bernese GNSS Software

Bernese is a high-precision positioning and timing determination software developed by the Astronomical Institute of the University of Bern (AIUB). It has features of processing multi-GNSS satellite systems, such as GPS and GLONASS, as well as one of the processing technique utilizing DGNSS principle. Fundamentally, the initial process in Bernese consists of seven main stages.

- **RNXSMT:** this initial process involves of detecting the cycle slips and poor observations in RINEX data by processing both code pseudorange and phase observations for all satellites.
- **CODSPP:** by utilizing the code pseudorange data observations, the receiver clock errors can be estimated and synchronized to the actual time reference, e.g., GPS time.

- **SNDGIF:** the previous process resulting such data referred as zero-difference results from each receiver. The so-called zero-difference results can be used to to do another baseline-based differential process, which the output is single difference observation data.
- **MAUPRP:** another cycle slips detection process is done to estimate multiple ambiguities for the phase observations for the single difference data.
- **RESRMS:** this step involves screening and producing the residuals for outliers data detection.
- **RESCHK:** such anomalies during the observations in both stations and antenna are identified in this process by examining the summary results from previous step.
- **SATMRK:** the final step is to mark particular observations from RESRNS that are recognized as outliers data.

Moreover, these initial processes and results can be used for further positioning determination by utilizing another processing technique such as double difference, since through these stages it is only single difference method applied [30].

2.8.2 Precise Point Positioning (PPP)

Unlike the DGNSS technique, the Precise Point Positioning (PPP) method does not primarily rely on differential operation. This processing method for position determinations does not require station reference(s) because only a single receiver is needed. Hence, PPP is considered non-differential since the user receives the satellite clock and ephemeris data directly estimated by a ground network. These estimations replace the broadcast information from individual satellites [2].

In principle, the PPP technique operates under the assumption that global satellite orbits and clocks are treated as strongly constrained. Additionally, the mathematical models employed in the PPP method are aligned with global network solutions, from which the estimations of orbits and clocks are derived. To ensure consistency between the global data of orbits and clocks and the PPP solutions, they should be aligned using similar reference system standards, such as IERS (International Earth Rotation and Reference Systems) [31]. The fundamental principle of PPP is to utilize dual-frequency of code pseudorange or carrier phase observations to produce the so-called ionospheric-free signals [2], as previously mentioned in Section 2.6.1.1.

On its initial procedure, PPP necessitates the estimation of phase ambiguities for all satellites since the carrier phase measurement is utilized, which therefore is used for the determinations. Despite only a single station receiver is required in PPP method, the calculation of the observed satellite orbits and clocks essentially relies on utilizing the global network. The final result of PPP model consists of several parameters, i.e., station positions (X, Y, Z), receiver clock estimations (τ), zenith tropospheric delay (ZTD), and carrier phase ambiguities (B). These final result parameters are aligned with global reference system, indicated by its consistency with the global GNSS orbit and clock solutions [31]. One of the GNSS software utilizing

PPP method is known as GipsyX, which is briefly explained in the following section.

2.8.2.1 GipsyX

The GipsyX software is developed by the NASA Jet Propulsion Laboratory (JPL) for positioning, navigation, timing, and Earth science applications. The software is able to utilize three different geodetic measurements, i.e., GNSS (Global Navigation Satellite Systems), SLR (Satellite Laser Ranging), and DORIS (Doppler Orbitography and Radiopositioning Integrated by Satellite). The main principle of GipsyX utilizes Kalman filter methodology to estimate such final parameters data for both real-time or post-processing observations. These final estimated parameters encompass station coordinates and velocities, satellite orbits and clocks, orientation of the Earth, as well as inospheric and tropospheric delays [32].

GipsyX is the newer version of GIPSY-OASIS and Real Time GIPSY (RTG) combined featuring more functions and capabilities, while still utilizing the same fundamental concept. In basic principle, GipsyX involves two different parts of determination, or can be referred as the computed and the observed determinations. The observed determination ($P_{observed}$) is computed directly by utilizing the desired data observations from receiver station. On the other hand, the computed determination ($P_{computed}$) utilizes the global network, which can be calculated by utilizing the precise satellite orbits and clocks provided by the International GNSS Services (IGS) [33].

The computed ($P_{computed}$) data results are treated as the initial guesses by modeling the the precise errors of geophysical properties, receiver station and antenna details to compute the distance between the satellites and the ground receiver. Moreover, the observed ($P_{observed}$) data is determined by utilizing the dual-frequency method directly to the desired observations data from receiver to form the ionospheric-free signals model for code pseudorange (P_3) or carrier phase (L_3) measurements [33]. The ionospheric model can be formed by employing two different frequency observations into the Equation 2.15 (as previously mentioned in Section 2.6.1.1).

Taking an example of dual-frequency in GPS system, the ionspheric-free model of L3 and P3 are formed in the following Equation 2.34 and 2.35.

$$L3 = 2.546L1 - 1.546L2 \tag{2.34}$$

$$P3 = 2.546P1 - 1.546P2 \tag{2.35}$$

where L1 and L2 are the measured carrier phase, as well as P1 and P2 are the code pseudorange data, while in this case observed by f_1 (1575.42 MHz) and f_2 (1227.60 MHz). A brief process of GipsyX algorithm is illustrated in Figure 2.10.

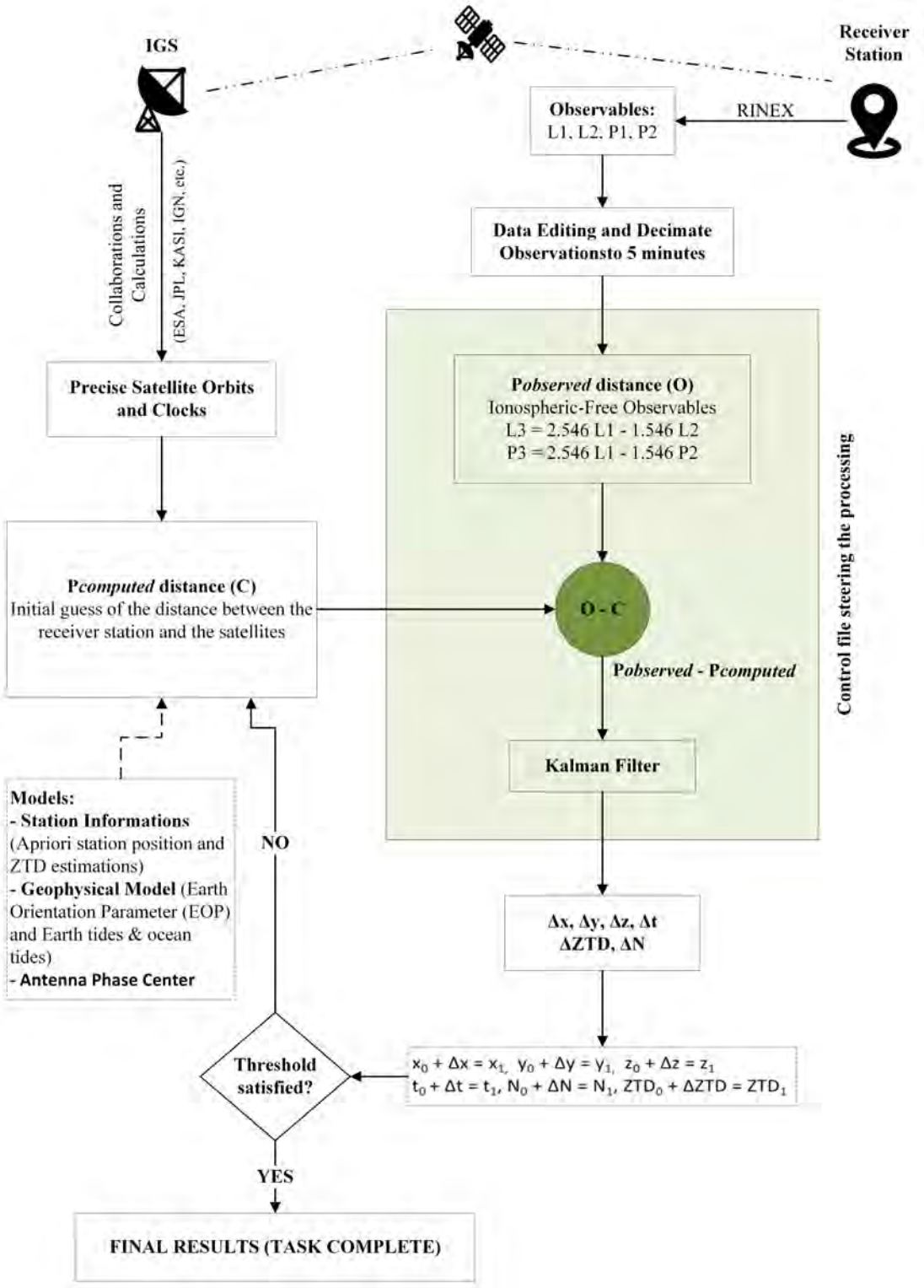

Figure 2.10: GipsyX algorithm process.

3
Methods

The accuracy of GNSS observations and measurements are significantly impacted by a variety of error sources, as previously discussed in Section 2.6. Therefore, it is crucial to take all error sources into account during the observation measurements, as well as post-processing. Although there are multiple GNSS constellations available for observation and measurement, only GPS satellite signals were utilized in this project.

The project involves several procedures during its implementation and experiment. This section elaborates mainly the details of the experiment setup, desired approaches to conduct and process the measurements, error source compensations, assessments and validations of the results, as well as its reasoning.

3.1 Antenna Station Setup

The experiment was conducted at the Onsala Space Observatory (OSO). Multiple coordinate points, particularly those near the 20 m telescope, were utilized for GNSS observations and measurements. The project involved five different GNSS stations, one station (ONSA) contributed to the IGS global network, while the remaining stations were part of the local GNSS network. All stations were placed within a total area of approximately 75 m.

The chosen positions were selected based on their long-standing establishment, particularly ONSA, which has been part of the global IGS network for decades. As a result, there are already finalized positional data available from previous experiments or research, which can be utilized for further validation in this study. The experiment involved five different stations: ONSA, A302, B303, C304, and D501.

Figure 3.1 illustrates the observation setup map of all five stations. Green marker of the station indicates as part of the global IGS network, while blue marker represents the local network.

Figure 3.1: Observation setup map of the stations

In an ideal experiment, it is preferable to use similar types of antennas and receivers for observations. Different types of receivers or antennas can influence the observed data due to varying specifications and behavioral characteristics. In this project, all five stations used the same type of antenna from Leica Geosystem AG. However, two different types of receivers were utilized due to unavailability of one particular receiver type in the inventory.

The main objective of the project is to implement a new observation method by tilting the antennas at a few degrees. Notably, only the four antennas (A302, B303, C304, and D501) of the local network were tilted in specific directions for the experiment, while ONSA remained in its original position as part of the global network. The purpose of tilting the antennas is to introduce geometric constraints that affect the position determinations. These geometric constraints, resulting from the tilted antennas, are then utilized to investigate the phase-center calibration corrections of each antenna, as previously mentioned in Section 1. Table 3.1 summarizes the detail setup specification of the desired antenna stations.

Table 3.1: List of stations specification and setup

Station	Antenna Type	Receiver Type	Tilt Direction	Tilt (°)
ONSA	AR20 (with radome)	Septentrio	-	-
A302	AR20	Septentrio	South	9.5237
B303	AR20	Trimble	West	10.2846
C304	AR20	Septentrio	East	9.4903
D501	AR20	Trimble	North	9.6391

It is noted that the initial idea was to tilt the four antenna stations in 10° in four different directions measured using Leica DISTO 501 range finder with embedded 360° tilt sensor. However, a more precise of distance and position determination was

conducted by utilizing laser tracker measurement. This laser tracker measurement is considered to have higher accuracy including able to project such object orientation in a ground plane, particularly in this case the antennas due to the tilting.

3.2 Antenna Station Calibrations

The desired antenna stations required calibration to characterize their phase-center behaviors, particularly to determine the phase-center offset (PCO) and phase-center variation (PCV). Therefore, four antennas (A302, B303, C304, and D501) were sent to Geo++ GmbH in Germany to undergo absolute robot calibration. However, station ONSA was not calibrated as it has been actively operating as part of the global network for years and could not be deactivated for calibration.

Table 3.2: Antenna station calibrations

Station	Antenna Type	Calibration Type	Date of Calibration
ONSA	AR20 (with radome)	-	-
A302	AR20	Robot (absolute)	2021-02-06
B303	AR20	Robot (absolute)	2021-02-02
C304	AR20	Robot (absolute)	2021-02-04
D501	AR20	Robot (absolute)	2021-04-28

The phase-center offset (PCO) and phase-center variation (PCV) for the four different antenna stations, obtained from Geo++ GmbH, are then used to compensate for errors during position determinations. Additionally, they are utilized to investigate the errors associated with antenna phase-center caused by geometric constraints due to the tilted antenna positions.

3.3 GNSS Observations and Laser Tracker Measurements

In this study experiment, carrier phase measurements are primarily utilized for station observations and position determinations, considering they produce more precise measurement results than the code pseudorange. The GNSS signal measurements during this project were initially conducted over a period of 41 days, from 2023-03-18 to 2023-04-27. Unfortunately, due to unknown reasons, only 11 days of observation data could be retrieved. Thus, this project only processed and assessed the GNSS signals from 2023-03-17 to 2023-03-27.

In principle, all the selected receiver types are highly capable of tracking and observing multiple GNSS constellations, including GPS, GLONASS, Galileo, BeiDou, and SBAS (Satellite-based Augmentation Systems). However, due to time constraints, only GPS signals were utilized from all five receiver stations in this project.

3.3.1 External Measurement Reference

An external measurement is required to serve as a reference for result validation. In this project, laser tracker measurement is utilized as the reference due to its high accuracy. Since the project focuses on positioning determinations using GNSS data signals, the laser tracker is used to measure and determine the positions of four antenna stations (A302, B303, C304, and D501). Therefore, the measured data from the laser tracker serve as reference results for the positions calculated from GNSS signals.

In principle, tracker measurements involve tracking a small object, typically shaped like a ball or stick, as it moves, provided there is a clear line of sight with no visible obstacles. Therefore, the tracker is positioned in a location that ideally offers a clear line of sight to track the object on the antennas in the observation setup using laser-based measurements.

Figure 3.2: Laser tracker measurement

Figure 3.3: Small object of the tracker measurement on antenna

3.4 Data Processing Strategies

There are multiple processing techniques can be utilized for GNSS positioning determination, as previously elaborated in Section 2.8. In the initial plan of this project, DGNSS method particularly single difference principle was utilized to process the signal data, following the same processing technique was conducted in previous research [1]. The single differece processing was conducted by utilizing the Bernese GNSS software. However, another type of data processing, PPP (Precise Point Positioning), was also used during the project. Using GipsyX software to utilize PPP principle as an alternative option to analyze the data since the Bernese software has considerably more complex process and configuration.

Therefore, the project produced two different type of results, i.e., the single difference from Bernese and PPP from GipsyX. These final solutions consisting all station positions are analyzed in terms of the baselines between each station. The detail of the results from both different methods are presented and analyzed in the following section.

4

Results and Discussion

This section presents and discusses the overall results of the project. Initially, the intention was to employ the single difference technique to process and evaluate the satellite signals and determine the final position of all receiver stations. However, due to the complexity of the Bernese software program, the results obtained from the single difference method were not as optimal as expected. Additionally, a custom GNSS signal processing approach using the single difference method was developed using Matlab, but the results were generally even worse than those obtained with Bernese. Ideally, the single difference method should have been used for the processing technique and assessments, as conducted in previous research. However, due to the challenges encountered, the Precise Point Positioning (PPP) technique of GipsyX was utilized as an alternative to determine the station positions. These PPP results can also serve as a comparison to the results obtained from Bernese.

It is noted there is a lack of detail information on how the single difference method was implemented in the previous study [1]. Additionally, identifying the optimal approach to achieve high precise results posed a challenge due to the presence of unpredictable error sources that could highly influence the final outcomes.

The main assessments focus on the position determination of all receiver stations using both Bernese and GipsyX, the baseline length analysis resulting from GNSS signals and laser tracker measurements, and the residual results of the observations corresponding to errors in the phase-center antenna caused by tilting. The phase-center errors are analyzed with respect to the observed satellite elevations. Moreover, the received GNSS signal observations are processed with an elevation cut-off of 10° in the desired methods.

4.1 Examination of Antenna Calibration

Considering that the main project aims to investigate the antenna phase-center calibration error, the desired antennas were sent to Geo++ as the service provider to be calibrated for phase-center characterizations. As mentioned earlier, Geo++ characterized the antenna phase-center calibration, including the phase-center offset (PCO) and phase-center variation (PCV).

It is noted that only four antenna stations, namely A302, B303, C304, and D501, were characterized for phase-center calibrations. These antennas were calibrated using the absolute calibration method utilizing a robot. Although station ONSA was utilized in the project setup, it was impossible to calibrate the antenna station since it has been mounted in its location and operating for years. Taking the antenna off for calibration may influence its observation data as part of the IGS global network.

The phase-center correction is characterized with respect to elevation and azimuth angles. The absolute calibration conducted by Geo++ resulted in phase center errors for multiple satellite navigation systems based on their provided frequencies. These calibration results include GPS (L1, L2, and L5), GLONASS (R1, R2, R3, R4, and R6), BeiDou (B1, B2, B3, B5, B6, and B8), Galileo (E1, E5, and E6), etc. However, as previously mentioned, the project is only focused on assessing the GPS signals.

The characterized phase-center variation (PCV) correction for every four antenna stations are presented in the following figures in terms of polar plot coordinate corresponding to elevation (0-90°) angle and azimuth (0-360°) angle.

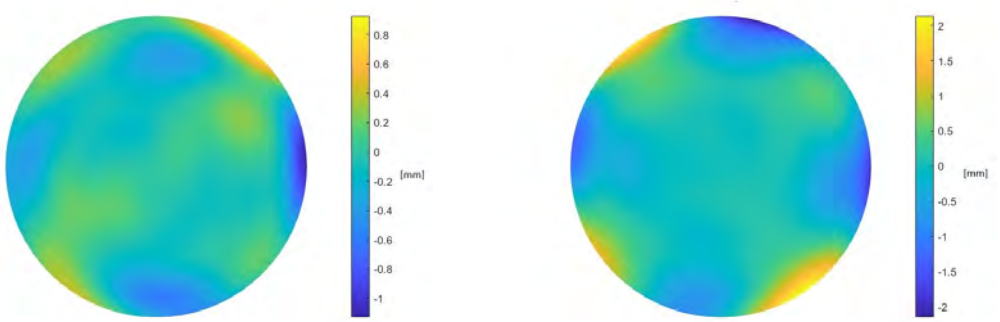

(a) L1 **(b)** L2

Figure 4.1: Station A302 antenna phase-center calibration

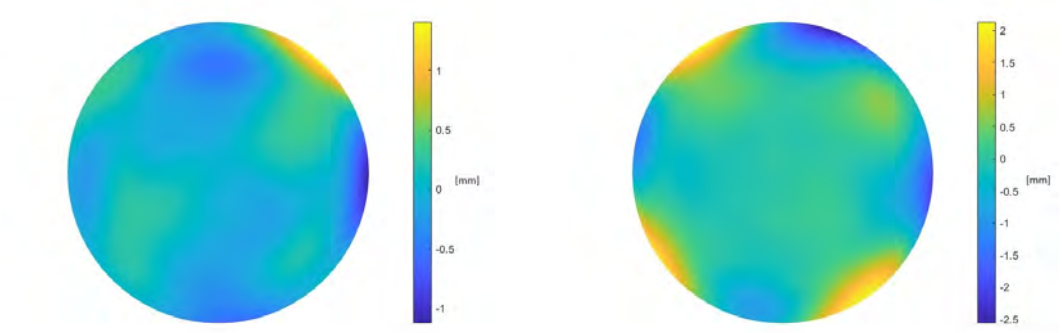

(a) L1 (b) L2

Figure 4.2: Station B303 antenna phase-center calibration

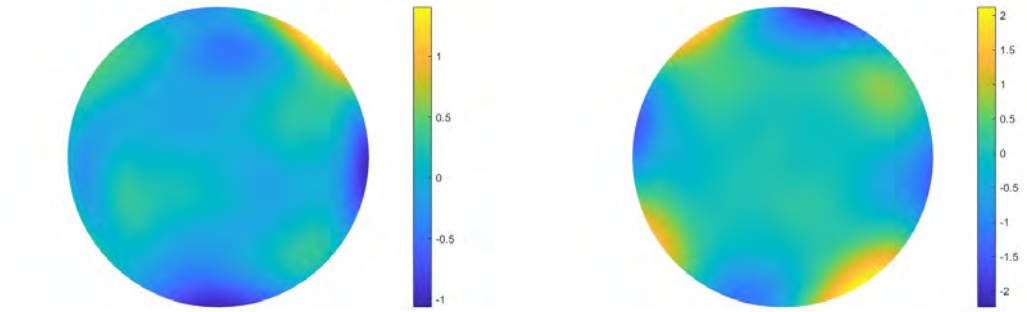

(a) L1 (b) L2

Figure 4.3: Station C304 antenna phase-center calibration

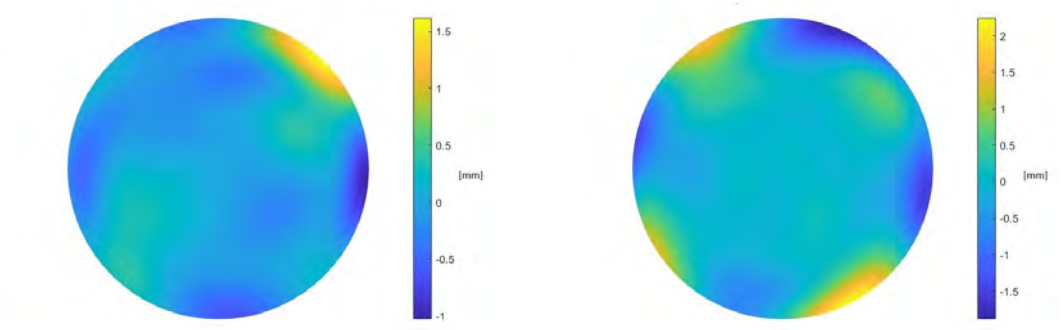

(a) L1 (b) L2

Figure 4.4: Station D501 antenna phase-center calibration

The PCV results are defined in millimeter unit and utilized as error corrections for the received carrier phase signals depending on satellite elevation and azimuth angles. The results in Figure 4.1-4.4 show only slight behaviour differences of characterized PCV between the four antennas. Although there are slight differences of PCV result between the antennas, the errors appear to be in the same magnitude order, particularly the PCV for L2 frequency.

High errors in the phase center likely occur at lower elevation angles, regardless of the position of azimuth angles. Lower elevation causes higher errors due to the longer signal path propagation and other error parameters such as multipath due to the surrounding environment of the receiver station.

In principle, higher-frequency satellite signals may experience a higher influence of errors during their signal propagation caused by atmospheric effects. In the case of antenna PCV, however, the PCV correction resulting from the absolute robot calibration shows that the lower frequency of L2 (1227.60 MHz) is influenced by a higher magnitude of error compared to the L1 frequency (1575.42 MHz). Thus, the PCV error from calibration is not solely defined by frequency dependence. Other parameters such as antenna design properties, along with the signal processing technique, also play crucial roles.

4.2 Determination of Station Positions

The following subsections elaborate on the final solutions of the desired receiver stations, calculated using two different methods of GNSS signal processing and software programs. Position results are determined by Bernese utilizing the single difference principle and by GipsyX using PPP. Furthermore, the final results of station positions are presented with respect to the frequency, as different methods are applied, utilizing different frequency processing.

4.2.1 Single Difference Result

The Bernese software offers to utilize DGNSS method of processing including the single difference and double difference, as previously described in Section 2.8.1.1. The following results of desired station position are processed only utilizing single difference method, as well as based on the L1 and L2 frequency separately. Employing the single difference processing method for the station determination is aligned with the initial aim from the previous research conducted [1].

The final solutions from Bernese's single difference method are provided in the local geodetic datum of IGS20, which is essentially an Earth-Centered, Earth-Fixed (ECEF) reference system. The position results are presented as time series data, reflecting observations conducted over 10 days. It is important to note that these final solutions are referenced to the antenna reference point (ARP). Figure 4.5-4.9 show the results of all the desired receiver stations.

It should be noted that the following station position results are presented in a particular scale in order to analyze the daily position changes much easier for all the five stations.

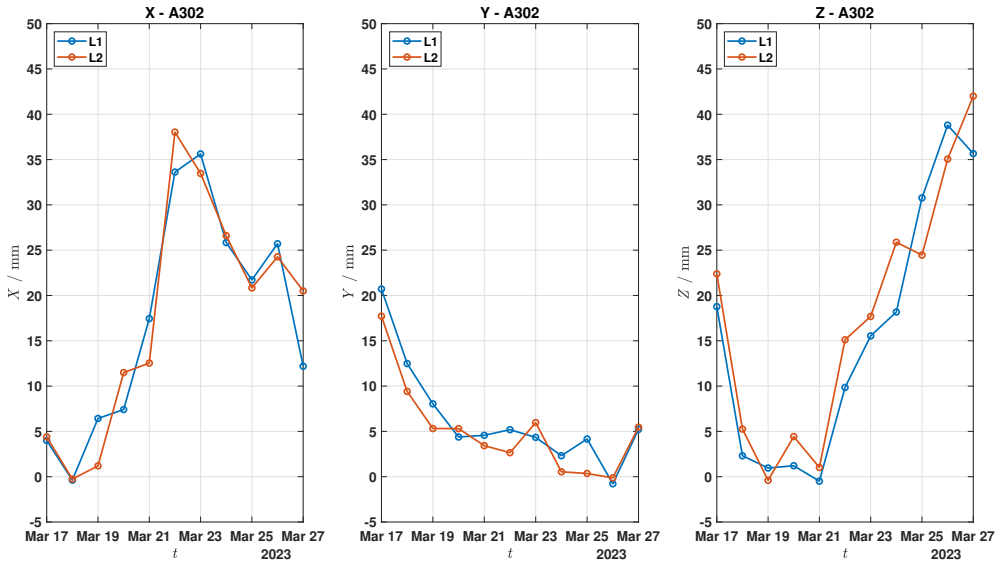

Figure 4.5: Bernese's A302 station position in ECEF coordinate system

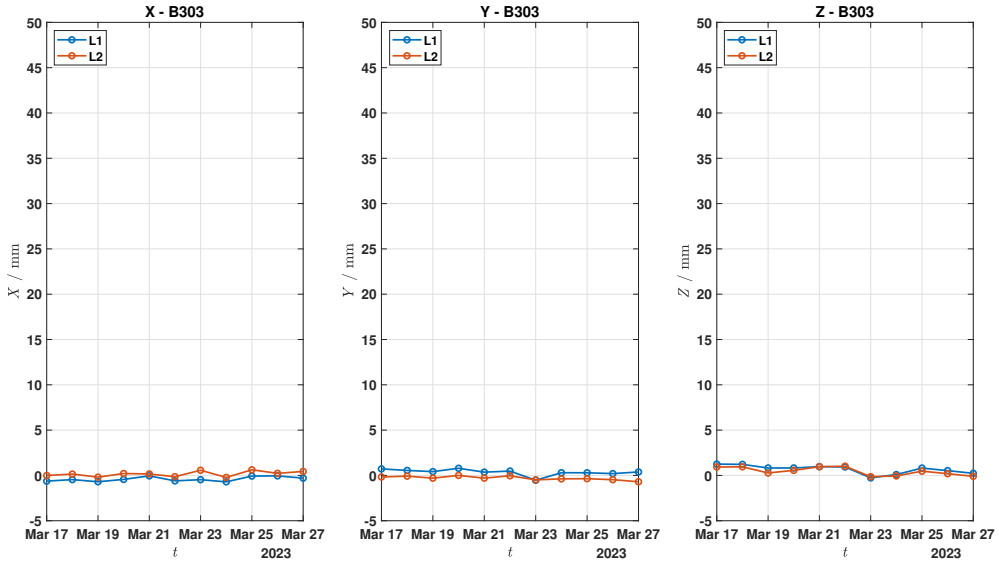

Figure 4.6: Bernese's B303 station position in ECEF coordinate system

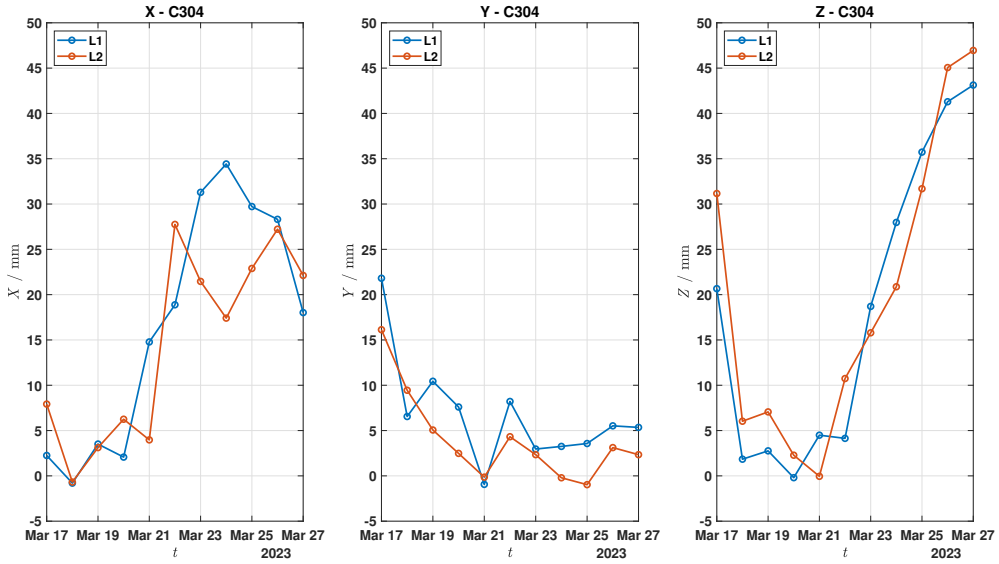

Figure 4.7: Bernese's C304 station position in ECEF coordinate system

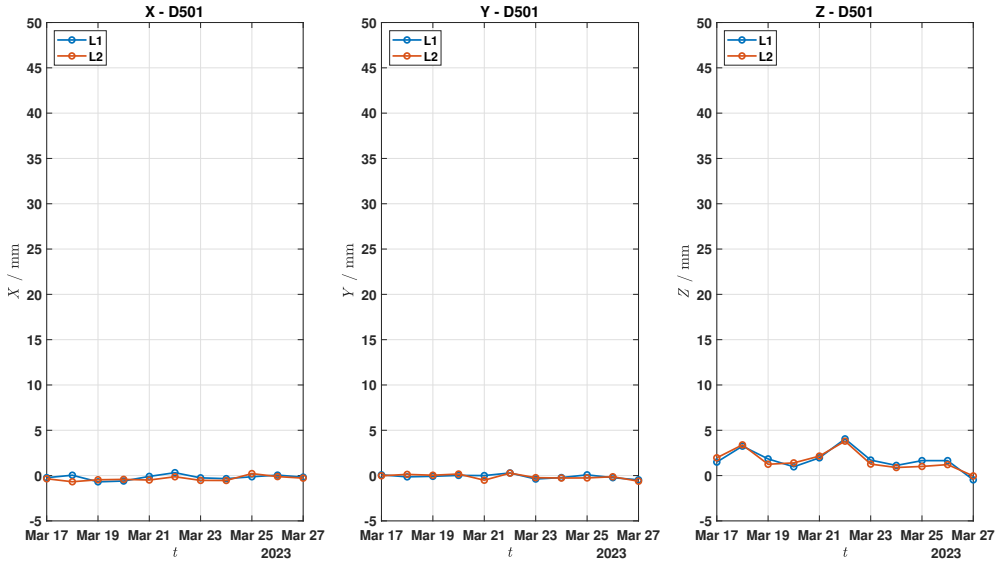

Figure 4.8: Bernese's D501 station position in ECEF coordinate system

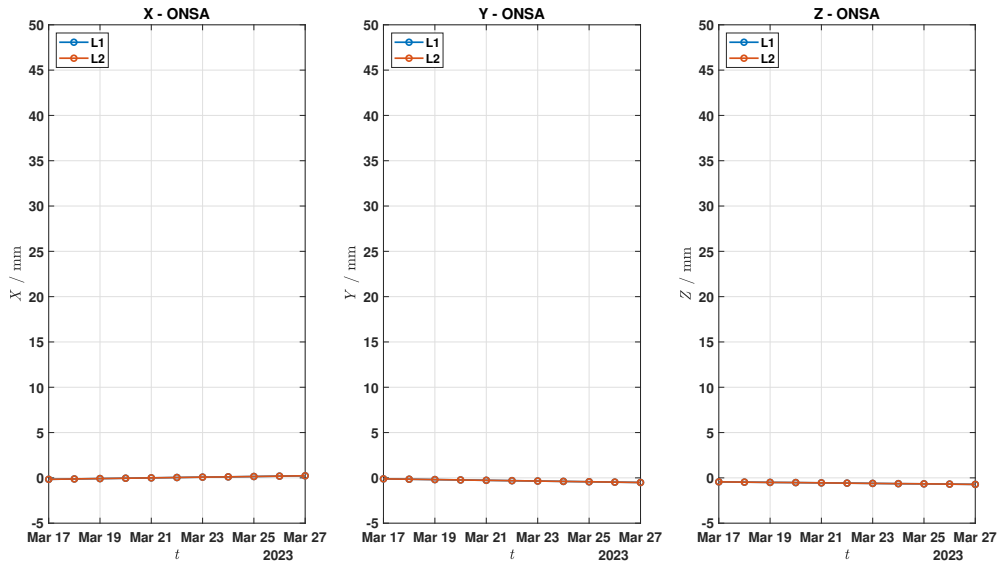

Figure 4.9: Bernese's ONSA station position in ECEF coordinate system

Given that the ONSA station is part of the IGS global network and unaffected by antenna tilting, it was made to be constrained during the Bernese processing. As a result, its final solutions between L1 and L2 frequencies are similar, as shown in Figure 4.9.

Furthermore, analyzing the day to day 3-axis positions (X-Y-Z) for all antenna stations, there are apparently two different behaviours in L1 and L2 frequencies position results. It appears there are unstable position results for both station A302 and C304, and is coincidence that both stations use the same type Septentrio receiver.

For station A302 in X-axis, for instance, both L1 and L2 results experience drastic daily changes for up to 1.6 cm and 2.5 cm, respectively. On the other hand in vertical position of Z-axis, such station also experiences changes for 1.6 cm in L1 and 1.7 cm in L2.

Moreover, in station D501, significant position changes also resulted in both X-axis and Z-axis. There is approximately position changes in X-axis for 1.2 cm in L1 and 2.3 cm in L2, as well as in Z-axis for 1.8 cm in L1 and 2.5 cm in L2.

4.2.2 PPP Result

In this case, the PPP method is employed in GipsyX processing to determine the station positions. GipsyX utilizes a frequency combination of L1 and L2 to generate the L3, also known as the ionospheric-free signal, as previously mentioned in Section 2.8.2.1.

Unlike Bernese, the final solutions computed using GipsyX are presented in terms

of latitude, longitude, and height coordinates. Therefore, specific calculations are needed to transform the geodetic coordinate system into ECEF. Figure 4.10-4.14 show the results of all the desired receiver stations computed using ionospheric-free signal of L3 frequency combinaiton in GipsyX. Similarly, the station position results are also presented in particular scale to make it easier for daily position changes analysis.

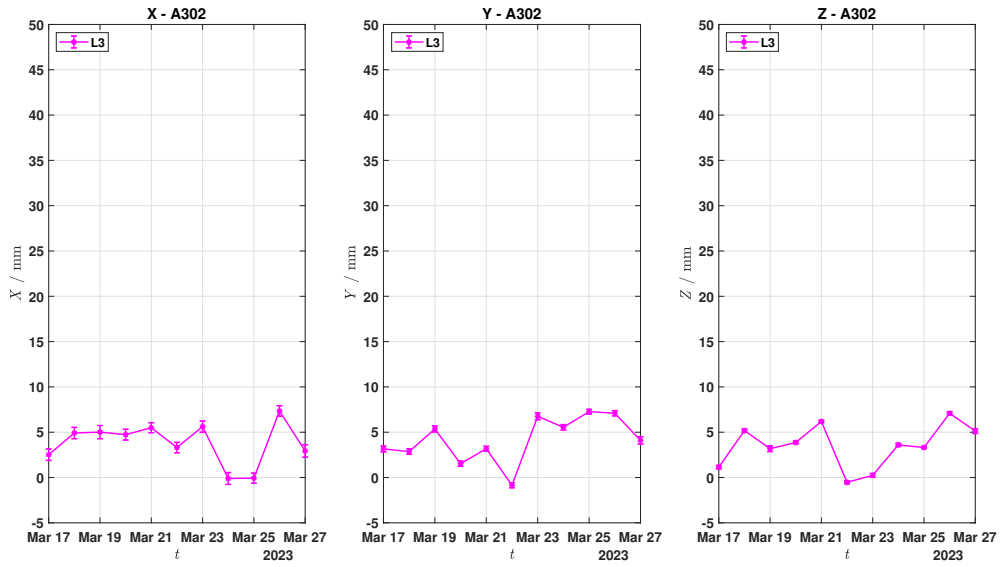

Figure 4.10: GipsyX's A302 station position in ECEF coordinate system

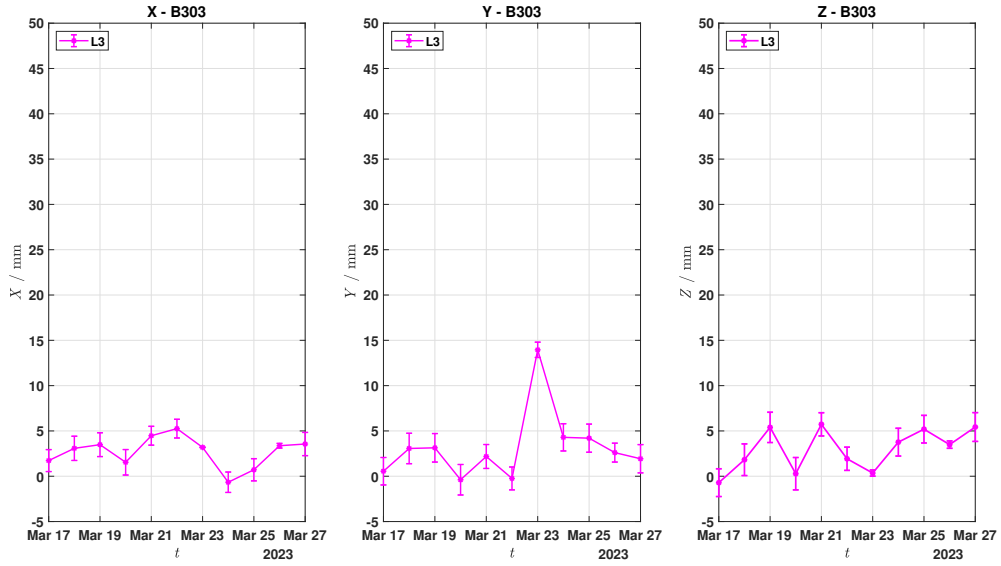

Figure 4.11: GipsyX's B303 station position in ECEF coordinate system

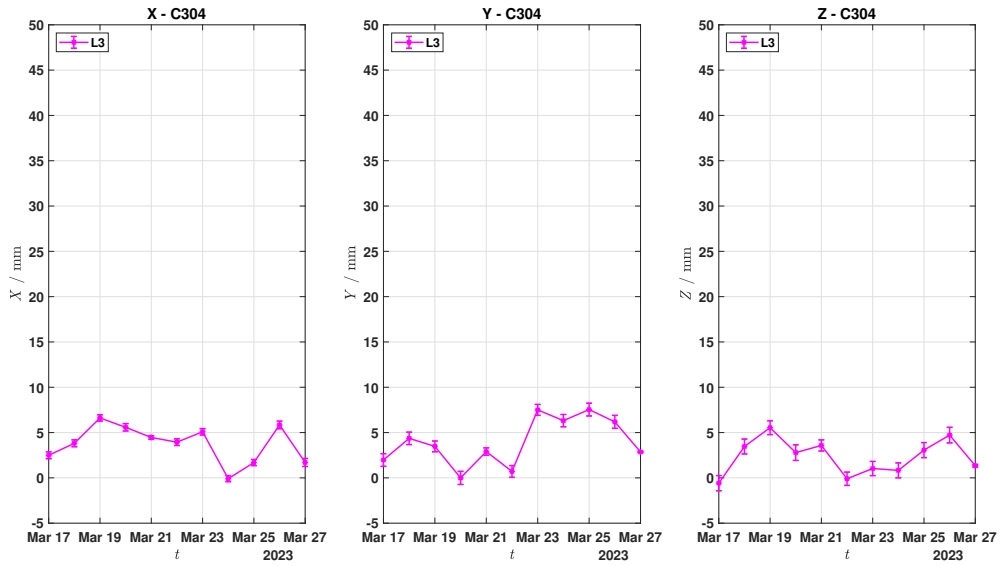

Figure 4.12: GipsyX's C304 station position in ECEF coordinate system

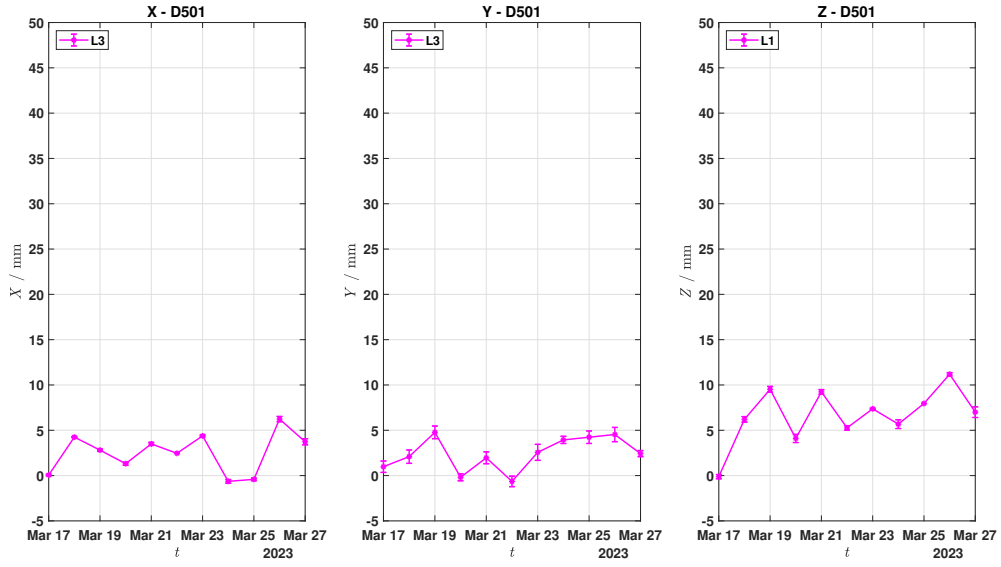

Figure 4.13: GipsyX's D501 station position in ECEF coordinate system

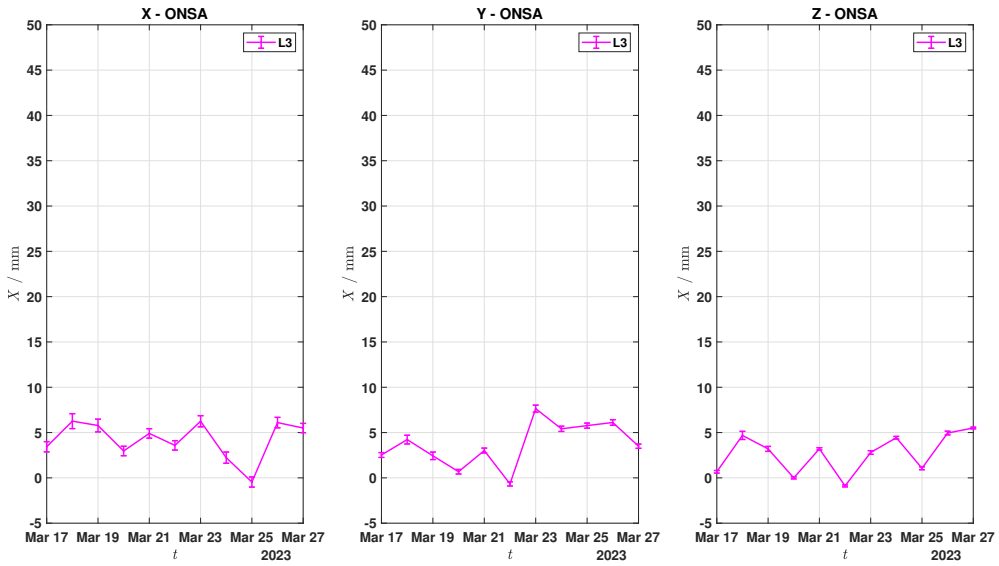

Figure 4.14: GipsyX's ONSA station position in ECEF coordinate system

The final solutions derived from the ionospheric-free signal of L3 frequency processed using GipsyX also exhibit a considerably similar behavior pattern across each day of observation for all stations. Notably, there is a sudden position jump in station B303, utilizing Trimble receiver, for up to 1.4 cm in Y-axis position.

4.3 Laser Tracker Measurement

The position determination is also conducted utilizing laser tracker and treated as the reference measurement since considered to have higher precision result, as previously mentioned in Section 3.3.1. Four antenna stations are measured using the laser tracker to determine their precise positions with respect to the antenna reference point (ARP). Figure 4.15 illustrates the conducted laser tracker measurement to the four antenna stations.

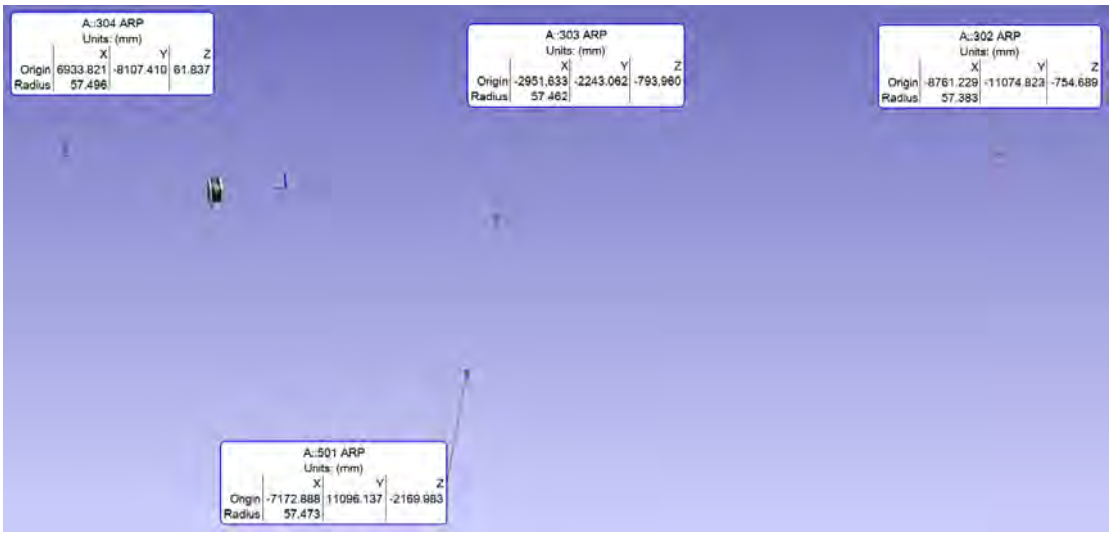

Figure 4.15: Laser tracker measurement setup

The result positions are measured in the tracker coordinate frame system in millimeter unit. In principle, the measured result is the distance between the antenna station and the tracker in three-dimension. The following Table 4.1 summarizes the measured four station positions from laser tracker.

Table 4.1: Measured station positions from laser tracker

Station	X [mm]	Y [mm]	Z [mm]
A302	-8761.229 ± 0.2	-11074.823 ± 0.2	-754.689 ± 0.2
B303	-2951.633 ± 0.2	-2243.062 ± 0.2	-793.960 ± 0.2
C304	6933.821 ± 0.2	-8107.410 ± 0.2	61.837 ± 0.2
D501	-7172.888 ± 0.2	11096.137 ± 0.2	-2169.983 ± 0.2

4.3.1 Reference System Transformation

It is acknowledged that the measurement results obtained from the laser tracker are considered to be of higher accuracy compared to GNSS signal positioning. However, it is important to note that the laser tracker results are measured in a local reference system. Thus, a specific transformation technique is necessary to convert between these two different reference frames by employing the Helmert transformation principle, as previously mentioned in Section 2.7.1.

The Helmert transformations involve four common points between the two different reference system frames. However, a slight challenge arises with the final solutions determined by both GNSS signal (E_G, N_G, U_G) and laser tracker measurements (E_t, N_t, U_t). While both types of calculations are referenced to the ARP, only the final position from the laser tracker measurement aligns exactly with the ARP. This discrepancy is attributed to the geometric constraint caused by the tilted antenna. Bernese and GipsyX do not account for this geometric constraint during their determinations. Figure 4.16 illustrates the difference between the computed

ARP from laser tracker and GNSS signal positioning.

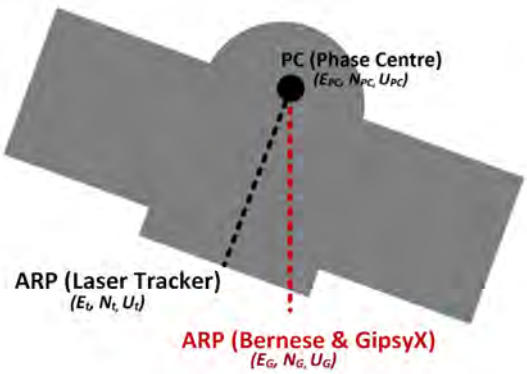

Figure 4.16: ARP illustration between laser tracker and GNSS signal

Hence, the ARP computed from the laser tracker needs to be adjusted to align with the calculated ARP of Bernese and GipsyX to establish a common point in the two different reference systems. This adjustment is achieved by considering the measured angle projection with respect to the tilting, along with the ARP information from the calibration data.

The offset between the ARPs of laser tracker and GNSS (Bernese and GipsyX) can be determined in Equation 4.1.

$$PC.\vec{n} = \begin{bmatrix} d_E \\ d_N \\ d_U \end{bmatrix} \tag{4.1}$$

where

$$PC = \begin{bmatrix} E_{PC} \\ N_{PC} \\ U_{PC} \end{bmatrix} \tag{4.2}$$

$$\vec{n} = \begin{bmatrix} n_x \\ n_y \\ n_z \end{bmatrix} \tag{4.3}$$

The phase center (PC) data in East-North-Up coordinates is provided by Geo++, the calibration agency, from the antenna calibration data. The vector $\vec{n}$ represents the normal projection data in three dimensions with respect to the tilt angle position of the antenna, as measured by the laser tracker.

Furthermore, it should be noted that the multiplication of Equation 4.2 and Equation 4.3 to determine the ARP offset $PC.\vec{n}$ includes only the vertical component of the phase center position. This is because the vertical component exhibits the greatest variation from the reference point of the antenna. Therefore, Equation 4.1

yields to the following Equation 4.4.

$$PC.\vec{n} = \begin{bmatrix} U_{PC}.n_x \\ U_{PC}.n_y \\ U_{PC} - |U_{PC}.n_z| \end{bmatrix} \tag{4.4}$$

Therefore, the exact ARP values measured by the laser tracker due to the geometric constraint caused by the tilted antenna that is aligned with the ARP of GNSS positioning (Bernese & GipsyX) is determined using Equation 4.5.

$$\begin{bmatrix} E_t^{'} \\ N_t^{'} \\ U_t^{'} \end{bmatrix} = \begin{bmatrix} E_t - d_E \\ N_t - d_N \\ U_t - d_U \end{bmatrix} \tag{4.5}$$

Seven Helmert parameters are estimated to facilitate the three-dimensional transformation between the two reference systems. These parameters are estimated based on the frequency signals used, as different frequencies may lead to varying final positions.

In practice, daily estimations yield multiple Helmert parameters due to the daily observations used in GNSS signal computations. However, for simplicity, the daily estimated seven Helmert parameters are averaged to obtain representative values.

Table 4.2 summarizes the estimated Helmert parameters. It is noted that k-scale is treated as a constant since there is no scale difference between two different reference frame systems. The reference transformation is done by utilizing the following Helmert parameters into Equation 2.20.

Table 4.2: Estimated Helmert parameters

Frequency	t_x **[mm]**	t_y **[mm]**	t_z **[mm]**	r_x [°]	r_y [°]	t_y [°]	k
L1	450.7 ± 3.1	9960.8 ± 5.0	216.1 ± 7.7	0.2745 ± 0.0423	-0.0044 ± 0.0292	-2.5919 ± 0.0165	1
L2	448.5 ± 2.5	9955.7 ± 4.6	217.7 ± 7.2	0.2686 ± 0.0437	0.0132 ± 0.0295	-2.6067 ± 0.0142	1
L3	454.5 ± 0.7	9943.7 ± 0.3	177.8 ± 2.5	-0.0028 ± 0.0063	-0.0247 ± 0.0070	-2.5822 ± 0.0024	1

4.4 Station Positions Analysis

The receiver stations measured by the laser tracker provide position data for three different frequencies. At this stage, the computed station positions from both the GNSS signals processed by Bernese and GipsyX, and the laser tracker, can be compared for validation since they are already in the same reference frame.

It should be noted that these transformed positions from the laser tracker measurement are referred to the projected ARP (red) according to the GNSS signal processing in Bernese and GipsyX, as illustrated in Figure 4.16. The results of four receiver antenna positions are presented in Table 4.3 with respect to the desired frequencies in ECEF coordinate system.

There are slight disagreements between each frequency in four antenna stations, particularly the difference result computed between L1 & L2 (Bernese) and L3 (GipsyX). One certain thing is that the L3 results from the GipsyX are calculated in so-called ionospheric-free signal, making it to be less influenced to the atmospheric errors compared to L1 or L2.

Table 4.3: Transformed ARP positions measured by laser tracker

Station A302			
Frequency	X **[m]**	Y **[m]**	Z **[m]**
L1	3370660.8916	711869.9814	5349785.9023
L2	3370660.8803	711869.9812	5349785.9064
L3	3370660.8370	711869.9679	5349785.8358
Station B303			
Frequency	X **[m]**	Y **[m]**	Z **[m]**
L1	3370652.2283	711873.6519	5349790.7407
L2	3370652.2332	711873.6522	5349790.7379
L3	3370652.2107	711873.6510	5349790.6980
Station C304			
Frequency	X **[m]**	Y **[m]**	Z **[m]**
L1	3370655.0513	711884.6563	5349788.5686
L2	3370655.0548	711884.6606	5349788.5690
L3	3370655.0222	711884.6478	5349788.4961
Station D501			
Frequency	X **[m]**	Y **[m]**	Z **[m]**
L1	3370641.6258	711866.5087	5349796.6119
L2	3370641.6311	711866.5075	5349796.6091
L3	3370641.6380	711866.5132	5349796.6281

4.4.1 Baseline Length Assessments

The transformed ARP of receiver stations measured using the laser tracker can be validated by comparing baseline lengths to the data positions computed using GNSS signals. It is noted that the comparison involves only the four antenna stations of the local network, thus forming six baseline formations to be assessed.

Table 4.4 summarizes the formed baseline length assessments based on the desired frequencies and between two different type of measurements. The overall results show that the error difference (Δ) of the baseline length computed by both GNSS signal and laser tracker measurement experience sub-millimeter level of error. Thus, with considerably small error differences, the Helmert transformation between local tracker refere frame and ECEF reference from from GNSS signal is conducted successfully.

Furthermore, the assessments on the L3 frequency particularly resulted in significantly lower error differences, up to the micrometer level, compared to L1 and L2,

making it more validated. This is caused by the dual-frequency combination of L3 processing, which produces the so-called ionospheric-free signal.

Table 4.4: Baseline length assessments between computed GNSS signal and tracker measurement

L1			
Baseline	**Length (Tracker) [mm]**	**Length (GNSS) [mm]**	**Δ [mm]**
B303 & A302	10 579.950	10 579.984	0.034
B303 & C304	11 566.472	11 566.572	0.100
C304 & A302	16 017.854	16 018.029	0.175
D501 & A302	22 314.283	22 314.284	0.001
D501 & B303	14 068.098	14 068.114	0.016
D501 & C304	23 964.053	23 964.154	0.101
L2			
Baseline	**Length (Tracker) [mm]**	**Length (GNSS) [mm]**	**Δ [mm]**
B303 & A302	10 563.775	10 563.807	0.032
B303 & C304	11 569.392	11 569.488	0.096
C304 & A302	16 015.962	16 016.129	0.167
D501 & A302	22 296.840	22 296.840	0.000
D501 & B303	14 068.478	14 068.494	0.016
D501 & C304	23 966.125	23 966.222	0.097
L3			
Baseline	**Length (Tracker) [mm]**	**Length (GNSS) [mm]**	**Δ [mm]**
B303 & A302	10 565.004	10 565.004	0.000
B303 & C304	11 562.067	11 562.066	0.001
C304 & A302	16 012.091	16 012.089	0.002
D501 & A302	22 293.682	22 293.682	0.000
D501 & B303	14 067.528	14 067.528	0.000
D501 & C304	23 960.959	23 960.958	0.000

Therefore, the estimated Helmert parameters are valid and can be used to transform the projected ARP from the laser tracker of the stations to the ECEF reference frame system. At this stage, the calculations have resulted in considerably the most accurate ARP of the desired antenna stations.

4.5 GNSS Error Assessments

Multiple error sources are compensated during the position determinations in both DGNSS's Bernese and PPP's GipsyX processing. In many cases, several error parameters can be inferred from the processing during its position determination. Moreover, it is also worthwhile to manually estimate and model certain error parameters using specific techniques to investigate their contribution to the final station position.

In this project, three error sources are estimated and modeled. The following subsections present both the estimated errors from the software processing and those modeled by certain methods.

4.5.1 Receiver Clock Estimations

It is crucial to estimate and compensate the receiver clock error parameter, considering such error highly influence the GNSS positioning determination. Both Bernese and GipsyX are capable to estimate the error caused by unsynchronized receiver clock. The following Figure 4.17-4.21 show the final solution of daily receiver clock error estimated by Bernese and GipsyX for all five desired stations. It is noted the estimations are conducted utilizing PPP method in both software programs. The results from Bernese and GipsyX are presented in yellow and blue color, respectively.

Figures 4.17 and 4.18 present the daily estimated receiver clock errors for station A302 (Septentrio) and B303 (Trimble). The estimated errors between the two different types of receivers are significantly different. For station A302, the daily average clock error is estimated to be 4.1653×10^4 m using Bernese and 4.1625×10^4 m using GipsyX. In contrast, for station B303, the daily average clock error is estimated to be -8.0241 m and -7.9025 m using Bernese and GipsyX, respectively.

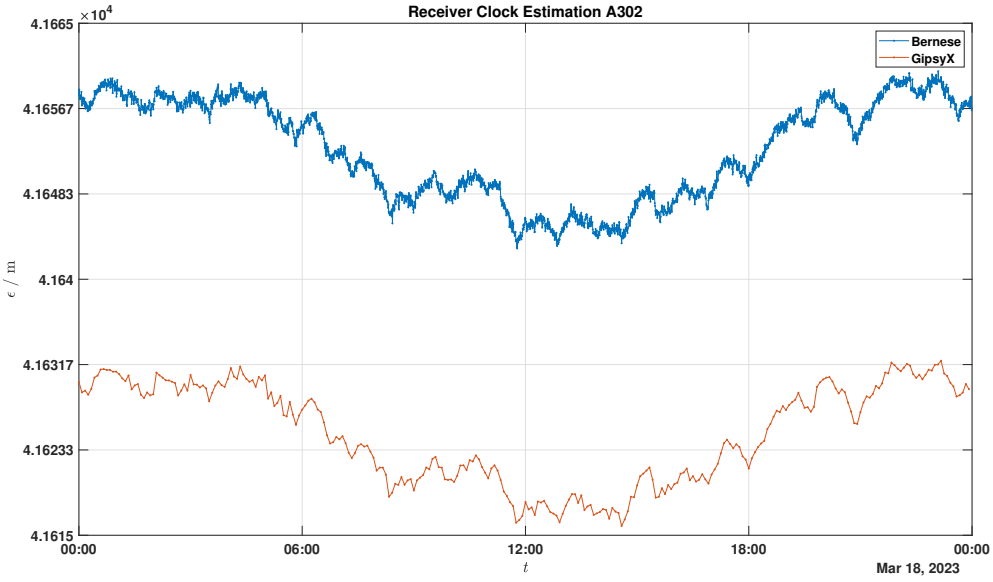

Figure 4.17: Receiver clock error station A302

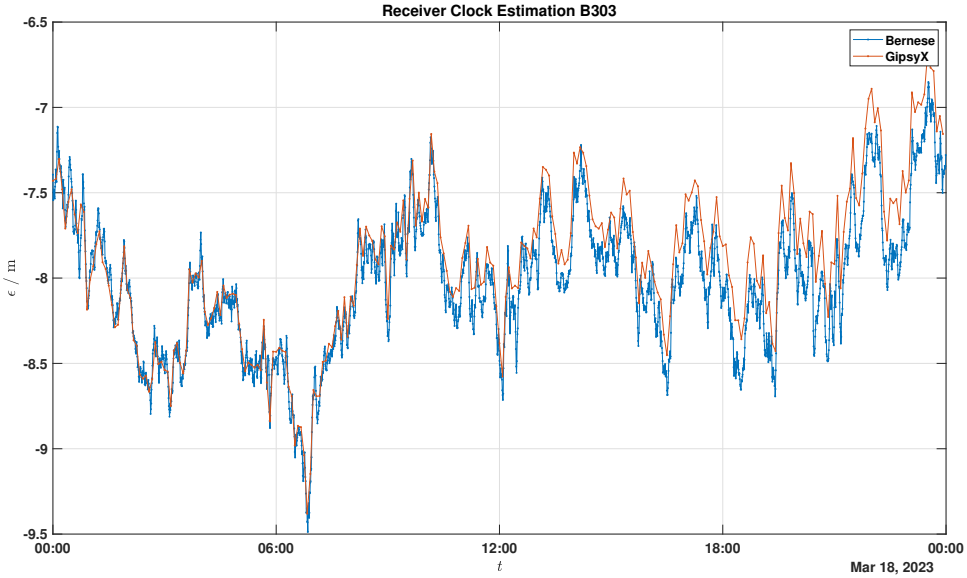

Figure 4.18: Receiver clock error station B303

Similarly, the estimated receiver clock errors for station C304 (Figure 4.19) with Septentrio and station D501 (Figure 4.20) with Trimble are much different. The daily average clock error for station C304 is estimated to be 4.4148×10^4 m using Bernese, while using GipsyX is estimated to be 4.4118×10^4 m. On the other hand, the daily average clock error for station D501 is estimated to be -6.9323 m and -6.9986 m using Bernese and GipsyX, respectively.

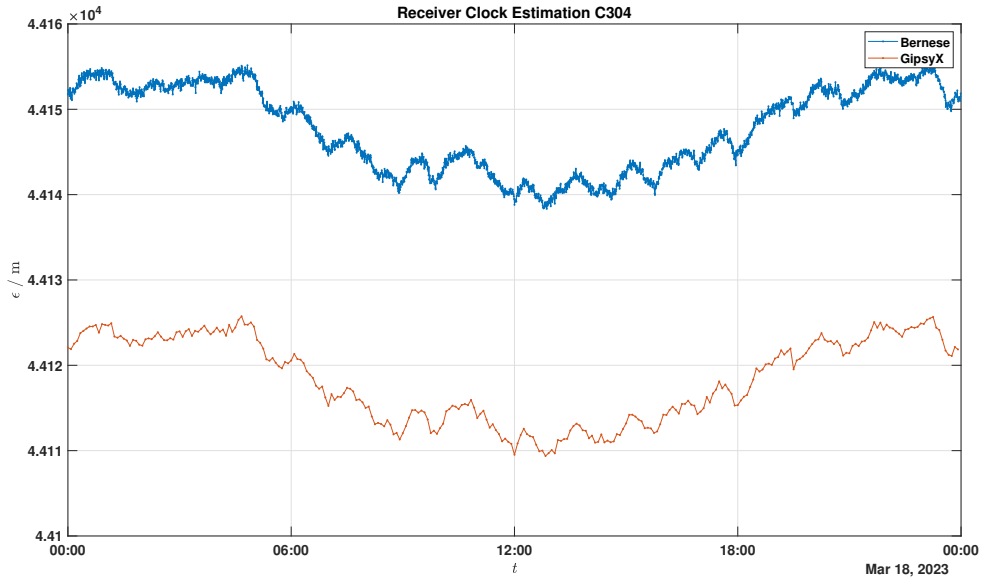

Figure 4.19: Receiver clock error station C304

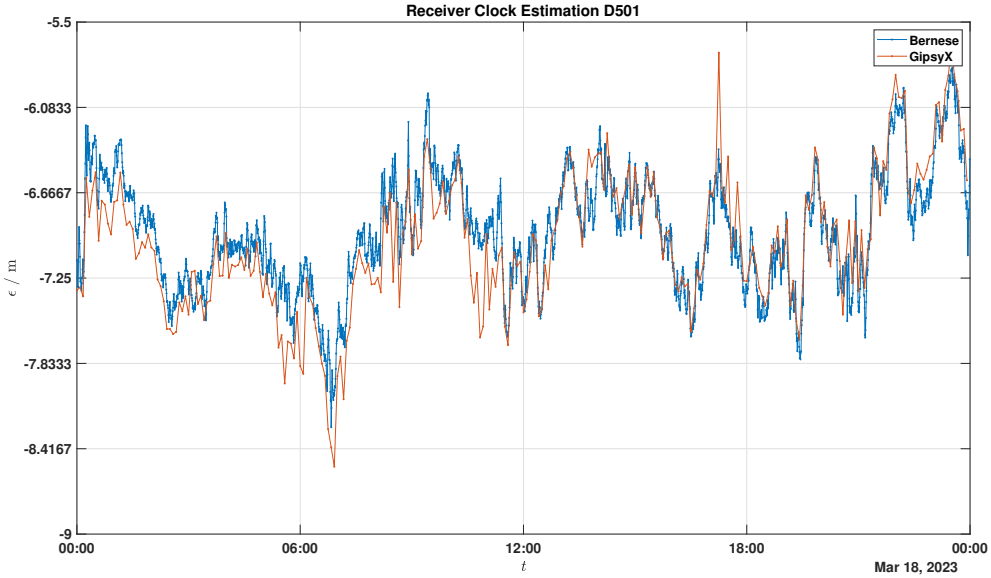

Figure 4.20: Receiver clock error station D501

Moreover, Figure 4.21 shows the daily estimated clock errors at station ONSA, utilizing a Septentrio receiver. On average, the daily receiver clock error is estimated to be -2.7547×10^4 m for Bernese and -2.7527×10^4 m for GipsyX.

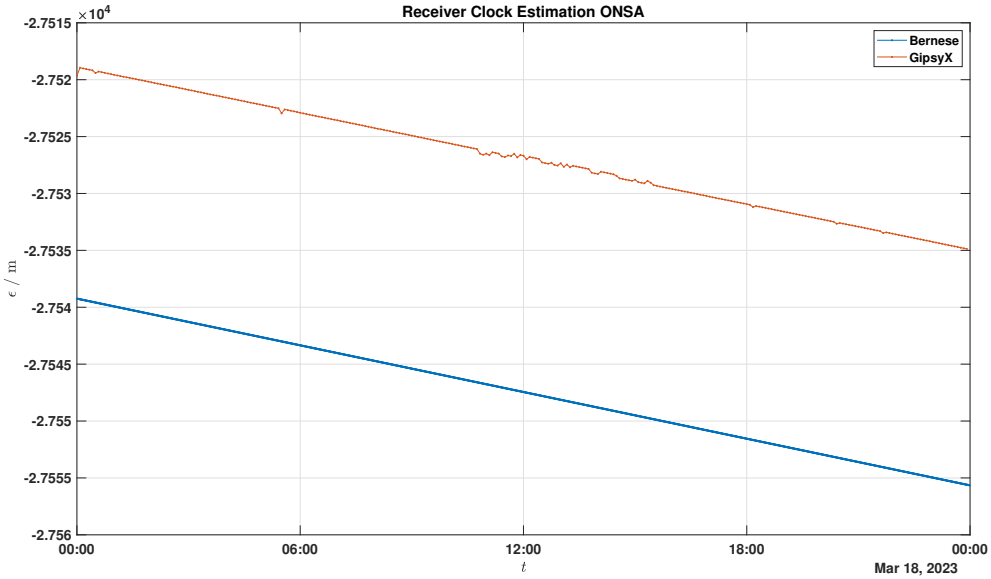

Figure 4.21: Receiver clock error station ONSA

The calculated receiver clock estimations (ϵ) generally exhibit similar patterns between the Bernese and GipsyX results. The Bernese estimations are calculated at 30-second intervals, while GipsyX's results are based on observations taken every 5 minutes. Moreover, the final estimated receiver clock error for all 10 days observations are presented in Appendix A.

It is evident from the results between the stations that there are significant differences in error magnitude, particularly between stations A302 & C304 compared to stations B303 & D501. Stations A302 & C304 are influenced by receiver clock errors of more than 40 km in distance, while stations B303 & D501 experience errors of less than 10 m. This discrepancy is likely caused by the different types of receivers used during the observations, resulting in behavioral differences between the receivers. The Septentrio receiver was used in stations A302 & C304, while the Trimble receiver was used in stations B303 & D501.

Although station ONSA also utilizes Septentrio receiver, it should be noted that an external clock oscillators are used for its daily observations. Thus, the estimated receiver clock in station ONSA (Figure 4.21) is clearly in much different behaviour pattern, compared to the rest of stations. Another noticeable difference is there are disagreements between the estimated receiver clock error from Bernese and GipsyX. Table 4.5 summarizes the average difference between two type of receiver from two different software programs.

Table 4.5: Mean difference of receiver clock error between Bernese and GipsyX

Receiver Station	**Mean Difference [m]**
Septentrio (A302 & C304)	-29.0977 – -27.2956
Trimble (B303 & D501)	0.2662 – 0.4162

4.5.2 Zenith Tropospheric Delay Estimations

In GipsyX, the Zenith Tropospheric Delay (ZTD) is modeled and estimated during the positioning determinations using the Precise Point Positioning (PPP) technique and the dual-frequency combination of L3. Tropospheric errors can significantly influence the transmitted signal from satellites because satellite signals are highly sensitive to atmospheric properties during propagation, as previously mentioned.

Figure 4.22 shows the daily estimated ZTD from GipsyX. The results for all stations show similar error delay behaviors caused by tropospheric parameters. It is noticeable that station A302 (blue) experiences higher tropospheric error delays than the rest of the stations. This can be attributed to the fact that station A302 is located at the lowest height coordinate position in the station setup, making it more susceptible to tropospheric delays as well as longer signal propagation. Final estimated ZTD (ϵ) errors for 10 days observations in the desired stations are presented in Appendix B.

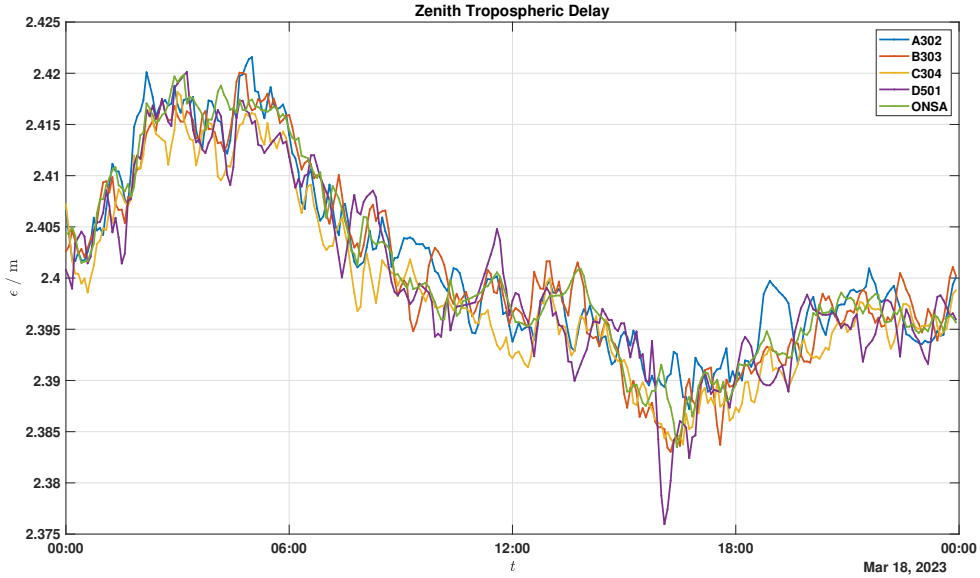

Figure 4.22: Daily ZTD estimation in the desired stations

Furthermore, upon more detailed investigation, the ZTD results among the five desired antenna stations do not exhibit large differences. This can be attributed to the setup and locations of all five stations in the field, as they are situated in close proximity to each other.

Closer investigation was conducted by taking differentials of the daily estimated ZTD with one particular station as a reference, in this case, station ONSA. Differential operations of estimated ZTD were performed between station ONSA and each of the four stations (A302, B303, C304, and D501), as shown in Figure 4.23.

Overall, the four differential operations resulted in considerably small tropospheric delay errors (ϵ), on the order of millimeter-level. Thus, when utilizing DGNSS technique for station positioning, the tropospheric delay error (ϵ) parameter can almost be cancelled out during the differential operation between two stations.

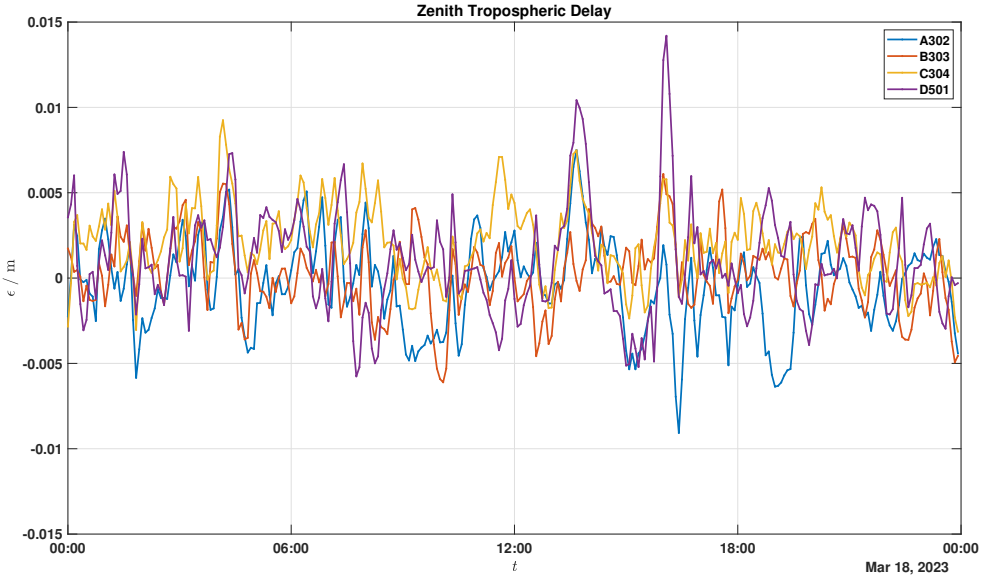

Figure 4.23: ZTD differences between ONSA and the four stations

4.5.3 Carrier Phase Wind-up Estimations

Although carrier phase wind-up error parameters are compensated in both Bernese and GipsyX processing, such error parameters can be estimated and modeled to assess their behaviors and the magnitude of errors produced during the observations.

In principle, the carrier phase wind-up effect should be almost the same across all stations since they are placed close to each other. However, in this project, geometric constraints are created due to the influence of tilted antennas, affecting the projection of the receiver coordinate system as well as the effective dipole vector of the receiver antenna in Equation 2.17.

Figure 4.24 shows the model estimation of carrier phase wind-up (ϵ) in all four receiver stations (A302, B303, C304, and D501). Utilizing the same daily observed satellite positions in all antenna stations every 5 minutes epoch interval, it can be clearly seen that there are differences of the estimated model errors caused by the geometrical constraints of tilted antenna.

Furthermore, differential approach is applied to assess the modeled carrier phase wind-up errors (ϵ). There are 6 carrier phase wind-up results, corresponding to the total baseline length in the experiment setup, as shown in Figure 4.25. Taking the average value of all the six baseline differences, the carrier phase wind-up effects are still in the decimeter-level of errors (up to 23 cm). This is also clearly caused by the created geometric constraints in all four antenna stations.

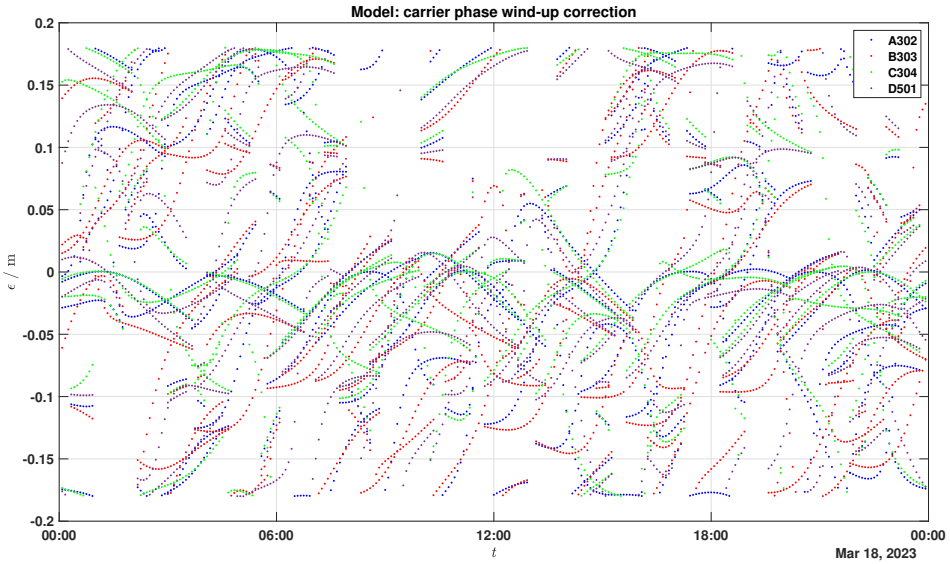

Figure 4.24: Daily carrier phase wind-up estimations

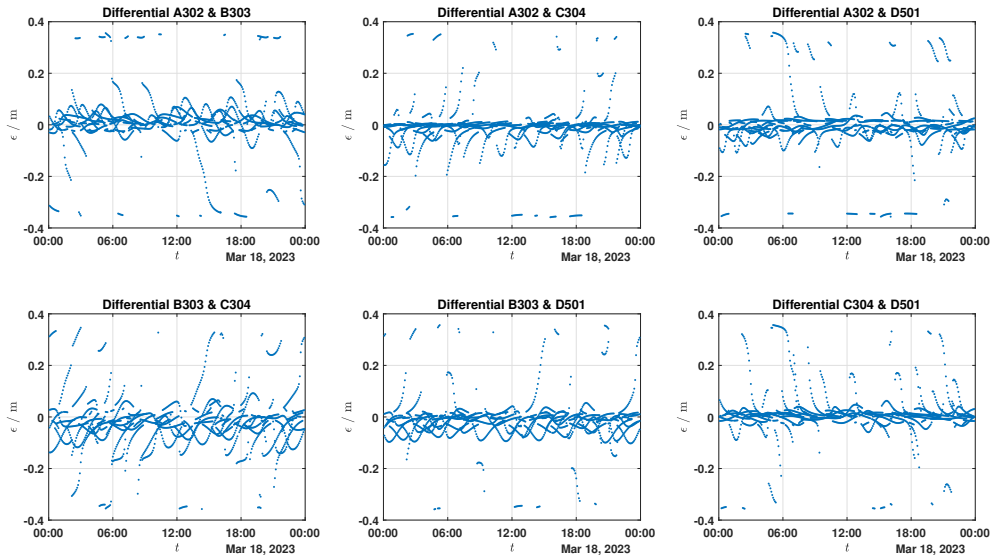

Figure 4.25: Carrier phase wind-up differences between receiver stations

4.6 Observation Residuals

Considering that two types of station determinations are utilized in this project, namely PPP and single difference (DGNSS), there are two sets of residuals produced. These residuals are presented with respect to the observed satellite signal elevation in the following subsections.

Furthermore, it is noted that the geometric constraints created due to the tilted

antenna clearly influence the received signal elevations with respect to the antenna phase center on the receiver stations. Therefore, corrections to the received signal elevations are applied in order to determine the actual received signals at the antenna phase center.

The corrections are calculated based on the amount of tilt angle with respect to the signal elevation, as well as the direction of the tilt corresponding to the signal azimuth angle. Figure 4.26 illustrates the influence of the tilted antenna position to the phase center of the antenna. For instance, satellite signal L is received with an elevation ϵ (red) on the antenna phase center, while the actual elevation on the antenna phase center is $\epsilon + c$ (blue) due to the geometric constraint.

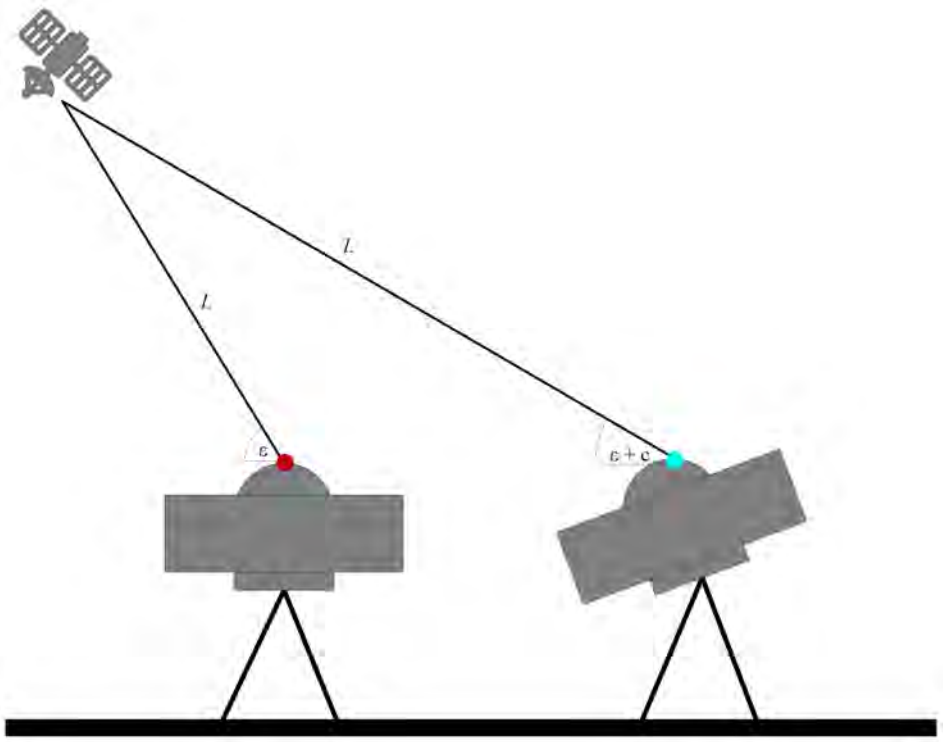

Figure 4.26: Illustration of normal phase center (red) and actual phase center when the antenna is tilted (blue) corresponding to the same received signal L

4.6.1 PPP Residuals

The following figures present the final residual results for the four antenna stations, i.e., A302, B303, C304, and D501, with the influence of geometric constraints caused by the tilted antenna positions. In station ONSA, however, it is noted there is no geometric constraint since such station is not tilted, thus no elevation corrections are conducted.

The final solutions for all the desired receiver stations are computed with an elevation cut-off 10°, as well as with the corrected elevation angle due to the created geometric constraints (except in station ONSA). From Figure 4.27–4.31, it can be

clearly seen that higher residual errors (ϵ) are present in the lower elevation angles. Thus, such phenomenon is correct and valid according to the the satellite signal principle, where the lower elevation angle experiences longer distance of signal propagation, as well as likely more influenced by higher error values during its transmission.

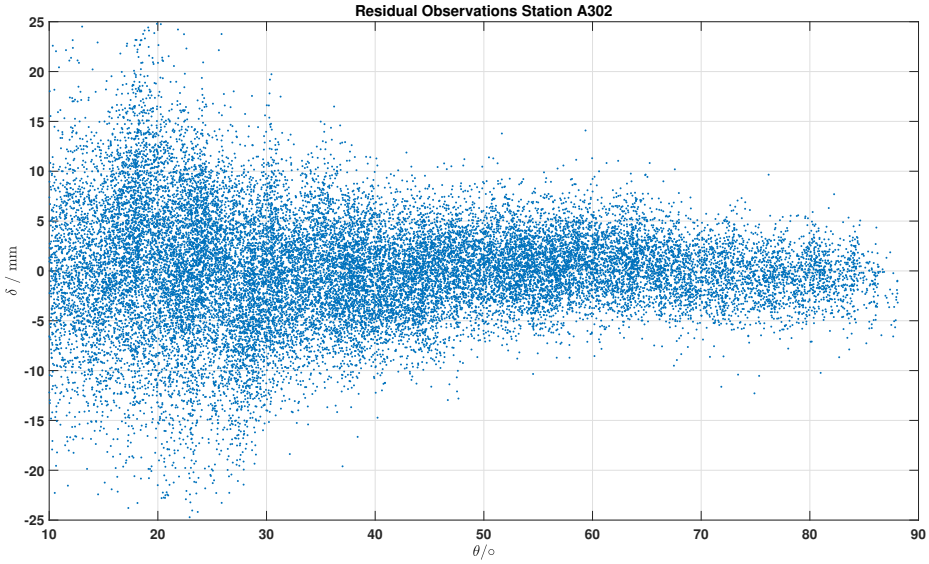

Figure 4.27: Residual data station A302

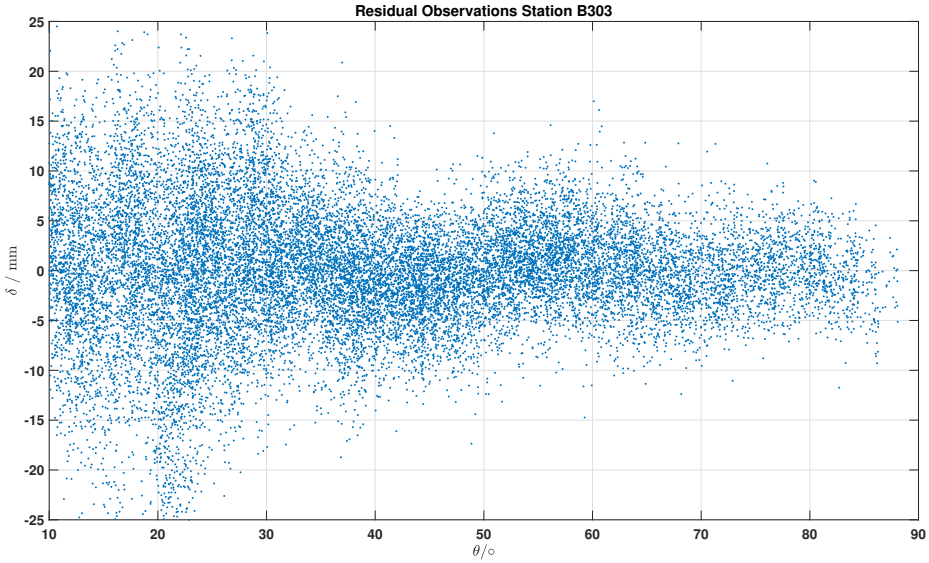

Figure 4.28: Residual data station B303

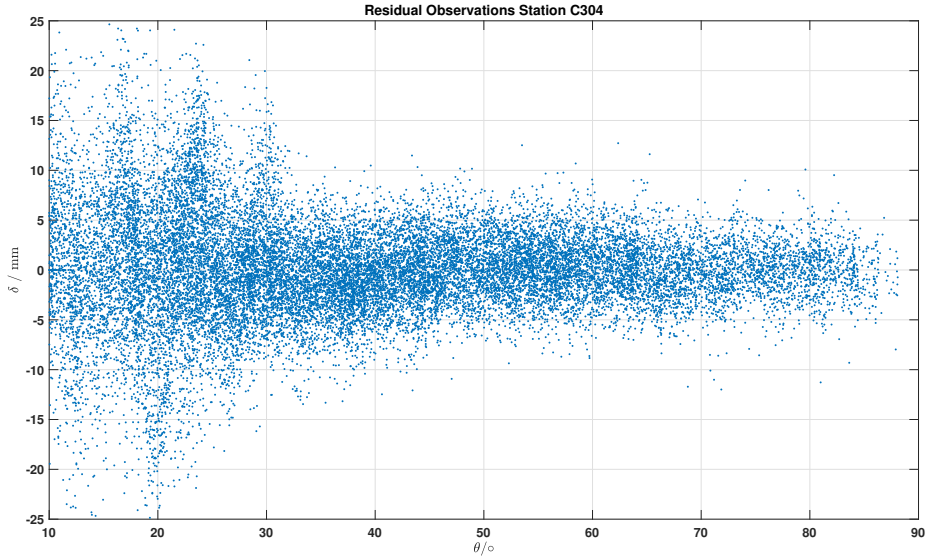

Figure 4.29: Residual data station C304

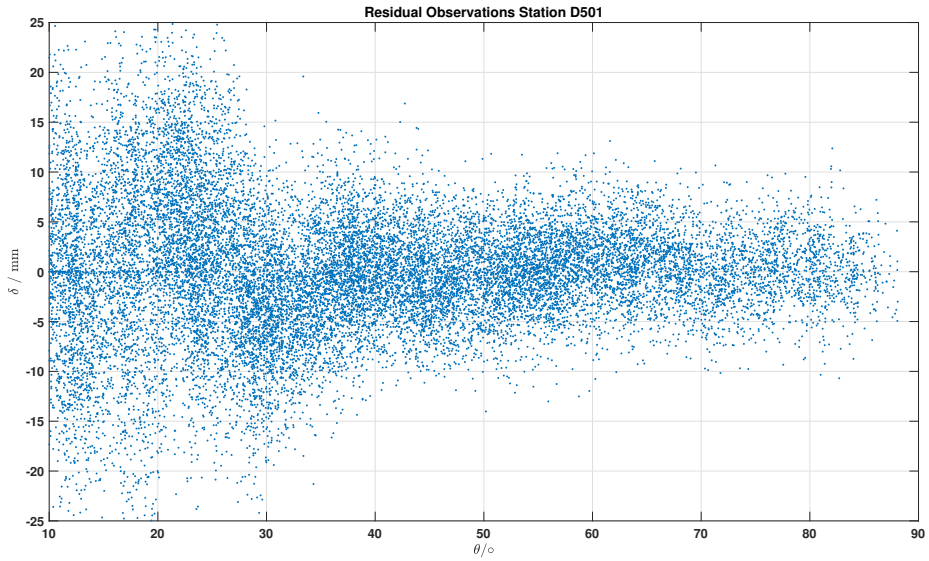

Figure 4.30: Residual data station D501

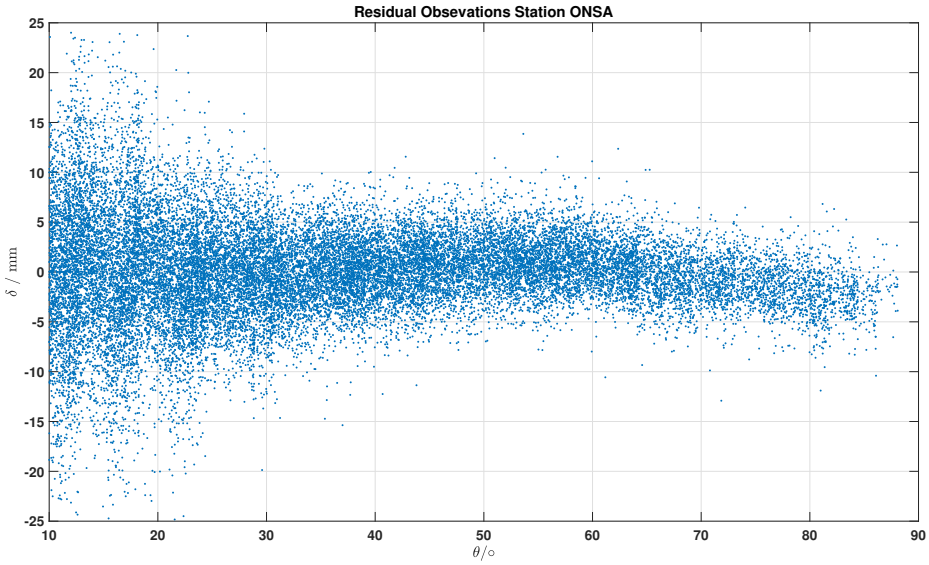

Figure 4.31: Residual data station ONSA

Furthermore, it is noted that these residual data results correspond to the elevation of antenna phase center errors for each station. Therefore, the data are computed in terms of mean phase residuals as the final estimated model errors with respect to the elevation angle of the phase center. These estimated model errors (ϵ) are then classified into elevation angles between 10° and 90°, with 5° differences. Figure 4.32 shows the final estimated model error with respect to elevation angles.

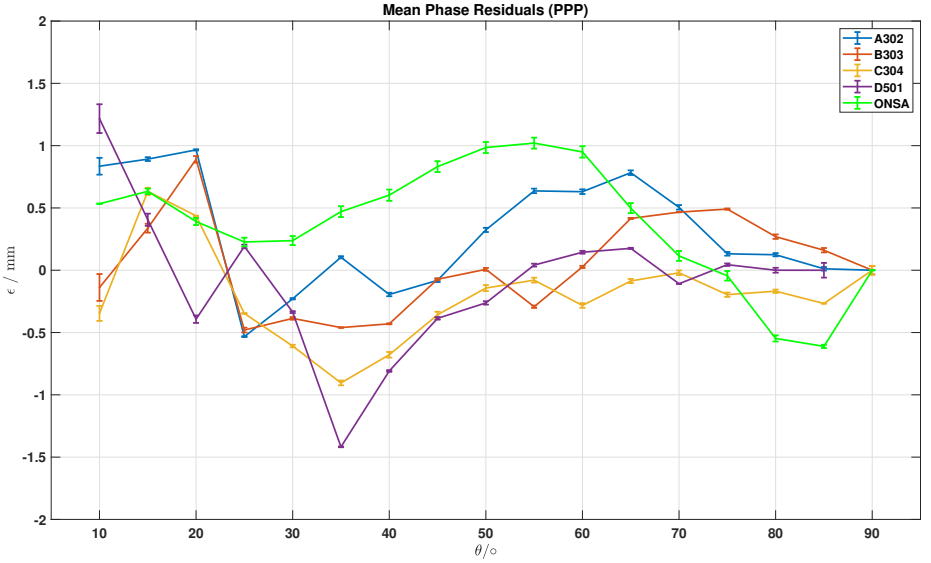

Figure 4.32: Final estimated model error of PPP phase residuals

Hence, a 30° elevation is considered as the benchmark for evaluation from all stations except ONSA. The averaged error models for the L3 frequency observation are found to be -0.3901 $\pm$ 0.0004 mm.

4.6.2 Single Difference Residuals

The final residual results computed by utilizing single difference method are also corresponding to the final estimated model errors with respect to the elevation angles of the phase center. However, unlike the PPP processing previously, the elevation cut-off of 3° is applied on the single difference determinations. Although the elevation cut-off is utilized to be relatively low, considering there is a geometric constraint of ±10° tilt angle, the final residual solutions are set to take 10° elevation cut-off into account.

Furthermore, since the final coordinate position of the desired stations is already computed using the laser tracker measurement, considered the most accurate, these final station coordinates can be used to compute single-difference distance projections with respect to the baseline and the satellite positions. Therefore, this tracker projection data is used as the reference for assessing the single-difference results calculated by Bernese. Moreover, the single-difference process in Bernese is conducted separately for frequency L1 and L2.

Figure 4.33 illustrates the method for determining the projection of the single difference between two stations using the measured laser tracker data. At this stage, the positions of station A, station B, and the satellite S are known and are all in the same coordinate reference system, i.e., ECEF.

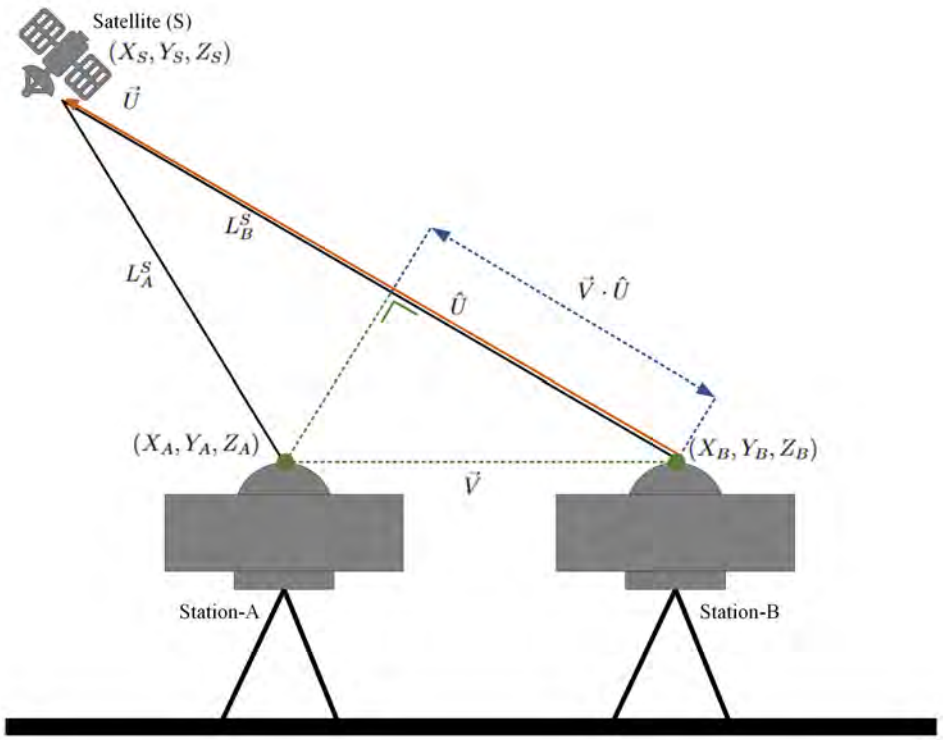

Figure 4.33: Tracker measurement projection for single difference between station-A and station-B

The vector $\vec{V}$ represents the baseline vector between station A and station B. The

illustration indicates that station B experiences a longer signal distance L_B^S to the satellite S compared to station A's signal distance L_A^S. Therefore, $\vec{U}$ is determined as the three-dimensional vector from station B to the satellite S, and $\hat{U}$ denotes its unit vector.

Furthermore, the projected single difference $(\vec{V} \cdot \hat{U})$ is computed as the dot product between the baseline vector of station A and station B $(\vec{V})$ and the unit vector to the satellite $(\hat{U})$. The results of the projected single difference correspond to the baseline between the two stations, which varies depending on the movement of the satellite. Therefore, the projected baseline can be analyzed in relation to the observed satellite elevations.

The maximum and minimum values resulting from both DGNSS and tracker projections correspond to the calculated baseline between the two station positions. As mentioned earlier, these baseline values vary due to satellite movements and observed elevations. For example, when the satellite is observed near the zenith direction (90° elevation), the signal distances measured from two different stations in close proximity are likely to be almost identical, resulting in a difference close to zero. In contrast, at lower satellite elevations, the measured signal distances from two different stations will exhibit more noticeable differences. This is because the satellite's position relative to the one of the stations is much closer during such epoch, as illustrated in Figure 4.33.

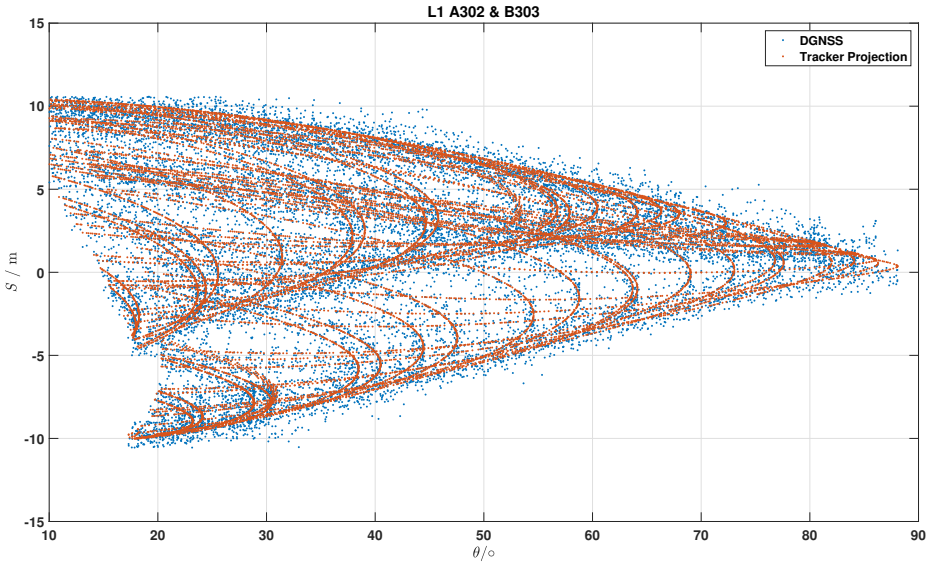

Figure 4.34: L1 single difference A302 & B303

Figures 4.34–4.39 present the results of the L1 single difference (S) between the observational data computed in Bernese and the tracker projection data across six different baseline formations. Overall, the final results exhibit behavior similar to

that of the tracker projection data, which is considered the most accurate. Moreover, the final results demonstrate behavior consistent with signal propagation principles, where signals at lower elevations are expected to experience longer signal distances.

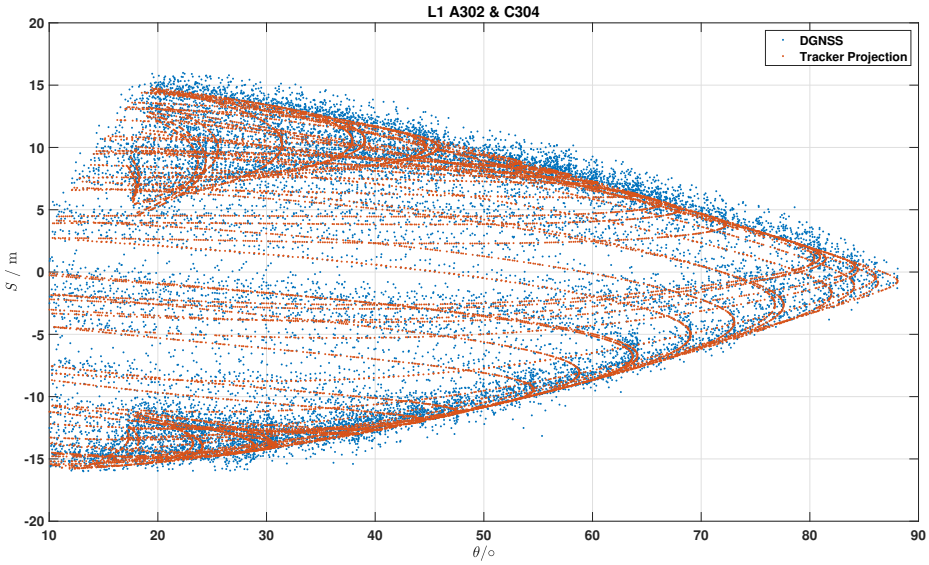

Figure 4.35: L1 single difference A302 & C304

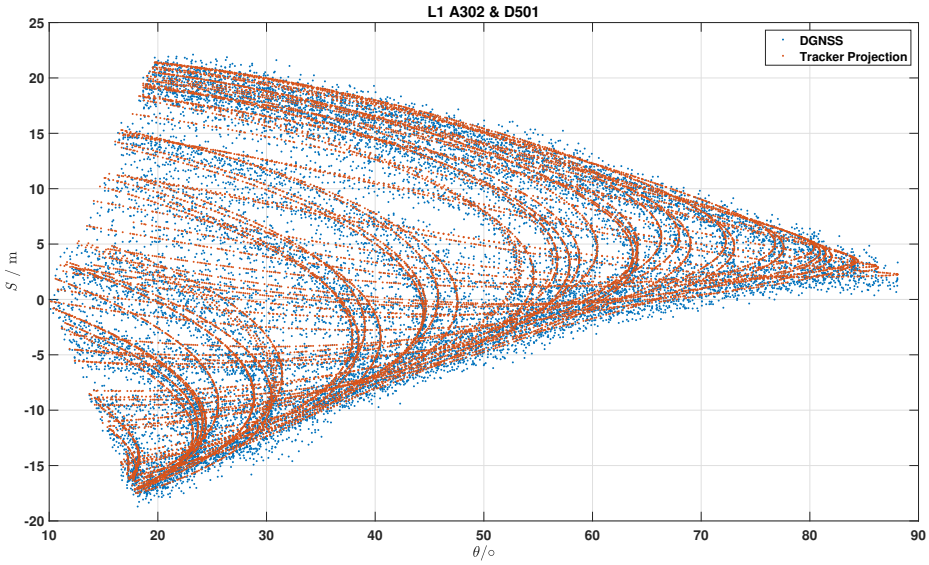

Figure 4.36: L1 single difference A302 & D501

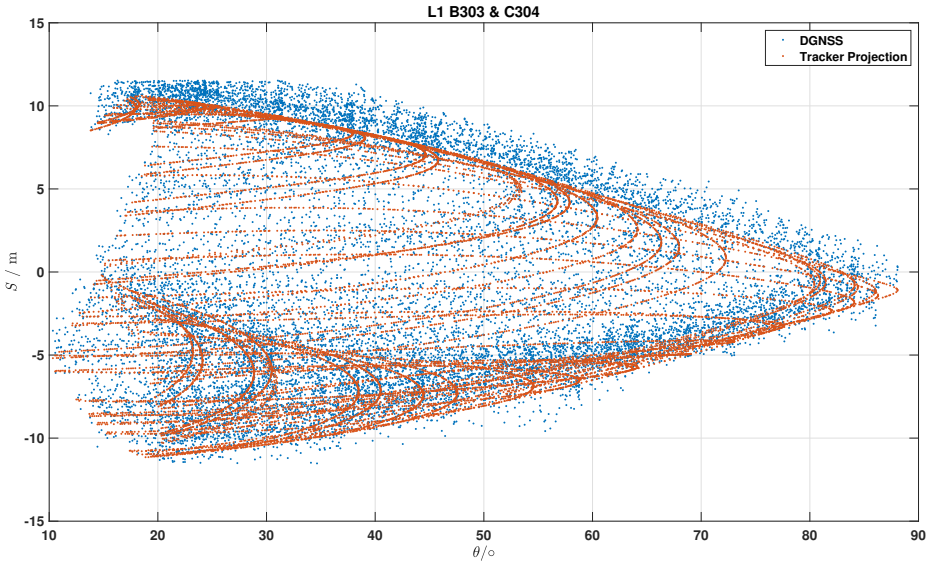

Figure 4.37: L1 single difference B303 & C304

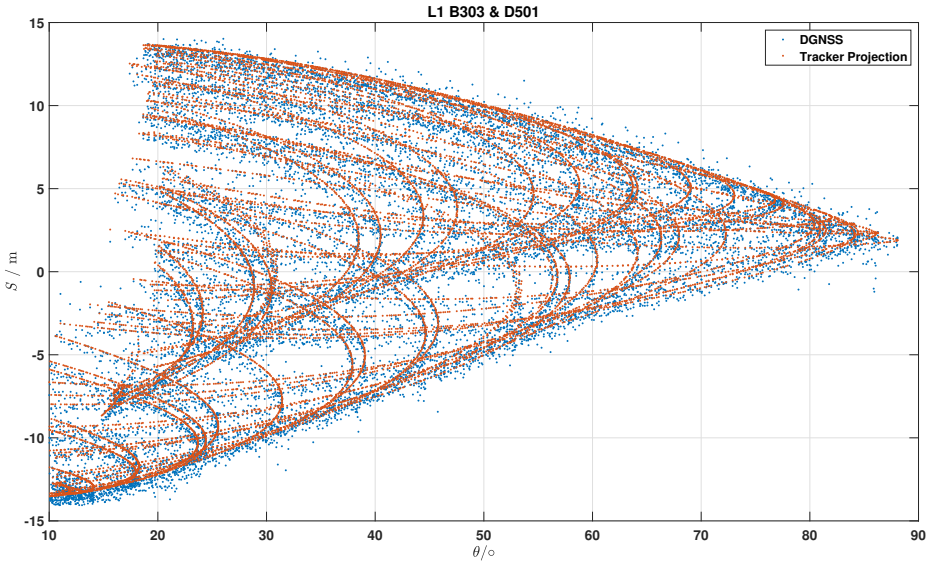

Figure 4.38: L1 single difference B303 & D501

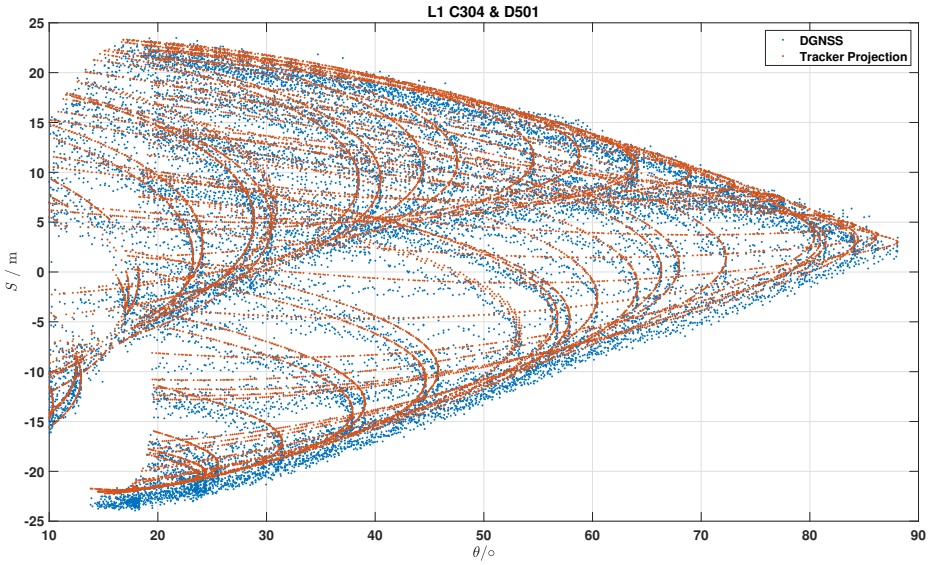

Figure 4.39: L1 single difference C304 & D501

Unfortunately, due to unknown reasons, the L2 single-difference data did not yield the expected results according to the tracker projection. Thus, only the L1 signal residual results are presented in terms of mean phase residuals as the final estimated model errors with respect to the elevation angle of the phase center. The results of L2 Bernese's single difference and tracker projection (S), as well as the final estimated model error of L2 Bernese's single difference (ϵ) are included in Appendix D.

However, unlike the residual results computed by PPP's GipsyX where it is produced through the whole algorithm process explained in Figure 2.10, the Bernene's single difference results are retrieved in its initial stage of processing. Subsequently the residuals of Bernese's single difference are calculated by taking the differential between the data of single differences and tracker projections.

Moreover, a further technique so-called additional ambiguity is applied to fit the the single difference data to the tracker projection results, producing the error differences to be lower than a wavelength of the signal. This is done by taking the differential results and defined as the integer wavelength ($N\lambda$), which then are applied back to the single difference data to be more fitted to the tracker projections.

The differential results both from Bernese's single difference (sd) and tracker projection (tp) can be defined in a new term, as expressed in Equation 4.6 and 4.7.

$$S_{sd} = N_{sd}\lambda + Frac_{sd} \tag{4.6}$$

$$S_{tp} = N_{tp}\lambda + Frac_{tp} \tag{4.7}$$

where S is the differential result, N is the integer ambiguity, and $Frac$ is the fractional value of the differential. Considering that previously the so-called additional

ambiguities are applied to the Bernese's single difference data, this leads to $N_{sd}\lambda$ becomes equal and can be cancelled to the $N_{tp}\lambda$ when taking the error differences.

Therefore, only the fractional part ($Frac_{sd}$ and $Frac_{tp}$) remains in the differential signal (S) in both of them. The final residuals are then computed by taking the differentials between $Frac_{sd}$ and $Frac_{tp}$.

$$Residual = S_{tp} - S_{sd} \tag{4.8}$$

$$Residual = Frac_{tp} - Frac_{sd} \tag{4.9}$$

These residuals are taken in average with respect to the elevation angles, as well as computed to be the final estimated error (ϵ) of L1 signal observations. The final estimated model error (ϵ) of L1 Bernese's single difference for the antenna stations is shown in Figure 4.40.

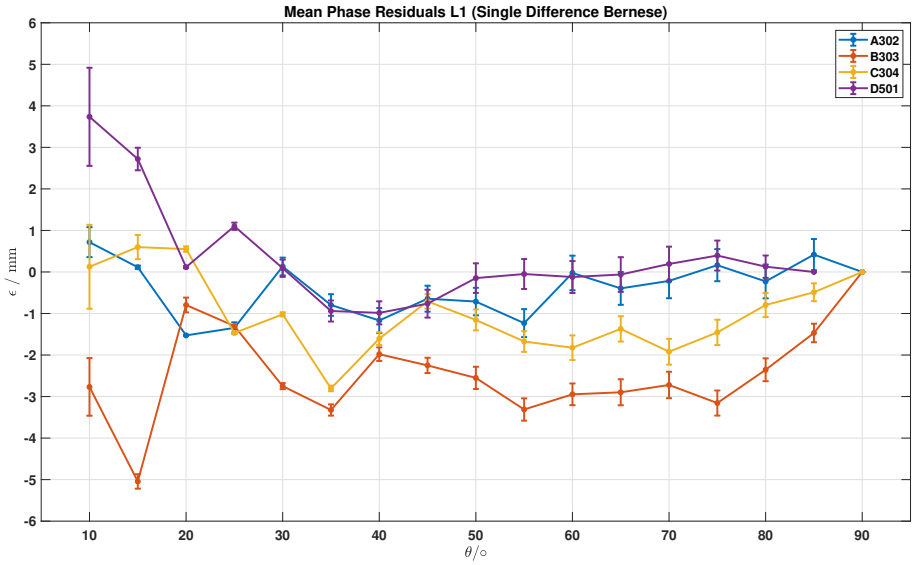

Figure 4.40: Final estimated model error of L1 single difference (Bernese)

Hence, a 30° elevation is also taken into account as the benchmark for evaluation across all antenna stations. The averaged error model for L1 frequency observations resulted in -0.8867 ± 0.1362 mm.

5

Conclusion

It is crucially important to assess the errors of GNSS observations in order to achieve more precise signal accuracy for certain applications or studies, such as space geodesy, geodynamics, and vehicle monitoring. These error parameters are caused by various aspects, including ground receiver-related, antenna-related, or environment-related factors in the surrounding location. This project is focused on examining the influence of errors, particularly in the phase center of the ground antenna.

The initial stage of assessing the error influence in the ground antenna phase center involves purposely tilting the antennas at several degrees of angle in different directions. This tilting process creates a geometrical constraint in the physical position and orientation of the antenna during GNSS signal observation. This constraint is then utilized to investigate the error of the antenna phase center. The geometrical constraint significantly affects the applied antenna phase center calibration correction data during position determination, as it is typically applied under normal antenna orientation and position. Moreover, this also impacts the position of the antenna reference point (ARP), as neither Bernese nor GipsyX can account for antenna tilting in a particular direction.

An external measurement using a laser tracker, which offers considerably higher accuracy than GNSS signals, is employed to calculate the desired station positions within its own reference frame. By utilizing the Helmert technique to transform the data points of the antenna stations between different reference frames, the laser tracker measurement results are then used as references for validation and comparison to the final results of station positions obtained from Bernese and GipsyX. The validation process involves comparing the formed six baseline formations between four antenna stations in two different reference frames, the laser tracker reference frame and the ECEF reference frame.

It is crucial to thoroughly investigate various types of errors during the project. For instance, the analysis of ground receiver clock error revealed that the use of two different types of receivers significantly influences signal observations, leading to considerable differences in error magnitude. This discrepancy may pose challenges when utilizing the single difference method for position determination in DGNSS, as this method does not eliminate the receiver clock error parameter. Therefore, it is advisable for future studies to consider using the same type of receiver across multiple stations during GNSS observations. This approach could help mitigate dis-

crepancies caused by differences in receiver characteristics and improve the accuracy of position determinations.

Additionally, the estimation of zenith tropospheric delay (ZTD) reveals that station A302 is subject to the highest error compared to the other stations. This observation is particularly significant as station A302 is situated at the lowest height, resulting in longer propagation distances for GNSS satellite signals.

The process of determining the positions of the four stations (A302, B303, C304, and D501) involves two different techniques and software applications, GipsyX with PPP method and Bernese with DGNSS single difference. Carrier phase signal measurement is used in this determination process, as it offer more precise signal accuracy compared to code measurements. GipsyX employs its PPP technique with dual-frequency processing of L3 (a combination of L1 and L2), while Bernese uses the single difference method with L1 and L2 processed separately. As a result, the final outputs consist of mean phase residuals data, which account for corrections to the antenna phase center based on the frequency signals of L1, L2, and L3.

In the PPP determination process using GipsyX, the final positions of all four stations, along with the residuals of carrier phase measurements, are computed utilizing L3 dual frequency. The resulting residuals are averaged and weighted based on the elevation angles of antenna phase center corrections. The mean phase residuals of L3 are categorized according to the antenna stations, with errors varying approximately 1.5 mm (for station D501) at lower elevations and around -0.25 mm (for station A301) at zenith angles.

In the single difference method of Bernese, the final outputs of phase residuals for L1 and L2 are calculated, with additional phase ambiguity corrections manually applied. This adjustment is made because the differential between the result of Bernese's single difference and the tracker projection is still considerably large. Notably, the phase residuals for L2 are not as expected and are noticeably worse than those for L1. As a result, only the phase residuals for L1 are considered, and their average values are weighted based on the elevation angles of the antenna phase center corrections. Taking the benchmark values for 30° elevation as the cut-off angle, the average error values of the antenna phase centers from all four antenna stations are as follows, -0.8867 ± 0.1362 mm on L1, -1.5728 ± 0.2496 mm on L2, and -0.3901 ± 0.0004 mm on L3.

Furthermore, one of the reasons the L2 are resulted in much worse residuals is the utilization of L2W in GPS signal during the position determination. The L2W is considered to have much lower carrier-to-noise ratio (CN_0) and signal-to-noise ratio (SNR) than L2C or L1C signal, making it to likely have worse quality performance during the signal observation. For further studies, particularly for L2 signal examination, it is recommended to utilize L2C signal observations considering it has higher quality performance in terms of SNR and CN_0 than the L2W.

Bibliography

[1] Bergstrand, S., Jarlemark, P., & Herbertsson, M. (2020). *Quantifying errors in GNSS antenna calibrations: Towards in situ phase center corrections*. Journal of Geodesy, 94(10), 105.

[2] Kaplan, E. D., & Hegarty, C. (Eds.). (2017). *Understanding GPS/GNSS: principles and applications*. Artech house.

[3] Gebre-Egziabher, D., & Gleason, S. (2009). *GNSS applications and methods*. Artech House.

[4] Blewitt, G. (1997). *Basics of the GPS technique: observation equations*. Geodetic applications of GPS, 1, 46.

[5] Cardellach, E., & Xie, F. (2014). *GNSS remote sensing (Vol. 16)*. S. Jin (Ed.). Dordrecht: Springer.

[6] Subirana, J. S., Zornoza, J. M. J., & Hernández-Pajares, M. (2013). *Global Navigation Satellite Systems, Volume I: Fundamentals and Algorithms*. ESA Communications ESTEC, Noordwijk, the Netherlands, 238.

[7] The Space-Based Positioning Navigation & Timing of U.S. National Executive Commitee (2017), *Control Segment*.

[8] Bhatta, B. (2010). *Global navigation satellite systems: insights into GPS, GLONASS, Galileo, Compass, and others*. BS Publications.

[9] Hofmann-Wellenhof, B., Lichtenegger, H., & Collins, J. (2012). *Global positioning system: theory and practice*. Springer Science & Business Media.

[10] Maral, G., Bousquet, M., & Sun, Z. (2020). *Satellite communications systems: systems, techniques and technology*. John Wiley & Sons.

[11] Hegarty, C. J. (2017). *The global positioning system (GPS)*. Springer handbook of global navigation satellite systems, 197-218.

[12] Revnivykh, S., Bolkunov, A., Serdyukov, A., & Montenbruck, O. (2017). *Glonass*. Springer Handbook of Global Navigation Satellite Systems, 219-245.

[13] Falcone, M., Hahn, J., & Burger, T., (2017). *Galileo* Springer handbook of global navigation satellite systems, 247-272.

[14] Beard, R., & Senior, K. (2017). *Clocks*. Springer handbook of global navigation satellite systems, 121-164.

[15] Meurer, M., & Antreich, F. (2017). *Signals and Modulation*. Springer handbook of global navigation satellite systems, 91-119.

[16] The United States of America, Department of Defense (2020). *Global positioning system standard positioning service performance standard*.

[17] van Diggelen, F. (2014). *Who's your daddy*. INSIDE GNSS Magazine.

[18] Hofmann-Wellenhof, B., Lichtenegger, H., & Wasle, E. (2007). *GNSS–global navigation satellite systems: GPS, GLONASS, Galileo, and more*. Springer Science & Business Media.

[19] Langley, R., B., Teunissen, P., J., G., & Montenbruck, O.(2017). *Introduction to GNSS*. Springer handbook of global navigation satellite systems, 3-23.

[20] Eissfeller, B., & Won, J-H. (2017). *Receiver architecture*. Springer handbook of global navigation satellite systems, 365-400.

[21] Maqsood, M., Gao, S., & Montenbruck, O. (2017). *Antennas*. Springer handbook of global navigation satellite systems, 505-534.

[22] Rao, B. R., Kunysz, W., Fante, R., & McDonald, K. (2013). *GPS/GNSS Antennas*. Artech House.

[23] Subirana, J. S., Zornoza, J. M. J., & Hernández-Pajares, M. (2011). *Receiver Antenna Phase Centre* . European Space Agency.

[24] Grewal, M. S., Andrews, A. P., & Bartone, C. G. (2020). *Global navigation satellite systems, inertial navigation, and integration*. John Wiley & Sons.

[25] Wu, J. T., Wu, S. C., Hajj, G. A., Bertiger, W. I., & Lichten, S. M. (1992). *Effects of antenna orientation on GPS carrier phase*. Astrodynamics 1991, 1647-1660.

[26] Hauschild, A. (2017). *Basic observation equations*. Springer handbook of global navigation satellite systems, 561-582.

[27] Subirana, J. S., Zornoza, J. M. J., & Hernández-Pajares, M. (2011). *Reference systems and frames*. European Space Agency.

[28] Boucher, C., & Altamimi, Z. (2001). *ITRS, PZ-90 and WGS 84: current realizations and the related transformation parameters*. Journal of Geodesy, 75, 613-619.

[29] Tran, D. T., Nocquet, J. M., Luong, N. D., & Nguyen, D. H. (2023). *Determination of Helmert transformation parameters for continuous GNSS networks: a case study of the Géoazur GNSS network*. Geo-Spatial Information Science, 26(1), 125-138.

[30] Dach, R., & Walser, P. (2015). *Bernese GNSS Software Version 5.2*. Astronomical Institute, University of Bern.

[31] Kouba, J., Lahaye, F., & Tétreault, P. (2017). *Precise Point Positioning*. Springer handbook of global navigation satellite systems, 723-751.

[32] Bertiger, W., Bar-Sever, Y., Dorsey, A., Haines, B., Harvey, N., Hemberger, D., ... & Willis, P. (2020). *GipsyX/RTGx, a new tool set for space geodetic operations and research*. Advances in space research, 66(3), 469-489.

[33] Lichten, S. M., Bar-Sever, Y., Bertiger, W., Heflin, M., Muellerschoen, R. J., ... & Zumberge, J. (1995). *GIPSY-OASIS II: A high precision GPS data processing system and general satellite orbit.*. JPL Open Repository.

A

Estimated Receiver Clock Errors

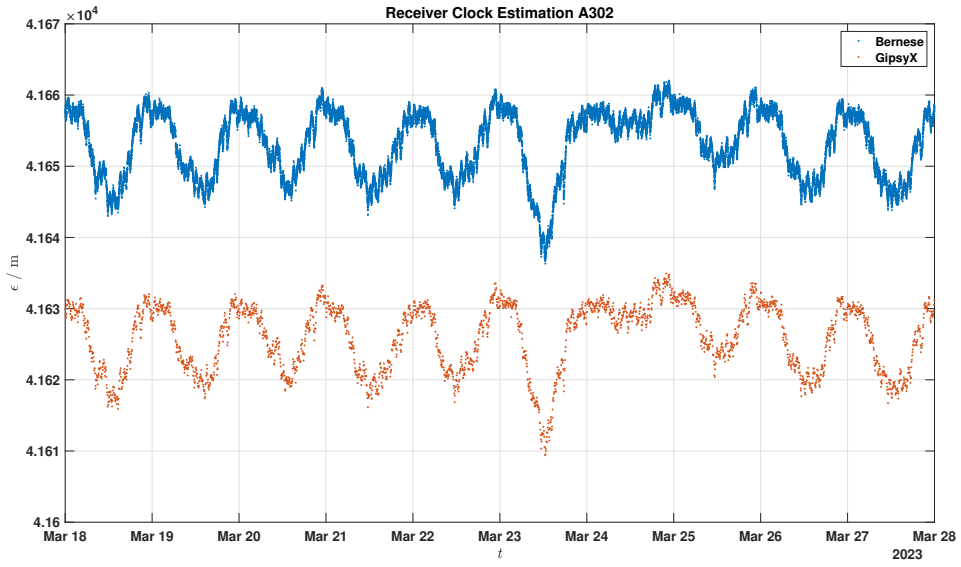

Figure A.1: Receiver clock error station D501 (10 days observations)

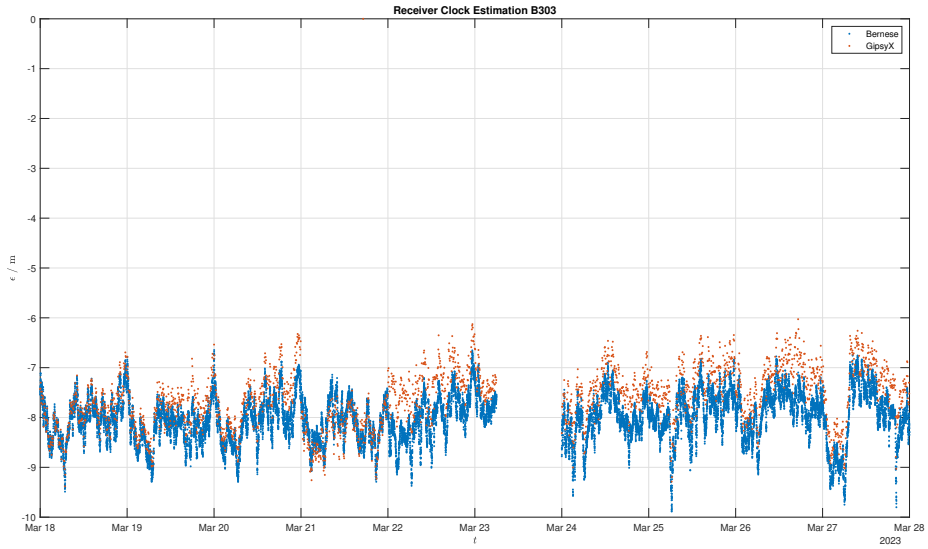

Figure A.2: Receiver clock error station D501 (11 days observations)

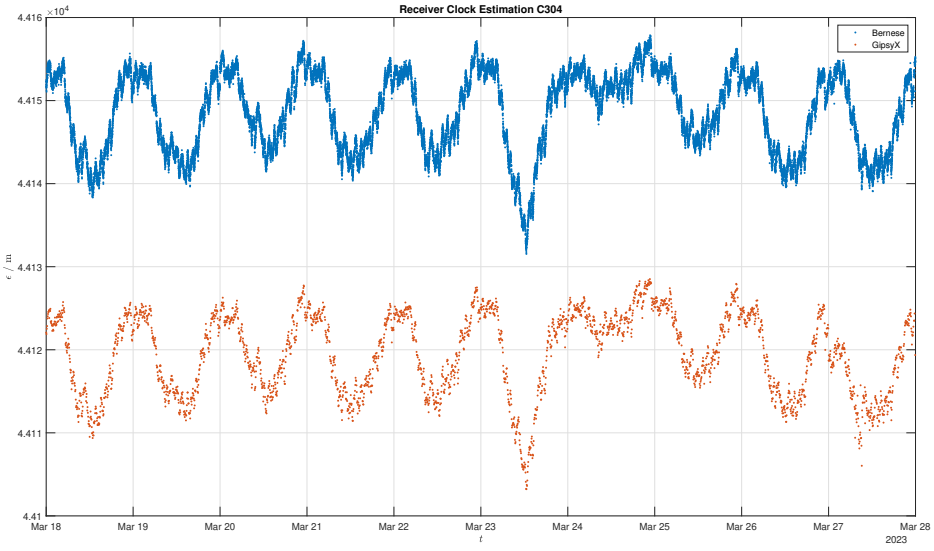

Figure A.3: Receiver clock error station D501 (10 days observations)

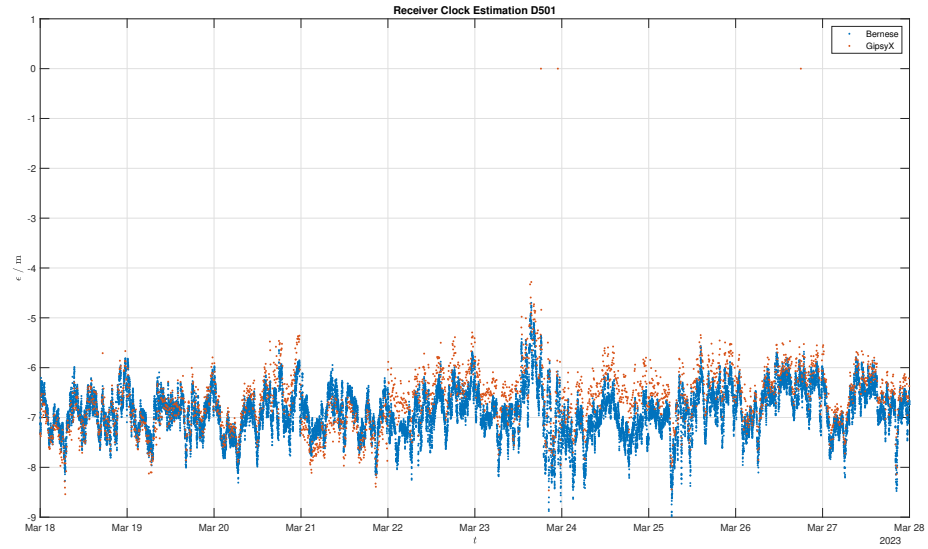

Figure A.4: Receiver clock error station D501 (11 days observations)

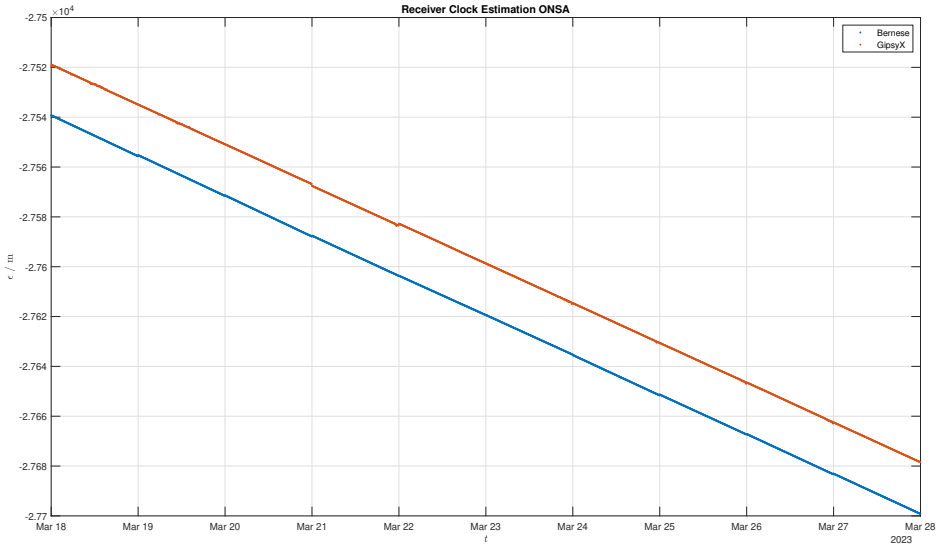

Figure A.5: Receiver clock error station D501 (11 days observations)

B

Estimated Zenith Tropospheric Delay

Figure B.1: Final estimations of ZTD in all five stations (11 days observations)

C

Estimated Integer Ambiguity Errors

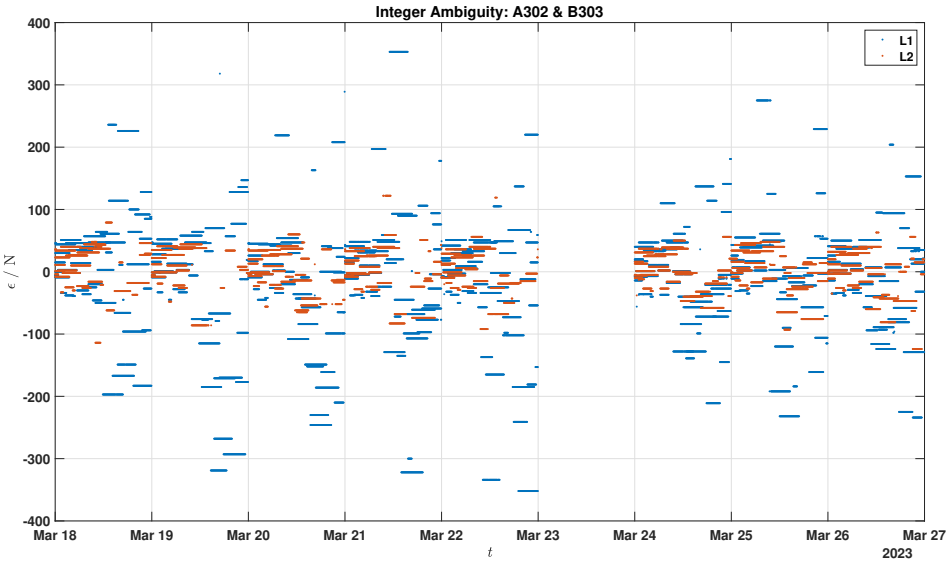

Figure C.1: Integer ambiguities between A302 and B303

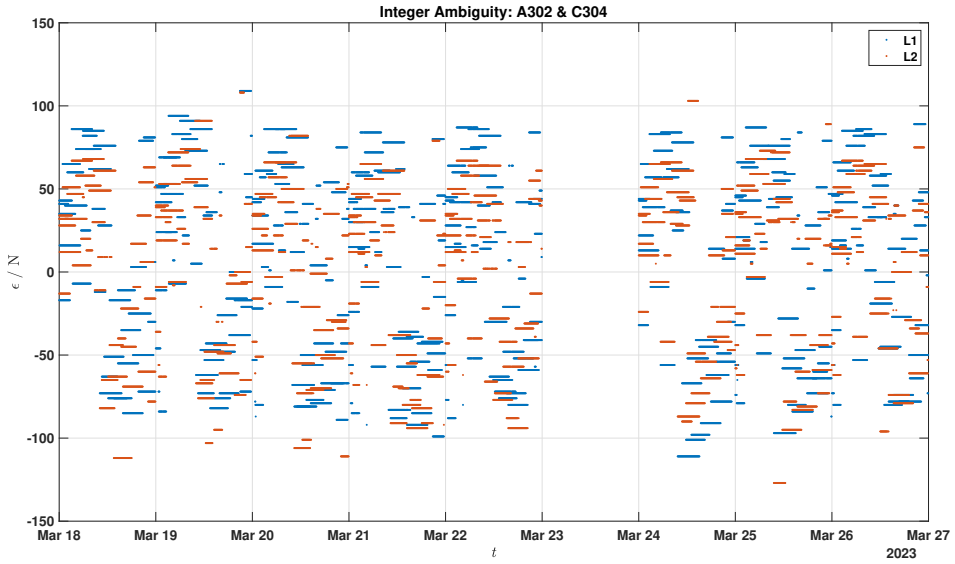

Figure C.2: Integer ambiguities between A302 and C304

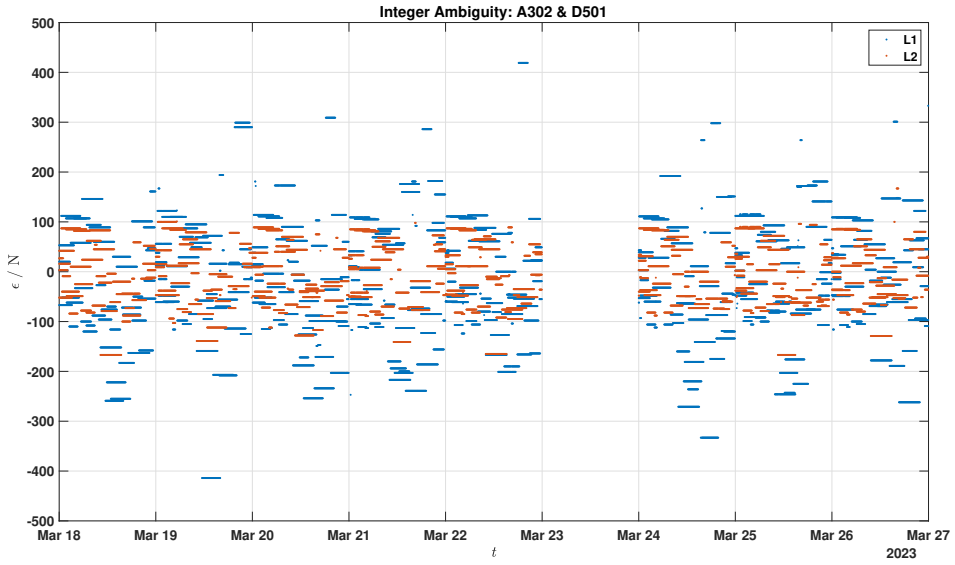

Figure C.3: Integer ambiguities between A302 and D501

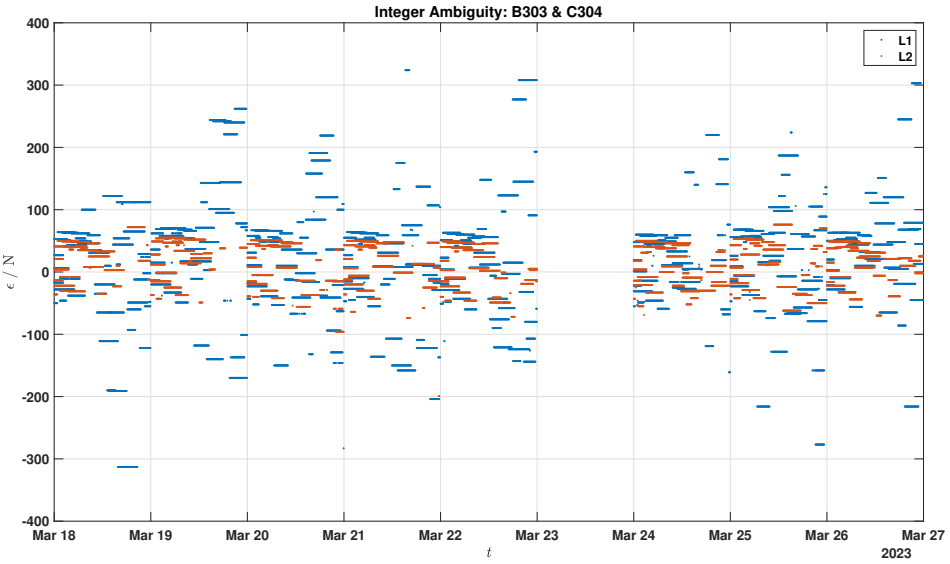

Figure C.4: Integer ambiguities between B303 and C304

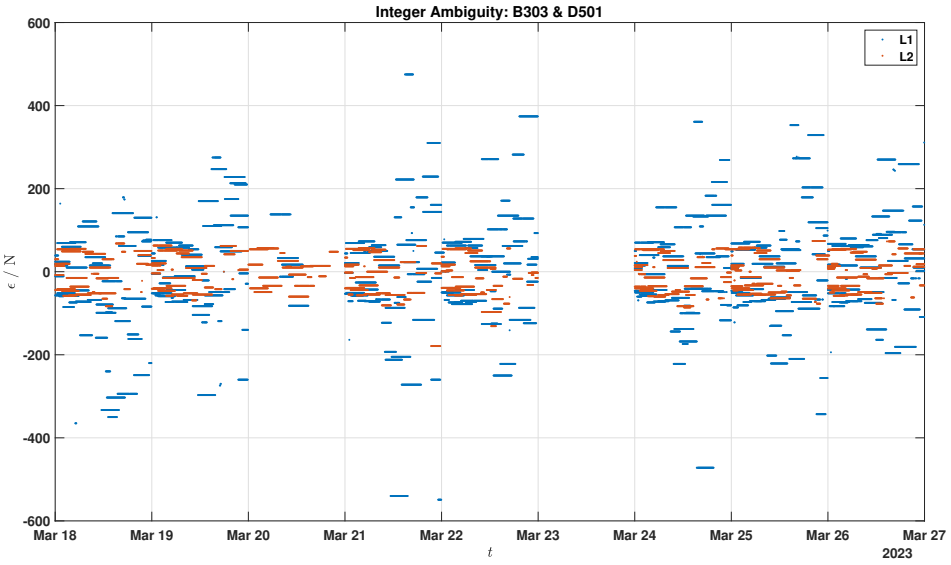

Figure C.5: Integer ambiguities between B303 and D501

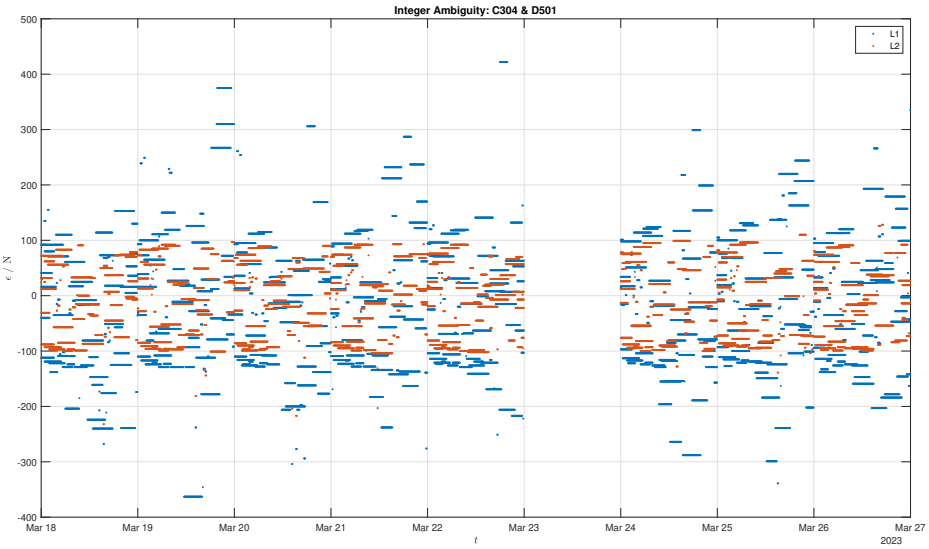

Figure C.6: Integer ambiguities between C304 and D501

D

L2 Single Difference & Tracker Projection

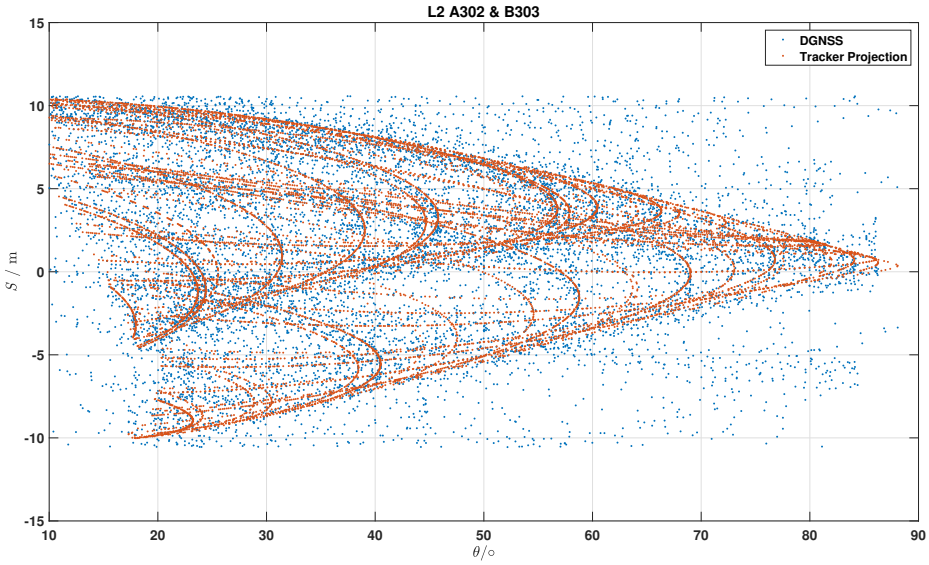

Figure D.1: L2 single difference A302 & B303

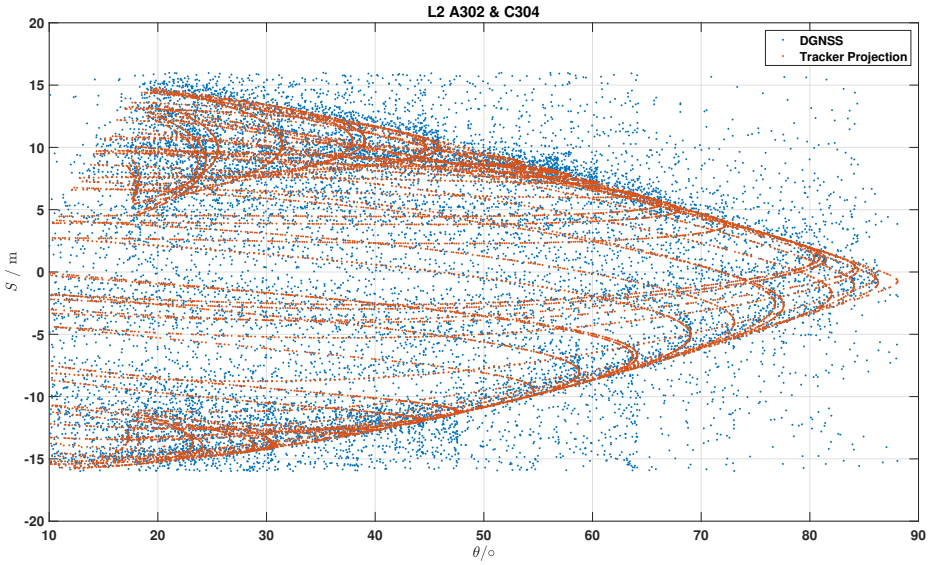

Figure D.2: L2 single difference A302 & C304

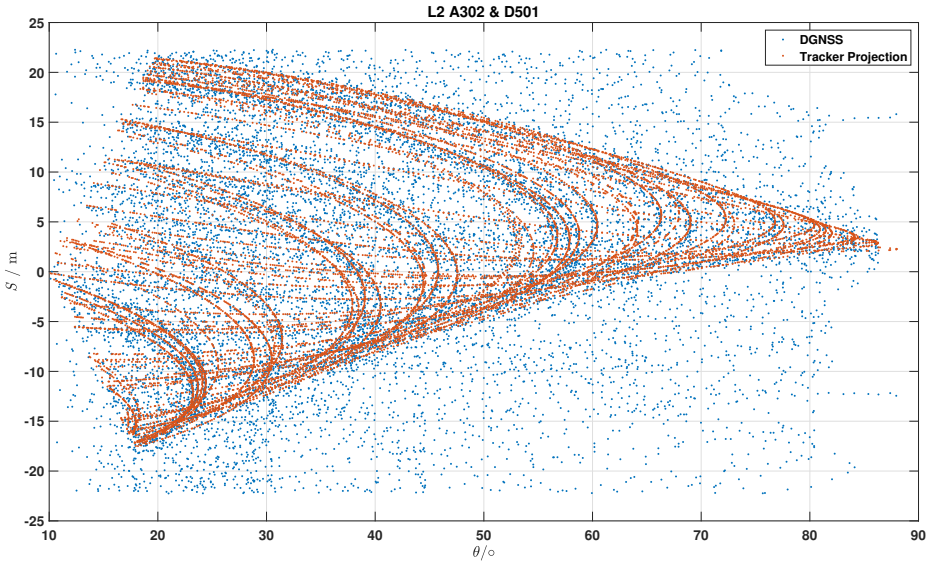

Figure D.3: L2 single difference A302 & D501

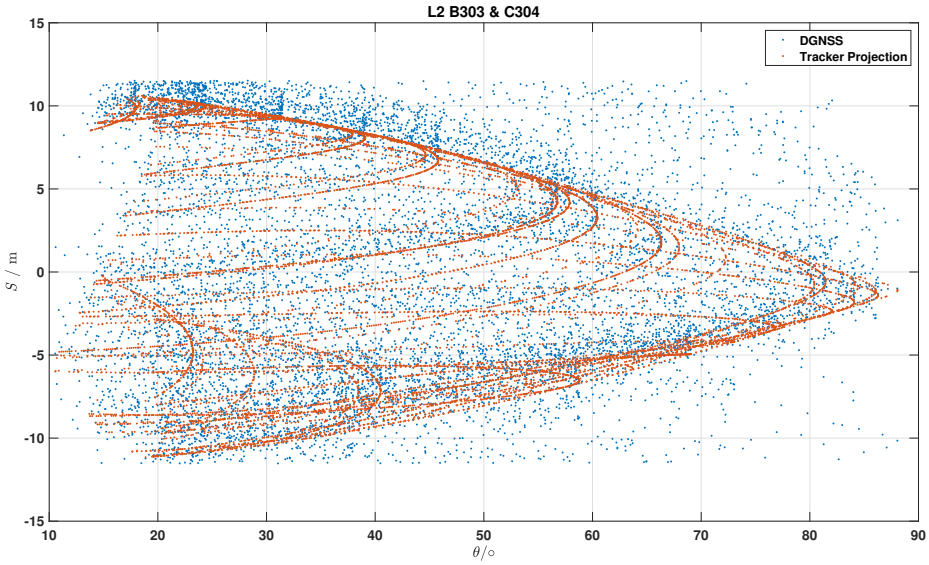

Figure D.4: L2 single difference B303 & C304

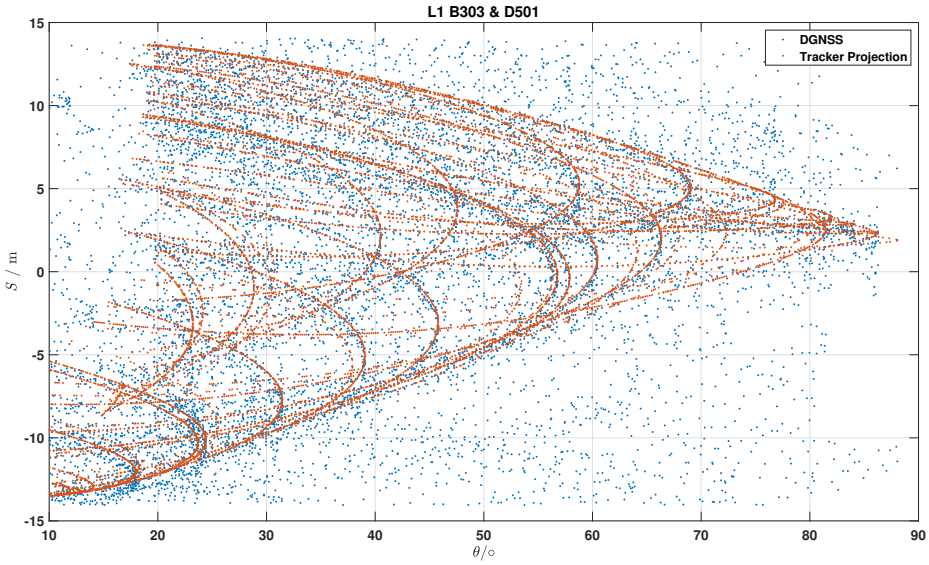

Figure D.5: L2 single difference B303 & D501

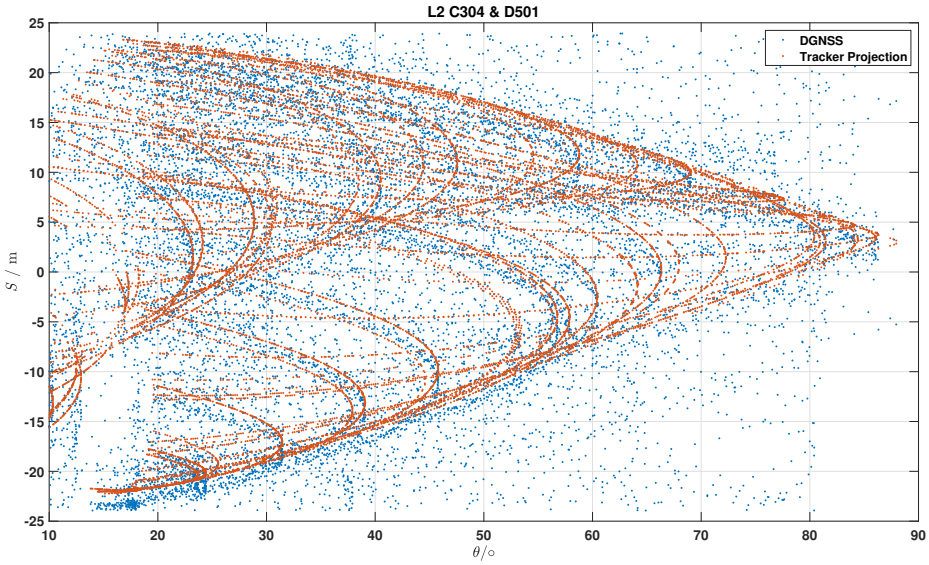

Figure D.6: L2 single difference C304 & D501

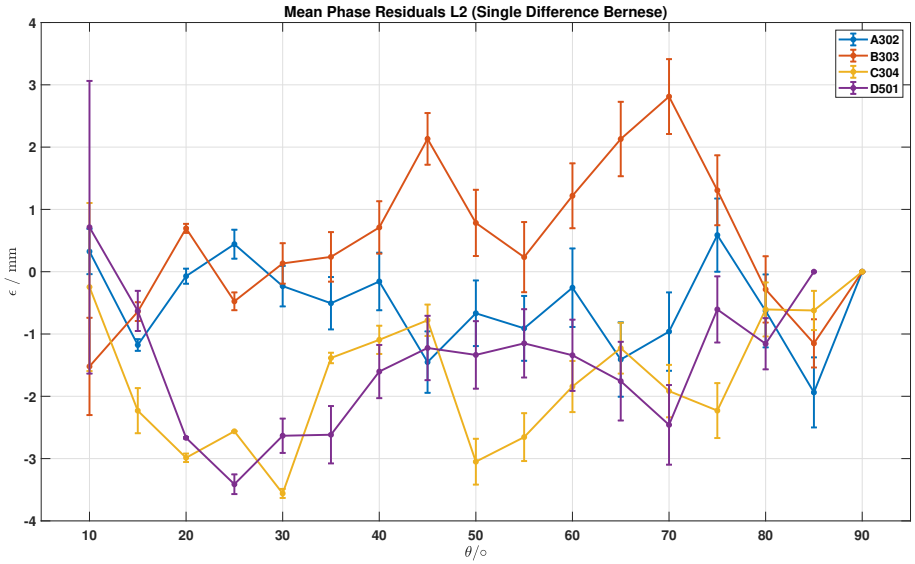

Figure D.7: Final estimated model error of L2 single difference (Bernese)

E

Mean Phase Residual Comparisons

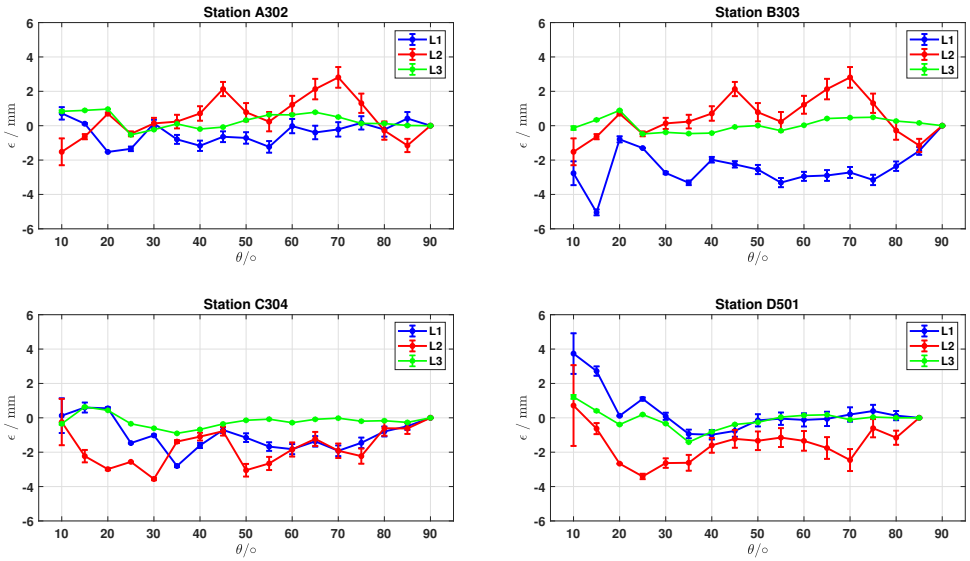

Figure E.1: Mean phase residual comparisons in each station